

10-20-2022

## Effect of Fine Aggregate and PVA Fiber Content on the Properties of Metakaolin-Based Engineered Geopolymer Composites

Ruwa Abufarsakh

*Louisiana State University and Agricultural and Mechanical College*

Follow this and additional works at: [https://digitalcommons.lsu.edu/gradschool\\_theses](https://digitalcommons.lsu.edu/gradschool_theses)

---

### Recommended Citation

Abufarsakh, Ruwa, "Effect of Fine Aggregate and PVA Fiber Content on the Properties of Metakaolin-Based Engineered Geopolymer Composites" (2022). *LSU Master's Theses*. 5661.  
[https://digitalcommons.lsu.edu/gradschool\\_theses/5661](https://digitalcommons.lsu.edu/gradschool_theses/5661)

This Thesis is brought to you for free and open access by the Graduate School at LSU Digital Commons. It has been accepted for inclusion in LSU Master's Theses by an authorized graduate school editor of LSU Digital Commons. For more information, please contact [gradetd@lsu.edu](mailto:gradetd@lsu.edu).

# **EFFECT OF FINE AGGREGATE AND PVA FIBER CONTENT ON THE PROPERTIES OF METAKAOLIN-BASED ENGINEERED GEOPOLYMER COMPOSITES**

A Thesis

Submitted to the Graduate Faculty of the  
Louisiana State University and  
Agricultural and Mechanical College  
in partial fulfillment of the  
requirements for the degree of  
Master of Science in Engineering Science

by  
Ruwa Murad Abufarsakh  
B.A., Louisiana State University, 2019  
Decemeber 2022

## **ACKNOWLEDGMENTS**

The author would like to express her gratitude to her parents, Dr. Murad AbuFarsakh and Mrs. Seham AbuFarsakh, along with her siblings for their support and encouragement during this time. The author would like to express her gratitude to her advisor Dr. Marwa Hassan for the amazing opportunity she provided her within conducting her research. Furthermore, her support, guidance, encouragement, and infectious enthusiasm were invaluable throughout this journey. Moreover, the author is exceptionally grateful to Dr. Gabriel Arce for his support, intelligence, advice, and continuous patience as he was an essential part throughout every step of this journey. Additionally, the author would like to express her gratitude to the members of her supervisory committee, Dr. Ayman Okeil, and Dr. Isabellina Nahmens, for providing her with their valuable time and insight.

The author would also like to thank Dr. Jose Milla, Norris Rosser, Leon Goudeau, and Austin Gueho, members of the Louisiana Transportation Research Center (LTRC) concrete laboratory, for their assistance in her research. Furthermore, the author would like to thank Tran-SET for the financial support which made this research possible.

The author would also like to thank her friends and colleagues at LSU for their continuous support and encouragement. A special thanks to my friend and colleague Sujata Subedi for her assistance during the research work.

## TABLE OF CONTENTS

ACKNOWLEDGMENTS .....	ii
LIST OF TABLES .....	iv
LIST OF FIGURES .....	v
NOMENCLATURE, SYMBOLS, AND ACRONYMS .....	vii
ABSTRACT .....	viii
1. INTRODUCTION .....	1
2. LITERATURE REVIEW .....	7
3. EFFECT OF FINE AGGREGATE AND PVA FIBER CONTENT ON THE PROPERTIES OF METAKAOLIN BASED ENGINEERED GEOPOLYMER COMPOSITES .....	57
4. SUMMARY AND CONCLUSIONS .....	92
5. FUTURE WORK .....	95
APPENDIX. COPYRIGHT PERMISSION .....	96
REFERENCES .....	97
VITA .....	109

## LIST OF TABLES

Table 2.1. Fly Ash Chemical Requirements (ASTM C618, 2019).....	23
Table 2.2. GGBFS Typical Chemical Composition .....	24
Table 2.3. Properties of PVA Fibers (NYCON, 2022) .....	26
Table 2.4. Properties of UHMWPE Fibers .....	27
Table 2.5. Properties of ST Fibers ( <i>Advanced Steel Fibers for Ultra High Performance Concrete</i> , 2020).....	27
Table 2.6. Comparison between Geopolymer and Conventional Concrete (Berndt et al., 2013) .....	53
Table 3.1. Mixture Proportions (units in kg/m <sup>3</sup> ).....	70

## LIST OF FIGURES

Figure 2.1. Classification of FRCCs According to Recommendations for Design .....	8
Figure 2.2. Typical stress-strain or stress-elongation curve in tension up to complete separation in (a) Conventional strain softening FRCC, and (b) Strain hardening FRCC or HPFRCC (Naaman, 2008) .....	9
Figure 2.3. Fiber bridging relation, $\sigma(\delta)$ curve (adapted from (Noorvand et al., 2019)) .....	13
Figure 2.4. Stress vs. strain behavior of cementitious materials in tension (adapted from (Noorvand et al., 2019)) .....	15
Figure 2.5. Geopolymerization process (Arce et al., 2020) .....	17
Figure 2.6. Association and Dissolution .....	18
Figure 2.7. Three Types of 3-Dimensional Amorphous Polymer Structures (Davidovits et al., 2015) .....	19
Figure 2.8. Fly Ash Stockpiles .....	22
Figure 2.9. MasterGlenium 7500 Superplasticizer Degrading in Alkali Silicate Activator Solution .....	36
Figure 2.10. Starch Modified with (a) Sodium Sulfonate and (b) CHPTAC .....	43
Figure 2.11. Drying Shrinkage and Creep Strains (Hardjito et al., 2004) .....	47
Figure 2.12. Mechanism of Alkali Silica Reaction (Annapurna et al., 2020) .....	51
Figure 3.1. (a) Fiber Bridging Relation ( $\sigma$ - $\delta$ Curve) (b) Stress vs. Strain Behavior of Cementitious Materials in Tension (Adapted from (Noorvand et al., 2019)) .....	64
Figure 3.2. Secondary Electron SEM Images of (a) Metakaolin, (b) Microsilica Sand, (c) Silica Sand, and (d) PVA Fiber .....	66
Figure 3.3. Particle Size Distribution of River Sand, and Microsilica Sand .....	67
Figure 3.4. Geopolymer Manufacturing (a) Vacuum Shear Mixer (b) Mixing Procedure (c) Modified Mixing Procedure .....	70
Figure 3.5. Casting and Curing of GP Materials (a) Dogbone Specimens after Casting (b) Cube Specimens during Curing .....	71
Figure 3.6. Experimental Setup for Compressive Strength Test .....	72
Figure 3.7. (a) Dog-bone Specimen Dimensions (in mm) and (b) Uniaxial Tensile Test Setup ..	73

Figure 3.8. Epoxy Impregnated and Polished GP Materials for SEM Analysis.....	74
Figure 3.9. GP Binders and Mortars (a) Average 28-Day Compressive Strength (b) Density.....	76
Figure 3.10. GP Composites (a) Average 28-Day Compressive Strength (b) Density.....	76
Figure 3.11. Compressive Strength Failure Mode of K321 EGCs .....	78
Figure 3.12. Tensile Stress vs. Strain Curves of (a) K321 GP-RS-1.6%PVA (b) K321 GP-MS-1.6%PVA (c) K321 GP-MS-1.6% Using Modified Mixing Procedure .....	81
Figure 3.13. Average Tensile Test Results (a) Tensile Strain Capacity (b) First-Cracking Strength and Tensile Strength.....	84
Figure 3.14. BSE Images of (a) K321 GP Binder (b) K331 GP Binder .....	85
Figure 3.15. Atomic Ratio Plot for (a) K321 and (b) K331 GPs .....	86
Figure 3.16. Setting Time Experimental Results .....	88

## NOMENCLATURE, SYMBOLS, AND ACRONYMS

ASTM	American Society for Testing and Materials
CV	Coefficient of Variation
DI	Deionized
GP	Geopolymer
GGBS	Ground-Granulated Blast-Furnace Slag
ECC	Engineered Cementitious Composite
EDS	Energy Dispersive Spectroscopy
EGC	Engineered Geopolymer Composite
$E_m$	Modulus of Elasticity of the Matrix
FA	Fly Ash
FRC	Fiber Reinforced Concrete
$J'_b$	Complementary Energy of the Fiber-Bridging Relation
$J_{tip}$	Crack-Tip Matrix Toughness
JSCE	Japan Society of Civil Engineers
$K_m$	Fracture Toughness of the Matrix
LOI	Loss on Ignition
LVDT	Linear Variable Displacement Transducer
MK	Metakaolin
MS	Microsilica Sand
PCC	Portland Cement Concrete
PSH	Pseudo Strain Hardening
PVA	Polyvinyl Alcohol
RS	River Sand
SE	Secondary Electron
SEM	Scanning Electron Microscopy
STD	Standard Deviation
UHMWPE	Ultra-High Molecular Weight Polyethylene
XRF	X-ray Fluorescence Spectroscopy
$\sigma_{fc}$	First Cracking Strength
$\sigma_0$	Fiber-Bridging Capacity
$\delta_0$	Crack Opening Corresponding to $\sigma_0$
$\sigma(\delta)$	Fiber-Bridging Relationship



## ABSTRACT

The mechanical and physical properties of novel metakaolin (MK) based Engineered Geopolymer Composites (EGCs) consisting of locally available river sand (RS) or manufactured microsilica sand (MS) reinforced with polyvinyl alcohol (PVA) fiber were studied. Plain geopolymer (GP) binder, GP mortars, and fiber-reinforced composites were also studied. Aspects of the material composition that were investigated in this study include binder composition, aggregate type, and PVA fiber content. Per the compressive strength results, GP mortars presented greater compressive strength than GP binder where the GP mortars manufactured with lower water to solids ratio exhibited greater compressive strengths. Furthermore, the incorporation of PVA fiber produced an important increment in compressive strength. Moreover, an enhancement in compressive strength of the composite was seen with an increase in fiber content. Additionally, MS tended to produce composites with higher strength compared to those using RS. All the composites evaluated in this study exceeded the compressive strength of regular concrete (i.e., 30 MPa) while exhibiting low densities (i.e., 1.80-1.94 g/cm<sup>3</sup>). Moreover, K321 GP-MS-1.6%PVA EGC presented the highest compressive strength of 57.5 MPa, thus classifying it as high strength concrete per ACI Committee 363. Furthermore, per uniaxial tensile test, tensile pseudo strain-hardening (PSH) behavior was observed for the MK-based GP composites manufactured where MS produced higher tensile strength and strain capacity compared to RS. However, due to the lack of proper fiber dispersion (i.e., fiber clumping), robust PSH behavior was not achieved. According to Scanning Electron Microscopy (SEM), several unreacted metakaolin particles were encountered indicating incomplete geopolymerization in both GP binders evaluated in this study. Additionally, there was good agreement between the intended chemical composition of the manufactured GP binders and the actual chemical

composition found in the specimens examined via energy dispersive X-ray spectroscopy (EDS) in the geopolymer gel.

## 1. INTRODUCTION

As one of the most widely utilized material for civil infrastructure, concrete is a low cost, widely available, durable, versatile, and workable material that possesses high compressive strength. However, concrete is weak in tension due to its low tensile strength and ductility. Therefore, when subjected to high tensile stresses, concrete will begin to crack leading to brittle failure. When concrete cracks, its durability is negatively affected as detrimental agents such as water and chlorides penetrate the structure enhancing deterioration. As a response, researchers around the world developed a new class of fiber-reinforced cementitious composites known as Engineered Cementitious Composites (ECCs) to mitigate the brittle nature of concrete. Unlike conventional concrete, ECCs have high tensile strain capacity ranging between 1 to 8% (i.e., 100 to 800 times that of regular concrete) and is achieved at relatively low fiber contents (i.e., typically 1.5 to 2% volume fraction) (Alrefaei & Dai, 2018; Li, 2008; Li et al., 2004; Nematollahi, Sanjayan, & Ahmed Shaikh, 2015; Ohno & Li, 2018). To attain this, ECCs are distinctively designed based on micromechanics and fracture mechanics concepts to transform the Griffith crack propagation mode of regular concrete and fiber-reinforced concrete (FRC) to a steady-state flat crack propagation mode. Consequently, this enables a tensile pseudo strain-hardening (PSH) behavior in ECCs through the formation of multiple steady-state microcracks, which gives rise to the extraordinary tensile ductility of these composites (Li, 2003).

Like conventional concrete, the ECCs mix design consists of cement, supplementary cementitious materials (SCMs), fine aggregate, water, and admixtures. However, coarse aggregates are not incorporated in ECCs. Additionally, ECCs are reinforced with microfibers such as Polyvinyl alcohol (PVA) and ultra-high-molecular weight polyethylene (UHMWPE) (Arce et al., 2019; Li, 2003, 2019b; Li et al., 2002; Reda Taha et al., 2002). PVA fibers have been predominantly used in the manufacturing of ECCs (Kan et al., 2019, 2020; Li et al., 2002,

2004; Ling et al., 2019; H. Ma et al., 2015; Nematollahi, Sanjayan, & Ahmed Shaikh, 2015; Nematollahi, Sanjayan, & Shaikh, 2015; Pakravan et al., 2018; Redon et al., 2001a), whereas UHMWPE fibers have been used to manufacture high performance ECCs due to its high cost (Alrefaei & Dai, 2018; Choi et al., 2016; Ding et al., 2018; Li et al., 2002; Osman et al., 2019; Yu et al., 2018). Since ECCs do not use coarse aggregates, the amount of cement used to manufacture ECCs increases compared to conventional concrete. This in turn increments ECCs environmental impact as the cement industry is accountable for nearly 8% of the carbon dioxide (CO<sub>2</sub>) global anthropogenic emissions (N. B. Singh, 2018). As such, there is a significant push to develop a more sustainable alternative to cement binder without negatively affecting the mechanical properties of ECC. A promising alternative is the use of geopolymer binders, which can reduce CO<sub>2</sub> emissions by 44-64% compared to ordinary Portland cement (OPC) (Komnitsas, 2011; McLellan et al., 2011; Turner & Collins, 2013). These composites implementing geopolymer binders are recognized in the literature as strain hardening geopolymer composites (SHGC) or Engineered Geopolymer Composites (EGCs). Previous studies suggest that geopolymer matrices exhibit comparable compressive strengths to cementitious matrices while exhibiting lower fracture toughness (C. Ma et al., 2018; Nematollahi et al., 2016; Nematollahi, Sanjayan, & Ahmed Shaikh, 2015; Ohno & Li, 2014). In turn, EGCs can achieve high tensile ductility at remarkably low fiber contents (i.e., less than 2%) (Nematollahi et al., 2014, 2016; Nematollahi, Sanjayan, & Shaikh, 2015; Ohno & Li, 2014, 2018).

### **1.1. Problem Statement**

Many researchers have evaluated fly ash based geopolymer composites with metakaolin or slag as a precursor partial replacement while achieving remarkable strengths and ductility without maintaining the geopolymer binder chemistry. However, pure metakaolin based geopolymer

composites has not been evaluated. The present study will evaluate the effect of novel metakaolin (MK) based polyvinyl alcohol (PVA) fiber reinforced EGCs as a sustainable construction material alternative with superior mechanical performance. To this end, the effect of binder composition, aggregate type, and fiber content, on the mechanical and physical properties of MK-PVA-EGCs. Furthermore, the geopolymer binder chemistry was controlled by manufacturing the activator solution in the laboratory.

## **1.2. Research Objectives**

Aiming to resolve the previously stated problem statement, the following is the study's objective:

(1) determine the best geopolymer binder composition; (2) produce geopolymer mortars utilizing two types of sand (i.e., river sand and microsilica sand) at a sand to binder ratio of 0.36; (3) develop fiber reinforced geopolymer composites (i.e., engineered geopolymer composites) utilizing three different levels of PVA fiber content; (4) assess the mechanical properties of the specimens by conducting compressive strength and uniaxial tensile tests; (5) evaluating setting time of the different geopolymer binder compositions; (6) characterize the microstructure of the geopolymer binders via scanning electron microscopy (SEM) along with energy dispersive x-ray spectroscopy (EDS).

## **1.3. Research Approach**

In order to achieve the previously stated objectives, the study was performed in three phases consisting of the following tasks:

## Phase 1: Geopolymer binder compositions

### *Task 1: Manufacture the activator solution*

The alkali silicate activator solution was manufactured in the laboratory through a dissolution process where potassium hydroxide and silica fume were dissolved in deionized water.

### *Task 2: Produce the different geopolymer binders*

The alkali silicate activator solution was mixed with metakaolin to produce geopolymer binder compositions consisting of two different water to geopolymer solid contents (i.e.,  $H_2O / (SiO_2 + Al_2O_3)$ ), which were 2 and 3, were investigated.

### *Task 3: Conduct compressive strength test on cubes*

After 28 days, the geopolymer binder compositions were subjected to compressive strength test to evaluate the effect of water content on this property.

## Phase 2: Geopolymer mortars

### *Task 4: Produce the different geopolymer mortars*

For both geopolymer binders, locally available river sand (RS) and microsilica sand (MS) were evaluated at a constant sand to binder ratio (i.e.,  $sand / (SiO_2 + Al_2O_3 + KOH)$ ) of 0.36.

### *Task 5: Conduct compressive strength test on cubes*

After 28 days, the geopolymer mortars were subjected to compressive strength test to evaluate the effect of sand type on this property.

### Phase 3: Engineered Geopolymer Composites (EGCs)

#### *Task 6: Produce the different EGCs*

Three different levels of PVA fiber content (i.e., 0.8%, 1.2%, and 1.6% volume fraction) were evaluated.

#### *Task 7: Conduct compressive strength test on cubes*

After 28 days, the engineered geopolymer composites were subjected to compressive strength test to evaluate the effect of PVA fiber content on this property.

#### *Task 8: Conduct uniaxial tensile test on MK-PVA specimens*

Along with compressive strength test, the specimens consisting of PVA fibers were subjected to uniaxial tensile test to determine the tensile strength and ductility of the geopolymer composites.

#### *Task 9: Conduct uniaxial tensile test on MK-PVA specimens with a different mixing procedure*

After conducting uniaxial tensile test on the geopolymer composites mixed via vacuum shear mixer, the best performing composite was mixed using a planetary tabletop mixer to better disperse the fibers to fully exfoliate the material tensile strength and ductility.

### Phase 4: Characterization of the geopolymer binder

#### *Task 10: Setting time of geopolymer binder*

The setting time of the geopolymer binders were evaluated to determine its applicability for transportation applications.

*Task 11: SEM/EDS analysis on the geopolymer binder*

The vacuum epoxy impregnated, polished, and platinum sputter coated geopolymer binders were subjected to SEM analysis via backscattered electron imaging to determine whether there is any unreacted metakaolin in the geopolymer binder. Furthermore, EDS analysis was conducted in order to validate the composition of the geopolymer materials produced.



## **2. LITERATURE REVIEW**

The American Society of Civil Engineers (ASCE) presents a report card every four years that illustrates America's infrastructure's condition and performance. In 2021, the overall grade increased from a D+ in 2017 to a C- indicating a significant improvement. Recently, global attention has turned to the environmental impact of rebuilding the deteriorating civil infrastructure as this will require vast amounts of construction materials with Portland cement concrete (PCC) being at the forefront. However, the cement industry produces vast amounts of anthropogenic emissions such as CO<sub>2</sub>. As such, there is a need to develop sustainable alternatives to PCC that are less emission intensive and more energy efficient, durable, and resilient. To this end, geopolymer (GP) based materials have gained the attention of scientists worldwide.

### **2.1. Fiber Reinforced Cementitious Composites (FRCCs)**

The durability, low cost, and widespread availability of concrete make it an ideal material for construction applications in civil infrastructure (e.g., pavements, bridges, buildings, etc.). While achieving high compressive strength, unreinforced cementitious materials (i.e., cement paste, mortar, and concrete) have low tensile strength and ductility resulting in brittle failure and cracking. Whenever unreinforced cementitious materials are loaded or exposed to changing environmental conditions, cracks develop and propagate, allowing water and other detrimental agents to enter the structure and deteriorate it (Mindess et al., 2003). To counteract this problem, steel reinforcement is typically placed in the area of the concrete subjected to tensile stresses (McCormac & Brown, 2016). However, in the past 40 years, there has been an increase in use of continuous aligned or randomly oriented fibers as cementitious reinforcement to hinder crack growth and propagation thus mitigating concrete brittle failure.

Fiber reinforced cementitious composites (FRCCs) are composed of two primary constituents: matrix and reinforcing fibers. The matrix is typically comprised of Portland cement, water, supplementary cementitious materials (SCMs), aggregate, and admixtures depending on whether it is a paste, mortar, or concrete. Additionally, entrapped air voids in the matrix are considered as part of the matrix. The fibers are assumed to be discontinuous and randomly distributed within the composite. Due to the fiber/matrix interfacial bond, the fibers and matrix work together to make FRCCs.

According to Japan Society of Civil Engineers (JSCE) presented in Figure 2.1., FRCCs are classified based on strength and ductility level (Japan Society of Civil Engineers, 2008). Among the different classes of FRCCs, high performance fiber reinforced composites (HPFRCCs) and engineered cementitious composites (ECCs) are of particular interest and are outlined in the following subsections.

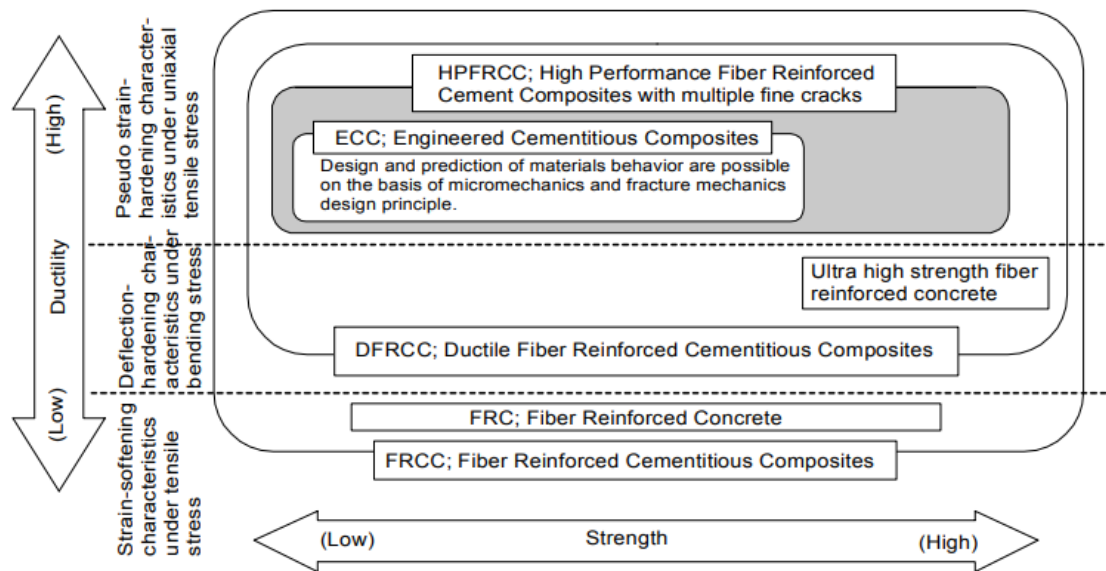


Figure 2.1. Classification of FRCCs According to Recommendations for Design and Construction of High Performance Fiber Reinforced Cement Composites with Multiple Fine Cracks (Japan Society of Civil Engineers, 2008)

### 2.1.1. High Performance Fiber Reinforced Cementitious Composites (HPFRCCs)

Traditional FRCCs present marginal improvement in tensile strength and ductility associated with strain-softening behavior after first crack in which there is single localized crack growth associated with a decrease in load carrying capacity when subjected to tensile stresses. On the other hand, HPFRCCs are a special class of FRCCs that exhibit strain hardening behavior in which there is multiple cracking associated with an increase in load carrying capacity when subjected under uniaxial tensile (Japan Society of Civil Engineers, 2008). Figure 2.2. presents typical stress vs strain curves for FRCCs and HPFRCCs. Over the past few decades, researchers around the world began to extensively study HPFRCCs leading to the development of various classes of HPFRCCs. The focus of this research paper is on one class of HPFRCCs known as Engineered cementitious composites (ECC), which will be discussed in the following section.

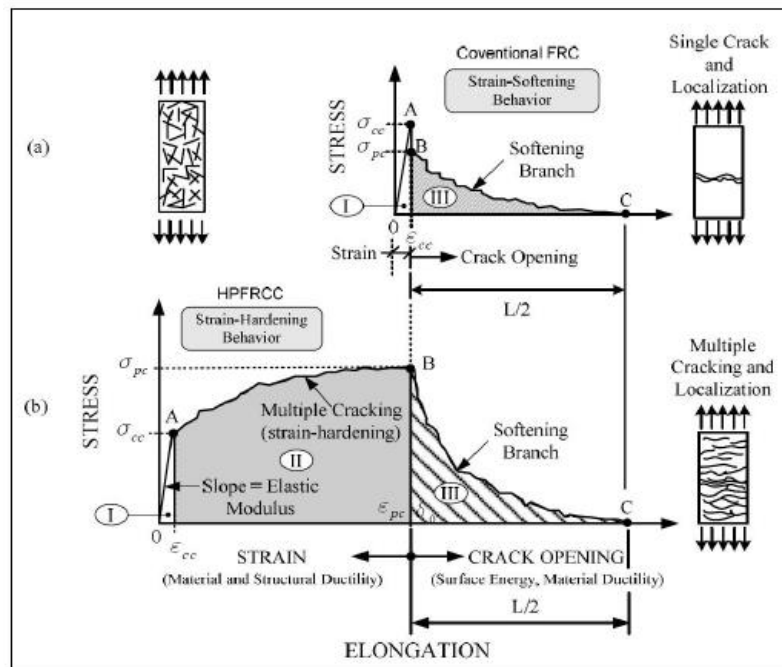


Figure 2.2. Typical stress-strain or stress-elongation curve in tension up to complete separation in (a) Conventional strain softening FRCC, and (b) Strain hardening FRCC or HPFRCC (Naaman, 2008)

## **2.2. Engineered Cementitious Composites (ECCs)**

To exhibit pseudo strain hardening (PSH) behavior with tensile strain capacity of about 1%, HPFRCCs utilize large amounts of randomly oriented and distributed short fibers (i.e., 4 to 20 vol.%) (Naaman, 2008, 2018). However, ECCs present tensile strain capacity greater than 2% while utilizing a small amount of fibers (i.e., less than 2 vol.%) (Alrefaei & Dai, 2018; Li, 2008; Li et al., 2004; Nematollahi, Sanjayan, & Ahmed Shaikh, 2015; Ohno & Li, 2018). This was achievable as ECCs are designed based on the micromechanics and fracture mechanics (i.e., synergetic interaction between the microstructural components) rather than the material microstructure (i.e., particle packing) for HPFRCCs. In other words, the fiber, matrix, and fiber/matrix interface are engineered to interact with one another when subjected to any load. Furthermore, the implementation of the fracture mechanics and micromechanics concepts transforms the Griffith crack propagation mode of regular concrete and FRC to a steady-state flat crack propagation mode (Li, 2019b). As such, this enables the formation of multiple steady-state microcracks, giving rise to the exceptional tensile ductility of these composites (Li, 2003).

### ***2.2.1. Materials in ECCs***

Similar to FRCCs, the ingredients used to manufacture ECCs are ordinary Portland cement (OPC), supplementary cementitious materials (SCMs), fine aggregate, water, and polymer microfibers (Arce et al., 2019; Li, 2003, 2019a; Li et al., 2002; Noorvand et al., 2019; Reda Taha et al., 2002). It is important to note that ECCs do not consist of coarse aggregates as their inclusion would increase the matrix fracture toughness, which in turn negatively affects the desirable PSH behavior of the composite. Typically, the water to cement (W/C) and sand to binder (S/B) ratios used in ECCs are below 0.5 (Li, 2019b). For the manufacture of ECCs, PVA fibers have been primarily used (Kan et al., 2019, 2020; Li et al., 2002, 2004; Ling et al., 2019;

H. Ma et al., 2015; Nematollahi, Sanjayan, & Ahmed Shaikh, 2015; Nematollahi, Sanjayan, & Shaikh, 2015; Pakravan et al., 2018; Redon et al., 2001a). However, ultra-high-molecular weight polyethylene (UHMWPE) fibers have also been used; yet, due to its high cost, these fibers have been limited to the development of high performance ECCs (Alrefaei & Dai, 2018; Choi et al., 2016; Ding et al., 2018; Li et al., 2002; Osman et al., 2019; Yu et al., 2018).

### ***2.2.2. Micromechanics and Fracture Mechanics Principles***

The design concept behind producing pseudo strain hardening behavior in fiber reinforced cementitious composites is based on tailoring the fiber, matrix, and fiber/matrix interface via micromechanics and fracture mechanics principles. Micromechanics is the study of the microscopic behavior linking the different components of the composite. On the other hand, fracture mechanics is the study of crack propagation in the composite. Knowledge in both areas is needed to successfully develop PSH behavior as crack initiation starts at a defect site (i.e., air voids, interfacial transition zone, etc.) then propagates in a steady state flat crack mode. In steady state flat crack propagation mode, at a constant load, the crack opening remains the same and the fibers bridging the crack sustain and transfer the load without rupturing or pulling out. As such, upon increasing the load, subsequent microcrack is initiated from another defect site. This phenomenon is repeated to form multiple cracking and PSH behavior until the Griffith crack propagation mode becomes dominant over the flat crack propagation mode in which the crack opening begins to infinitely increase and eventually exhausting the fiber bridging capacity due to fiber pullout or rupture. Since the fiber bridging capacity is reduced, no further crack can develop resulting in tensile strain softening behavior with a large opening of a single crack and eventually failure of the composite (Li, 2019b).

To attain PSH behavior, two conditions must be met: the energy criterion and the strength criterion as presented in Equation 2.1. and Equation 2.2., respectively (Li, 2019a; Ohno & Li, 2018; E. H. Yang et al., 2008). As demonstrated by Marshall and Cox (1988), the energy criterion guarantees that steady-state flat crack propagation will occur when the crack-tip matrix toughness ( $J_{tip}$ ) is lower than the complementary energy of the fiber bridging relation ( $J'_b$ ) (Marshall & Cox, 1988).

Equation 2.1.

$$J'_b = \sigma_0 \delta_0 - \int_0^{\delta_0} \sigma(\delta) d\delta \geq J_{tip} \approx \frac{K_m^2}{E_m}$$

where:

$J'_b$  = Complementary energy of the fiber-bridging relation;

$J_{tip}$  = Crack-tip matrix toughness;

$\delta_0$  = Crack opening corresponding to  $\sigma_0$ ;

$\sigma(\delta)$  = Fiber-bridging relationship;

$K_m$  = Fracture toughness of matrix; and

$E_m$  = Modulus of elasticity of matrix.

Based on Equation 2.1.,  $J_{tip}$  is dependent on the matrix composition as it is sensitive to  $K_m$  and  $E_m$ . On the other hand,  $J'_b$  is dependent on the fiber and fiber/matrix interface properties. Fiber properties include the fiber length ( $L_f$ ), diameter ( $d_f$ ), modulus of elasticity ( $E_f$ ), and tensile strength ( $\sigma_{fu}$ ) (Li, 2019a). Fiber/matrix micro-scale interfacial properties, which are referred as micromechanical parameters in the literature, include frictional bond ( $\tau_0$ ), chemical bond ( $G_d$ ), and slip-hardening coefficient ( $\beta$ ) (Li, 2019a). As such, both the fiber and fiber/matrix properties define the fiber-bridging relation ( $\sigma(\delta)$ ). In fact, Li and co-workers developed micromechanics-

based models to obtain the fiber-bridging relation of the composite from these properties (Li, 1993, 2019a; Li et al., 2002; E. H. Yang et al., 2008).

The energy criterion (Equation 2.1.) is determined by taking into account the energy changes that occur during steady-state flat crack propagation (Li, 2019b). The area under the  $\sigma(\delta)$  is the amount of energy consumed to propagate the crack. However,  $J'_b$  is the net energy available for crack propagation. It is determined by taking the difference between the external work energy and energy consumed by the fiber bridging action. On the other hand,  $J_{tip}$  is the energy required for the matrix to resist crack propagation. Figure 2.3. illustrates the energy balance. It is important to note that the energy criterion determines whether the crack will propagate via flat crack propagation mode or Griffith crack propagation mode (Li, 2019b).

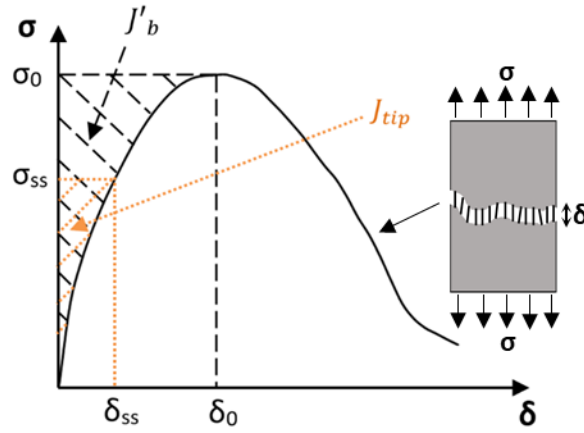


Figure 2.3. Fiber bridging relation,  $\sigma(\delta)$  curve (adapted from (Noorvand et al., 2019))

The strength criterion (Equation 2.2.) states that the fiber bridging capacity must exceed the first cracking strength in order to ensure that the composite will not fail via fiber rupture or pullout upon crack initiation from any defect site in the matrix (H. Ma et al., 2015; Ohno & Li, 2018; Redon et al., 2001a; E. H. Yang et al., 2008).

Equation 2.2.

$$\sigma_{fc} \leq \sigma_0$$

where:

$\sigma_0$  = Fiber-bridging capacity; and

$\sigma_{fc}$  = First-cracking strength.

Based on Equation 2.2.,  $\sigma_{fc}$  is defined by the matrix fracture toughness ( $K_m$ ) and the initial flaw size, while  $\sigma_0$  depends on the fiber and fiber/matrix interfacial properties (Nematollahi et al., 2016; Ohno & Li, 2018). It is important to note that for matrices exhibiting PSH behavior, the ultimate tensile strength ( $\sigma_u$ ) coincides with  $\sigma_0$ .

When both the energy and strength criterion are met, the composite will exhibit pseudo strain hardening. Otherwise, the composite will exhibit tensile strain softening similar to conventional fiber reinforced concrete as illustrated in Figure 2.4. (E. H. Yang et al., 2008). It is important to note that JSCE classifies fiber reinforced composites as strain hardening in tension when the ultimate tensile strain capacity is greater than 0.5% (Japan Society of Civil Engineers, 2008).

For simplicity, Equation 2.1. and Equation 2.2. are commonly written as  $J'_b/J_{tip} \geq 1$  and  $\sigma_0/\sigma_{fc} \geq 1$  where the  $J'_b/J_{tip}$  and  $\sigma_0/\sigma_{fc}$  ratios are referred to as PSH energy and the PSH strength performance indexes, respectively. In fact, to successfully design ECCs, both the PSH strength and PSH energy indices must be greater than one. However, it is important to note that Equation 2.1. and Equation 2.2. assume a perfectly homogeneous material. Therefore, to achieve robust PSH behavior of the composite, it is necessary for the PSH performance indexes to be greater than one. Based on prior experimentation conducted by Kandra and Li (2006), it has been determined that PSH energy and PSH strength indices greater than 2.7 and 1.3, respectively, will



correlate with robust PSH performance in PVA reinforced ECCs (Kanda & Li, 2006). Figure 2.4. presents the robust PSH behavior of an ECC.

In comparison with cementitious based matrixes of cementitious materials, geopolymer (GP) based matrixes have a lower fracture toughness ( $K_m$ ) and a lower tensile strength ( $\sigma_{fc}$ ), but comparable compressive strengths (Ohno & Li, 2018). As such, in the design of pseudo strain hardening cementitious composites, GPs are more favorable for meeting both the strength and energy criteria (Ohno & Li, 2014). To this end, researchers began to develop engineered geopolymer composites (EGCs) as they can produce robust PSH behavior (i.e., high tensile ductility) at relatively low fiber contents (i.e., 1.5% volume fraction utilizing PVA fibers or even lower using UHMWPE fibers) considerably enhancing the greenness and cost-effectiveness of these novel composites (Ohno & Li, 2018).

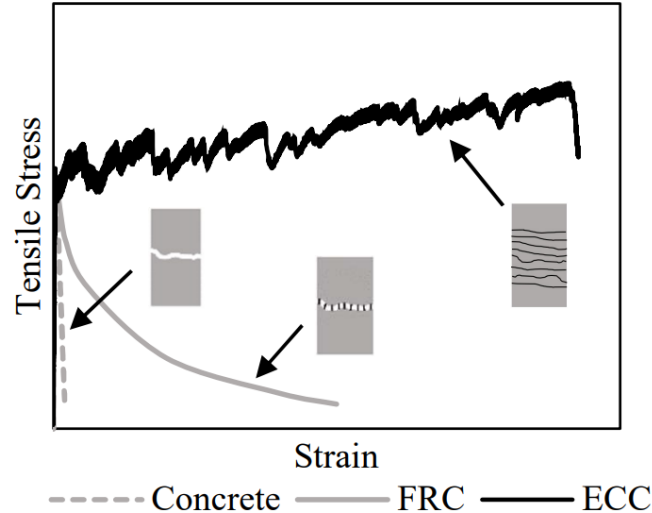


Figure 2.4. Stress vs. strain behavior of cementitious materials in tension (adapted from (Noorvand et al., 2019))

### 2.3. Geopolymers

The term polymer was coined from two Greek words: poly (meaning many) and meros (meaning part). In scientific terms, polymers are comprised of macromolecules, which are made up many

repeating subunits called monomers. The reaction of these monomers is called polymerization (Weissberger, 2020). Depending on their molecular structure, polymers may be either organic (i.e., carbon-based) or inorganic (i.e., silicon-based).

In the 1970s, the term geopolymers (GP) was coined by Joseph Davidovits to classify the inorganic polymers synthesized from rock-forming minerals of geological origin. Geopolymers are defined fully as amorphous inorganic aluminosilicate polymers manufactured at room temperature from industrial byproducts (e.g., fly ash, slag, rice husk ash, etc.) and natural sources (e.g., calcined clays, volcanic rocks, mine tailings, etc.) which serve as a rich source of soluble silicon (Si) and aluminum (Al) species (Davidovits et al., 2015; Provis & Deventer, 2009; Ryu et al., 2013). The formation of GP rigid gels is triggered by the geopolymerization of Al and Si species, which takes place when the GP precursor is activated by the alkaline solution or alkaline silicate solution.

Although geopolymers are newly innovative materials, they can be used for several applications such as coating, adhesives, waste encapsulation, binders for concrete, and most recently fiber-reinforced composites (Davidovits et al., 2015). In fact, for concrete applications, GPs have shown to prevent extensive corrosion of steel reinforcement in comparison to ordinary Portland cement (OPC) (A. M. Aguirre-Guerrero, R. A. Robayo-Salazar, 2017; C. Tennakoon, A. Shayan, J. G. Sanjayan, 2017; Huang, O. D., Kim, C., Lies, N. J., Castaneda, H., & Radovic, 2021; M. Sufian Badar, K. Kupwade-Patil, S. A. Bernal, J. L. Provis, 2014), are more resistant to acid attacks (Bakharev, 2005; Sata et al., 2012) and fire (Vickers et al., 2015), and can reach maximum strength faster than OPC. Furthermore, GPs are more energy efficient as they can reduce the CO<sub>2</sub> emission by 44-64% when compared to OPC (Komnitsas, 2011; McLellan et al., 2011; Turner & Collins, 2013).

## 2.4. Geopolymerization

Geopolymerization is a complex process involving the transformation of one or more aluminosilicate raw materials into 3-dimensional amorphous polymer structures consisting of covalently bonded Si, Al, and O. This process consists of multiple chemical reactions occurring at different rates to produce a strong, durable geopolymeric material. The geopolymer formation follows a bimolecular nucleophilic substitution ( $SN_2$ ) mechanism in which the amorphous aluminosilicate reacts with the alkaline activator solution (Michalske & Freiman, 1982). The geopolymerization chemical reactions occur as follows: association, dissolution, polymerization, and polycondensation. Figure 2.5. presents the complete geopolymerization process.

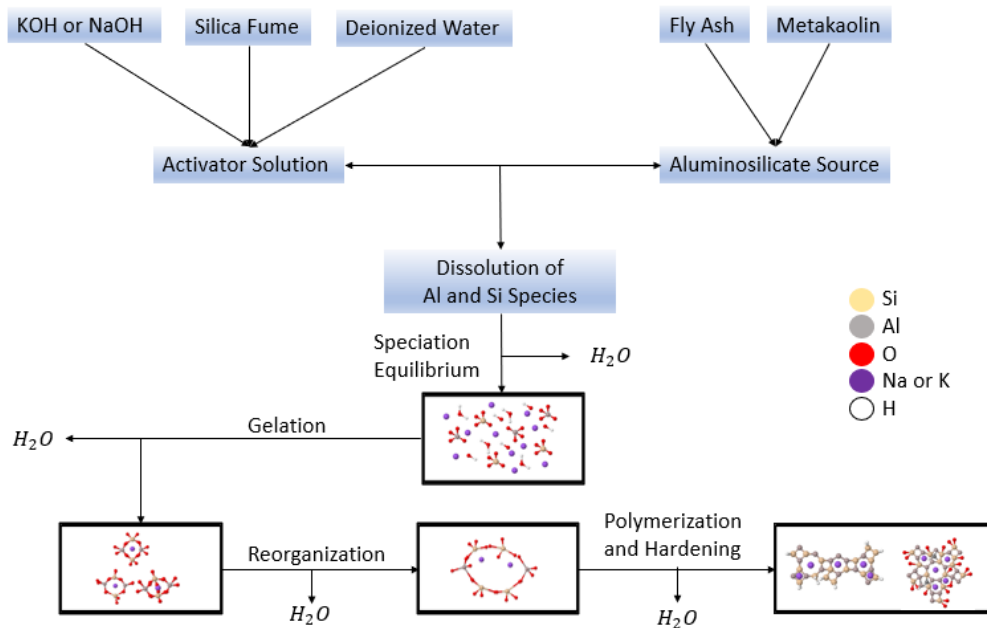


Figure 2.5. Geopolymerization process (Arce et al., 2020)

### 2.4.1. Association and Dissociation

Association occurs when the water molecules interact with the -Si-O-Si- and -Al-O-Al- bonds present in the amorphous aluminosilicate. As a result, highly reactive intermediate pentavalent

silicon and aluminum species form. The intermediate pentavalent silicon and aluminum exhibit a distorted trigonal bipyramid structure, and their extremely reactive nature makes them dissociate rapidly into silanols (-Si-O-H) and aluminols (-Al-O-H) (Davidovits et al., 2015; Provis & Deventer, 2009; Ryu et al., 2013). Figure 2.6. illustrates the association and dissolution of an -Si-O-Si- bond.

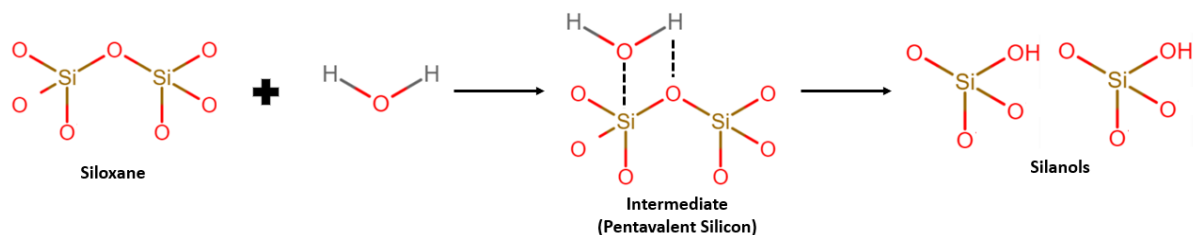


Figure 2.6. Association and Dissolution

#### 2.4.2. Polymerization and Polycondensation

Thy aluminols and silanols further react until they form hydrolyzed  $[\text{AlO}_4]^{5-}$  (aluminate) and  $[\text{SiO}_4]^{4-}$  (silicate) species. The hydrolyzed aluminate and silicate species react forming hardened polymer chains through the polycondensation process releasing water as it cures (Davidovits et al., 2015; Provis & Deventer, 2009; Ryu et al., 2013). During a geopolymerization reaction, three types of 3-dimensional amorphous polymer structures consisting of Si, O, and Al form (Figure 2.7.): poly-sialate (Si-O-Al-O-), poly-sialate-siloxo (Si-O-Al-O-Si-O), and poly-sialate-disiloxo (Si-O-Al-O-Si-O-Si-O) (Davidovits et al., 2015; Provis & Deventer, 2009; Ryu et al., 2013). Sialate refers to the Si-O-Al link, while siloxo refers to the Si-O-Si link. Equation 2.3. presents the chemical formula of the final GP composition.

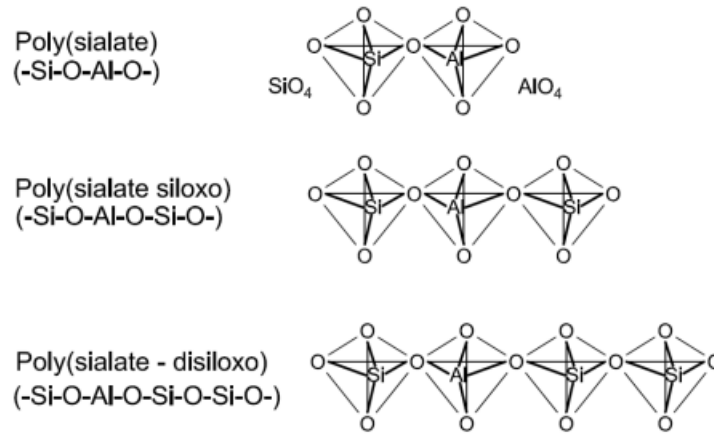


Figure 2.7. Three Types of 3-Dimensional Amorphous Polymer Structures (Davidovits et al., 2015)

Equation 2.3.

$$M_n[-(\text{SiO}_2)_z - \text{AlO}_2]_n \cdot w\text{H}_2\text{O}$$

where:

M = alkali metal cation (usually  $\text{Na}^+$  or  $\text{K}^+$ )

n = degree of polymerization

z =  $\text{SiO}_2/\text{Al}_2\text{O}_3$  ratio

w = the molar water quantity

Typically, geopolymers are prepared with  $\text{SiO}_2/\text{Al}_2\text{O}_3$  ratio of 1.8-2.2, a water to GP solids (i.e.,  $\text{H}_2\text{O}/(\text{Al}_2\text{O}_3 + \text{SiO}_2)$ ) ratio of 2.0-5.0, and a cation to aluminum (i.e., M/Al) ratio of 0.9-1.2 (Davidovits et al., 2015; Provis & Deventer, 2009; Ryu et al., 2013).

## 2.5. Raw Materials

### 2.5.1. GP Precursor

#### 2.5.1.1. Metakaolin

Feldspar is a mineral that makes up roughly 60% of Earth's crust. In the chemical breakdown of potassium feldspar, kaolinite is the most abundant clay mineral with a chemical composition of  $\text{Al}_2\text{O}_3 \cdot 2\text{SiO}_2 \cdot 2\text{H}_2\text{O}$ , which means each particle has a tetrahedral silica layer and octahedral alumina layer (Tarbuck et al., 2017). As such, these particles are held together via hydrogen bonds and Van der Waals forces; thus, preventing the water from entering the interlayer spaces at room temperature. Under surface conditions, kaolinite is very stable and is typically used as a coating high-gloss paper, such as that used in textbooks (Morsy FA, El-Sherbiny S, Hassan MS, 2014).

When kaolinite is thermally treated (i.e., calcinated within a definite temperature range, 600-800°C), metakaolin is formed as shown in Equation 2.4. through a process called dehydroxylation (Ilić et al., 2010). Dehydroxylation is an endothermic reaction that requires lots of energy to remove the chemically bonded hydroxyl ions, thus breaking down the kaolinite crystal structure into amorphous silica and alumina with high surface area. Metakaolin is a highly reactive pozzolan that is classified as an SCM (Ilić et al., 2010). Furthermore, it is a highly pure white mineral that can be used to replace part of the clinker in cement or replace cement in concrete mixtures (BASF, 2007). In fact, metakaolin is manufactured specifically for cementing applications to maintain high whiteness, high reactivity, ultrafine particle size distribution and consistency. It meets ASTM C-618 Class N pozzolans as well as strength activity index per ASTM C-1240 (BASF, 2007).

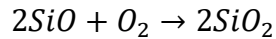
Equation 2.4.



#### 2.5.1.2. Silica Fume

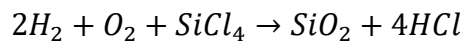
During the industrial manufacturing of elemental silicon or alloys (i.e., ferrosilicon steel) in electric arc furnaces, silica fume is formed as a byproduct (Davidovits et al., 2015; Panesar, 2019). When heated to over 2000 °C, high purity quartz reduces forming SiO gas, which mixes with oxygen, thus forming SiO<sub>2</sub>. At low temperature, the airborne SiO<sub>2</sub> condenses resulting in silica fume as shown in Equation 2.5. (Davidovits et al., 2015; Panesar, 2019).

Equation 2.5.



Silica fume is composed ultrafine amorphous SiO<sub>2</sub> sphere ranging from 50 to 100 nanometers in diameter with a specific surface area of 15000 to 30000 m<sup>2</sup>/kg (Davidovits et al., 2015). High purity silica fume can also be produced from the vapor phase hydrolysis of silicon tetrachloride (SiCl<sub>4</sub>) in a flame of hydrogen and oxygen as shown in Equation 2.6. (Davidovits et al., 2015). Silica fume is usually added to MK or FA to modify Si/Al ratio in GPs. The chemical reactions for both processes are as follows:

Equation 2.6.



#### 2.5.1.3. Fly Ash

Fly ash also known as coal ash is a byproduct of the combustion reaction of coal. During the combustion of coal, the mineral impurities in coal (i.e., quartz, feldspar, clay, etc.) fuse together and float out of the combustion chamber with the exhaust gases. As these materials rise, they cool down and solidify into spherical particles  $0.5\text{ }\mu\text{m}$  to  $100\text{ }\mu\text{m}$  in size, which are captured by electrostatic precipitators (ESP) or baghouses and subsequently by scrubber systems. They are then placed in stockpiles as shown in Figure 2.8.



Figure 2.8. Fly Ash Stockpiles

Fly ash is a very fine and light tan powder consisting mainly of silicon dioxide ( $\text{SiO}_2$ ) (amorphous and crystalline), aluminum oxide ( $\text{Al}_2\text{O}_3$ ), iron (III) oxide ( $\text{Fe}_2\text{O}_3$ ), and calcium oxide ( $\text{CaO}$ ). ASTM C618 identifies three different types of fly ash:

- Class N—Raw or calcined natural pozzolans that comply with the applicable requirements for the class as given herein, such as some diatomaceous earths; opaline cherts and shales; tuffs and volcanic ashes or pumicites, calcined or uncalcined; and various materials requiring calcination to induce satisfactory properties, such as some clays and shales.



- Class F—Fly ash that meets the applicable requirements for this class as given herein.  
This class of fly ash has pozzolanic properties.
- Class C—Fly ash that meets the applicable requirements for this class as given herein.  
This class of fly ash, in addition to having pozzolanic properties, also has some cementitious properties.

Table 2.1. presents the chemical requirements for Class N, Class C, and Class F fly ash per ASTM C618 based on the presence of CaO, SiO<sub>2</sub>, Fe<sub>2</sub>O<sub>3</sub>, and Al<sub>2</sub>O<sub>3</sub> as presented in. The main difference between Class N, Class C, and Class F fly ash is the total SiO<sub>2</sub>, Fe<sub>2</sub>O<sub>3</sub>, and Al<sub>2</sub>O<sub>3</sub> minimum oxide wt.%. Class C and Class F must present a minimum of 50% whereas Class N must present a minimum of 70% total SiO<sub>2</sub>, Fe<sub>2</sub>O<sub>3</sub>, and Al<sub>2</sub>O<sub>3</sub> (ASTM C618, 2019). On the other hand, the main difference between Class C and Class F fly ash is the CaO composition. Class F fly ash contains less than 18% CaO, while Class C fly ash contains of greater than 18% CaO (ASTM C618, 2019). It is important to mention that when Class C fly ash is used, the CaO interferes with the geopolymerization reaction forming calcium silicate hydrate as well as linear polymer chains and flash set properties (Davidovits et al., 2015).

Table 2.1. Fly Ash Chemical Requirements (ASTM C618, 2019)

	Class		
	N	F	C
Silicon dioxide (SiO <sub>2</sub> ) plus aluminum oxide (Al <sub>2</sub> O <sub>3</sub> ) plus iron oxide (Fe <sub>2</sub> O <sub>3</sub> ), min, %	70	50	50
Calcium oxide (CaO), %	report only	18 max	>18.0
Sulfur trioxide (SO <sub>3</sub> ), max, %	4	5	5
Moisture content, max, %	3	3	3
Loss on ignition, max, %	10	6	6

#### 2.5.1.4. Ground Granulated Blast Furnace Slag (GGBFS)

Blast furnace slag (BFS) is a byproduct of the steel industry that is typically obtained from the production of iron through a blast furnace. A combination of iron ore, coke, and limestone are blended to form an optimum mix. The mix is then quenched into a blast furnace where the oxygen reacts with the mixture to form molten iron at the bottom of the furnace followed by a layer of slag. The molten blast furnace slag is tapped off and quenched into water or steam to produce granular blast furnace slag. The granular BFS is then dried and ground into a fine powder forming ground granulated blast furnace slag (GGBFS) with a particle size  $<45\mu\text{m}$  and surface area between  $400\text{-}600\text{ m}^2/\text{kg}$  (ASTM C989, 2019). GGBFS consists of silicate, aluminate, and lime (Table 2.2.), yet the chemical composition depends on the raw materials used in the production process. ASTM C989 specifies the slag activity index (i.e., Grade 80, 100, and 120) where Grade 120 is most reactive (ASTM C989, 2019).

Table 2.2. GGBFS Typical Chemical Composition

Chemical Composition	wt. %
Silicon dioxide ( $\text{SiO}_2$ )	31-38
Aluminum oxide ( $\text{Al}_2\text{O}_3$ )	9-13
Calcium oxide ( $\text{CaO}$ ),	38-44
Magnesium oxide ( $\text{MgO}$ ), %	7-12

#### 2.5.2. *Fibers*

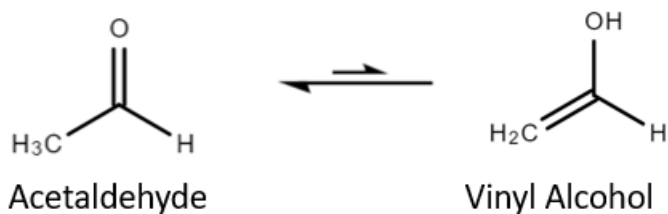
The fibers studied to produce engineered geopolymer composites with ductile PSH capabilities include 1.2 wt.% oil coated and uncoated PVA (Constâncio Trindade et al., 2020; Kan et al., 2019, 2020; Nematollahi, Sanjayan, & Ahmed Shaikh, 2015; Ohno & Li, 2018; Salami et al., 2016; Trindade et al., 2020; Zahid & Shafiq, 2020), ultra-high molecular weight polyethylene

(UHMWPE) (Alrefaei & Dai, 2018; Trindade et al., 2020), and copper coated steel fibers (Alrefaei & Dai, 2018).

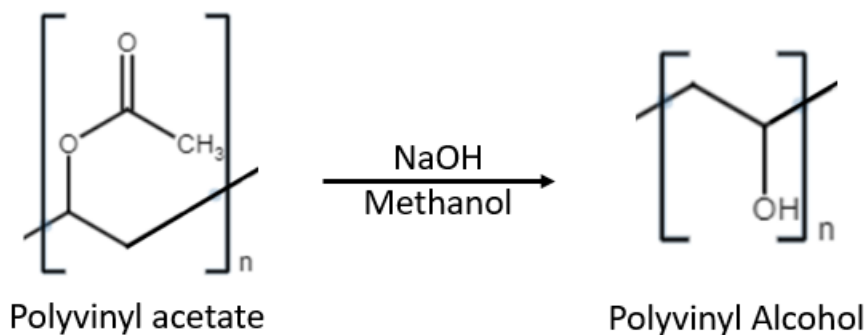
#### 2.5.2.1. Polyvinyl Alcohol (PVA)

Vinyl alcohol is an unstable monomer which undergoes tautomerization. Tautomerization is the process in which the protons transfer from one site to another. Acetaldehyde is vinyl alcohol's tautomer. As illustrated in Equation 2.7., acetaldehyde is the more stable tautomer. Therefore, producing polyvinyl alcohol from vinyl alcohol is not optimum. Instead, polyvinyl alcohol is produced by hydrolyzing polyvinyl acetate with sodium hydroxide and methanol as shown in Equation 2.8. Next, a nozzle is used to spin the polyvinyl alcohol fibers into a coagulating bath followed by wet or dry spinning to coagulate the PVA fiber (Inada et al., 2004).

Equation 2.7.



Equation 2.8.



The PVA fibers have a high modulus of elasticity and low elongation and creep, yet they can resist chemicals such as alkalis and acids which makes them an exceptional candidate for fiber reinforced concrete and composites. Furthermore, PVA fibers are hydrophilic meaning they have a high tenacity. As such, they tend to form a strong bond with the cementitious matrix. To this end, PVA fibers are one of the most common fibers used in fiber reinforced composites ranging from 1 to 2% volume fraction. In this study, the properties of the RECS15 PVA fibers from Nycon are presented in Table 2.3.

Table 2.3. Properties of PVA Fibers (NYCON, 2022)

Configuration	Monofilament
Tensile Strength	240 ksi (1600 MPa)
Flexural Strength	5700 ksi (40 GPa)
Filament Diameter	8 Denier (38 microns)
Available Lengths	0.375”(8mm)
Aspect-Ratio	210.52
Melting Point	435° F (225° C)
Water Absorption	<1% by Weight
Color	White
Elongation	6%

#### 2.5.2.2. Ultra-high Molecular Weight Polyethylene (UHMWPE)

Ultra-high molecular weight polyethylene fibers are highly oriented crystalline straight chain polyethylene structures that are manufactured through the catalysis of ethylene as shown in

Equation 2.9. (Chem Europe, n.d.). Compared to conventional polyethylene fibers with 700 to 1800 monomers, UHMWPE fibers consist of 100,000 to 250,000 monomers (Chem Europe, n.d.). Table 2.4. presents the typical properties of UHMWPE fibers.

Equation 2.9.

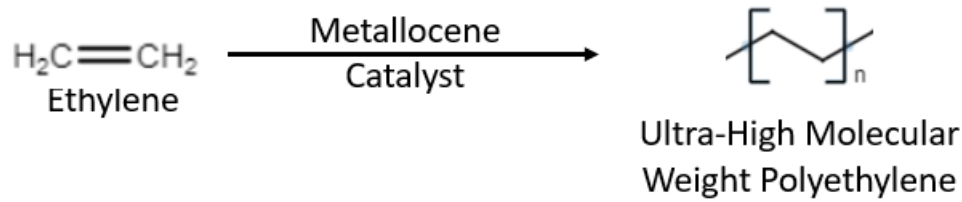


Table 2.4. Properties of UHMWPE Fibers

Diameter (μm)	24
Length (mm)	12-18
Aspect Ratio (L/D)	500-750
Elongation (%)	1-3
Specific Gravity	0.97-0.98
Modulus of Elasticity (GPa)	116
Tensile Strength (GPa)	3
Melting Point	144-152° C
Cross-section	Near round

#### 2.5.2.3. Steel (ST)

Steel fibers are short discontinuous steel strips manufactured with a brass coating to boost the fiber/matrix interface (*Advanced Steel Fibers for Ultra High Performance Concrete*, 2020). The properties of the steel fibers are shown in Table 2.5.

Table 2.5. Properties of ST Fibers (*Advanced Steel Fibers for Ultra High Performance Concrete*, 2020)

Diameter (μm)	20
Length (mm)	10-22
Aspect Ratio (L/D)	50-110
Specific Gravity	7.85
Tensile Strength (MPa)	2928
Elongation (%)	2-4
Copper Content (%)	66.8
Brass Weight (%)	4.83
Torsions (Turns/100d)	67
Melting Point	2760° F (1516° C)
Water Absorption	Nil

### ***2.5.3. Alkaline Activators***

Several different alkali activator solutions were used in manufacturing geopolymers. The alkali activators studied extensively by researchers include solutions of commercially-available aqueous sodium silicate ( $\text{Na}_2\text{SiO}_3$ ) and sodium hydroxide ( $\text{NaOH}$ ) pellets (Kan et al., 2019, 2020; Ohno & Li, 2018), aqueous 8 M  $\text{NaOH}$  and  $\text{Na}_2\text{SiO}_3$  (Nematollahi, Sanjayan, & Shaikh, 2015; Salami et al., 2016; Zahid & Shafiq, 2020), anhydrous sodium metasilicate powder (Alrefaei & Dai, 2018), aqueous 8 M  $\text{KOH}$  and potassium silicate ( $\text{K}_2\text{SiO}_3$ ) (Nematollahi, Sanjayan, & Shaikh, 2015), and waterglass solutions of potassium or sodium hydroxide pellets and silica fume dissolved in DI water (Constâncio Trindade et al., 2020; Trindade et al., 2020).

## **2.6. Geopolymer Composition and Microstructural Analysis**

X-ray Fluorescence (XRF), Scanning Electron Microscopy (SEM), and Energy Dispersive X-ray Spectroscopy (EDXS) are the three tools utilized to investigate the oxide composition, microstructure, and chemical elements of the raw materials and geopolymers in this work, respectively.

### ***2.6.1. X-Ray Fluorescence (XRF) Spectroscopy***

The X-Ray Fluorescence (XRF) analysis was conducted by Peter Norvath at Louisiana State University's Shared Instrument Facility (SIF) Laboratory. A PANalytical Epsilon 3XLE EDS XRF Spectroscopy system was used to determine the oxide composition of the metakaolin used in this study. The methodology is as follows: (1)  $0.6 \pm 0.006$  g of metakaolin were fused with a mix of 49.5% lithium metaborate, 49.5% lithium tetraborate, 0.5% lithium iodide (total mass of 6 g) at  $1065^\circ\text{C}$  using a Claiss LeNeo Fusion Fluxer to make glass disks. The resulting glass disks were placed in a 10-position carousel of the PANalytical Epsilon3XLE energy-dispersive XRF

spectrometer and analyzed using the Omnian programme of the Epsilon 3 software. Loss on ignition (LOI) values were calculated using the weight difference of the dry samples (before fusion) and the glass disks.

### ***2.6.2. Scanning Electron Microscope (SEM) and Energy Dispersive Spectroscopy (EDS)***

Scanning Electron Microscope (SEM) is a type of electron microscope that uses a high energy electron beam to scan a solid specimen in a raster scanning pattern (Swapp, 2017). As the incident electron beam comes in contact with the specimen, it penetrates the sample to a depth of a few micrometers (i.e., known as the interaction volume) based on the accelerating voltage, current, and density of the specimen. Several signals are generated from the specimen containing information about the surface morphology and composition (Swapp, 2017). These signals are secondary electron (SE), backscattered electrons (BSE), diffracted backscattered electrons (EBSD), characteristic X-Rays, visible light, and heat. SE and BSE are commonly used to show the surface morphology and contrast of the samples, respectively (Swapp, 2017). The characteristic X-Rays are produced when the electrons from the electron beam collide with the electrons in the orbitals of the atoms, exciting the electron to where it jumps to the next orbital (Swapp, 2017). When the electron returns to the lower energy state orbital, an X-Ray with a fixed wavelength (which is different for each element) is released and collected using an energy dispersive X-Ray spectroscopy (EDS) detector (Swapp, 2017).

In this study, the raw materials were sputter coated with platinum prior to imaging. However, the GP binder and mortars were vacuum impregnated with epoxy, polished using silicon carbide grit papers, then sputter coated with platinum. After polishing, the specimens were sputter coated with platinum. The images of the raw materials were taken using an SE detector whereas the GP binder and mortar images were taken using a BSE detector. Furthermore, the elemental

composition of the GP gel is determined via EDS analysis. For all materials studied, a 20kV accelerating voltage and 4nA current were used for imaging.

## **2.7. Properties Affecting Geopolymers**

There are several properties that affect the physical and mechanical properties of geopolymers. They include, but are not limited to,  $\text{SiO}_2/\text{Al}_2\text{O}_3$  ratio, water to GP solids ratio, cation to Aluminum ratio, curing regime, and plasticizers and retarders.

### **2.7.1. $\text{SiO}_2/\text{Al}_2\text{O}_3$ Ratio**

The  $\text{SiO}_2/\text{Al}_2\text{O}_3$  ratio is the fundamental factor influencing the properties of geopolymers. In fact, several studies suggested that an increase in  $\text{SiO}_2/\text{Al}_2\text{O}_3$  results in an increase in compressive strength, hardness, and fracture toughness, due to the GPs increased density and Si-O-Si bonds as it has been established that an Si-O-Si bond is stronger than Si-O-Al bond (Davidovits et al., 2015; Duxson et al., 2007; P. He et al., 2016). Typically, the  $\text{SiO}_2/\text{Al}_2\text{O}_3$  ratio by mol is preferred to be between 1.8 and 3. In this study, the  $\text{SiO}_2/\text{Al}_2\text{O}_3$  ratio is equal to 3.

### **2.7.2. $\text{Water}/\text{GP}_{\text{solids}}$ Ratio**

In the geopolymerization reaction, the water is used to hydrate the precursor, thus acting as a lubricating element (Davidovits et al., 2015). Furthermore, it is used for the association, dissolution, and transportation process indicating that water is a part of the first two steps in geopolymerization. However, the excess water tends to evaporate from the material in each step of the geopolymerization process as shown in Figure 2.5. As such, the addition of water is considered to increase workability and assumed to not be a part of the resulting hardened geopolymer structure.

Just like cement binders, there is an inverse relationship between  $\text{water}/\text{GP}_{\text{solids}}$  (i.e.,  $\text{H}_2\text{O}/(\text{Al}_2\text{O}_3+\text{SiO}_2)$ ) and mechanical properties as the excess water tends to evaporate from the



material, leaving a lower density solid with an increased open porosity (Lizcano, Gonzalez, et al., 2012; Nematollahi et al., 2016). As such, there must be a proper range of water/GP<sub>solids</sub> ratio to produce an optimum compressive strength while having a workable material. Therefore, in this research, water/GP<sub>solids</sub> ratios by mol of 2 and 3 are studied.

### ***2.7.3. Cation/Al Ratio***

It is theorized that the alkali cation acts as a chain terminator during the polycondensation (Lizcano, Kim, et al., 2012; Provis & Deventer, 2009). Therefore, an increase in the M/Al ratio can prevent the geopolymer chains from fully developing (Lizcano, Kim, et al., 2012; Provis & Deventer, 2009). As such, it is essential to provide an appropriate amount of alkali cation needed to balance the negatively charged IV-fold coordination of Al<sup>3+</sup> in an Si<sup>4+</sup> network and contribute to the catalysis of the condensation process (Duxson et al., 2007).

### ***2.7.4. Curing Regime***

Curing regime is a vital component in enhancing the geopolymerization reaction, and in turn, the strength of the geopolymer materials. There are two main types of curing regimes adapted by the geopolymer community: heat and ambient curing. Heat curing was introduced in the geopolymer community to accelerate the early age strength of the geopolymer materials. Heat curing is performed by placing the sample in a furnace at a designated temperature for a designated period of time. The elevated temperature and time period studied range from 30 to 90 degrees Celsius and 1 to 24 hours, respectively (Abdullah et al., 2012; Al-Shether et al., 2016; Ekaputri et al., 2017; Hake et al., 2015; Hardjito et al., 2004; Nurrudin et al., 2018; Ohno & Li, 2014; Perera et al., 2007; B. Rangan & Hardjito, 2005; Rovnaník, 2010; Vijai et al., 2010). Ambient curing was investigated for on-site construction. Ambient curing was performed keeping the specimens in their molds (or formwork for on-site construction) between 1 to 7 days, then exposing the

specimens to the air (i.e.,  $21 \pm 1$  °C) (Heah et al., 2011; Nuruddin et al., 2011; Patil et al., 2014; Perera et al., 2007; Rovnaník, 2010; Vijai et al., 2010; Yewale et al., 2016).

Perera (2007) investigated the effect of heat and ambient curing regime on the compressive strength, shrinkage, and open porosity of metakaolin based geopolymer activated with sodium silicate solution (Perera et al., 2007). It was concluded that mild heating (i.e., 40 to 60 °C) at low relative humidity produced similar compressive strength to ambient curing. Furthermore, the removal of the water in the geopolymer through evaporation played an important role in cracking and shrinkage as the capillary pressure which drives cracking depends on the microstructure and porosity of the geopolymer.

Rovnaník (2010) studied the influence of curing temperature ranging from 10 to 80 °C on the 1, 3, 7, and 28-day compressive and flexural strengths of metakaolin based geopolymer activated with sodium hydroxide and sodium silicate solutions (Rovnaník, 2010). It was concluded that a curing period of at least 20 hours is needed to achieve early strength, yet exposure to elevated temperatures immediately after casting can lead to large pores in the specimen (Rovnaník, 2010).

Hardjito et al. (2004) evaluated the effect of heat curing on the compressive strength of fly ash based geopolymer concrete at temperatures ranging from 30 to 90 degrees Celsius. It was concluded that the compressive strength is directly proportional to heat curing temperature (Hardjito et al., 2004; B. Rangan & Hardjito, 2005). Furthermore, increasing heat curing time enhanced the geopolymerization reaction thus increasing compressive strength (Hardjito et al., 2004; B. Rangan & Hardjito, 2005). However, exceeding 24 hours of heat curing did not have a significant effect on compressive strength.

Vijai et al. (2010) evaluated the effect of ambient and 24 hour 60 °C heat curing on the compressive strength of fly ash based geopolymer concrete activated with both sodium hydroxide, potassium hydroxide, and sodium silicate solutions (Vijai et al., 2010). It is important to note that the specimens were demolded after five days of casting to imitate construction sites formwork. It was concluded that heat curing substantially outperformed ambient curing. However, the compressive strength for heat curing does not increase substantially from 7 to 28 days.

Heah et al. (2011) investigated the effect of ambient and heat curing ranging from 40 to 100 °C for 1, 3, 7, and 28 days on the compressive strength and microstructure of metakaolin based geopolymer binder activated by sodium hydroxide and sodium silicate solutions (Heah et al., 2011). It was concluded that ambient curing delayed the setting time. Furthermore, as temperature increased, the geopolymerization reaction was enhanced, thus increasing the compressive strength. However, prolonged curing time at higher temperature tends to distort the geopolymerization reaction due to the formation of microcavities (Heah et al., 2011). The optimum heat curing temperature and time was determined to be 60 °C for 3 days where the samples presented a more compact and denser geopolymeric gel (Heah et al., 2011).

Nuruddin et al. (2011) investigated the effect of hot gunny, ambient, and external exposure curing on the 3, 7, 28, and 56 days compressive strength of fly ash and rice husk ash based geopolymer concrete activated with sodium hydroxide and sodium silicate solutions (Nuruddin et al., 2011). It was concluded that curing at elevated temperature presented higher compressive strength than ambient curing solutions (Nuruddin et al., 2011). Furthermore, the replacement of fly ash with rice husk did not significantly improve the compressive strength solutions (Nuruddin et al., 2011).

Patil et al. (2014) evaluated the effect of ambient and heat curing on the 7 and 28-day compressive strength of fly ash based geopolymer concrete activated with sodium hydroxide and sodium silicate solutions (Patil et al., 2014). It was concluded that the 7-day compressive strength of heat curing was six times that of ambient curing, whereas at 28-days the compressive strength doubled.

Kumaravel et al. (2014) investigated the effect of steam, hot air, and ambient curing on class F fly ash and blast furnace slag based geopolymer concrete activated with sodium hydroxide and sodium silicate solutions (Kumaravel, 2014). It was concluded that the compressive strength of heat cured concrete is greater than that of ambient cured concrete (Kumaravel, 2014). However, ambient cured geopolymer concrete possess similar compressive strength to OPC concrete (Kumaravel, 2014). Therefore, ambient cured geopolymer concrete can be used for on-site construction.

Yewale et al. (2016) investigated the effect of ambient, steam, water, and heat curing on class F fly ash based geopolymer concrete activated with sodium hydroxide and sodium silicate solutions (Yewale et al., 2016). 24-hour heat curing occurred for temperatures ranging from 40 to 140 °C at 20 °C intervals, whereas 18-hour steam curing occurred for temperature ranging from 60 to 110°C after demolding. All specimens were tested at 7 and 28 days. Experimental results revealed that 60 °C heat curing for 24 hours was the optimum curing method (Yewale et al., 2016). Furthermore, compared to water curing, ambient curing performed significantly better.

Out of the many geopolymer materials studied, heat curing proved to be a vital component in fly ash based geopolymer materials. This is due to the fact that the activation of fly ash is an endothermic reaction, therefore heat curing is an important element in the geopolymerization

reaction of fly ash based geopolymer materials (W. JIANG et al., 1993). Compared to fly ash based geopolymer materials, ambient cured metakaolin based geopolymer materials produce comparable compressive strengths to OPC concrete. As such, this study focuses on curing the metakaolin based geopolymer materials under ambient conditions.

## **2.8. Admixtures**

Superplasticizers are substances (typically liquid) that are added to a mix to increase the separation of particles, thus preventing the substance from clumping, therefore enhancing the workability. In OPC concrete, there are several types of superplasticizers: lignosulphonates, naphthalene, melamine-based, and modified Polycarboxylate. Polycarboxylate based superplasticizers are the latest superplasticizer to be used in OPC which utilize electrostatic interparticle repulsion and steric repulsion of the ether chains on the superplasticizer molecule. It is important to mention that the aforementioned superplasticizers are not designed to work on geopolymers. However, they have been studied by researchers in an attempt to improve the rheology of the geopolymer materials. Some superplasticizers have been deemed ineffective as they have been found to degrade once mixed with the alkaline activator solution as shown in Figure 2.9. However, some superplasticizers which resist the alkaline environment have been found to marginally improve the rheology of the geopolymer materials. The effect of the different superplasticizer on the workability, compressive strength, and rheological parameters of metakaolin, fly ash, and slag based geopolymer materials are discussed in the following subsections.



Figure 2.9. MasterGlenium 7500 Superplasticizer Degrading in Alkali Silicate Activator Solution

### ***2.8.1. Ground Granulated Blast Furnace Slag***

Douglas and Brandstetr (1990) investigated the effect of sodium lignosulphonate (i.e., 0.2, 0.5 and 1 wt.% of binder) and sulfonated naphthalene (i.e., 0.5, 1, 5 and 9 wt.% of binder) based superplasticizers on the workability and early age compressive strength of ground granulated blast furnace slag based geopolymer mortars activated with sodium silicate solution (Douglas & Brandstetr, 1990). It was concluded that the addition of sodium lignosulphonate and sulfonated naphthalene did not improve the workability of the slag based geopolymer mortar (Douglas & Brandstetr, 1990). Furthermore, both superplasticizers reduced the 1 day compressive strength compared to the specimens without superplasticizers (Douglas & Brandstetr, 1990).

Bakharev et al. (2000) investigated the effect of naphthalene and lignosulphonate based superplasticizers on the workability and shrinkage of ground granulated blast furnace slag based geopolymer concrete activated by three different activator solutions (i.e., combinations of sodium silicate glass, sodium hydroxide solution, and/or sodium carbonate) (Bakharev et al., 2000). It was concluded that the addition of lignosulfonate based superplasticizer increased the

workability for all three activator mixtures, yet naphthalene based superplasticizer increased the initial workability followed by a flash set (Bakharev et al., 2000). Furthermore, lignosulfonate based superplasticizer reduced the shrinkage whereas naphthalene based superplasticizer increased the shrinkage of the geopolymer concrete (Bakharev et al., 2000).

Puertas et al. (2003) investigated the effect of vinyl and polyacrylate copolymer superplasticizers on the workability and 2 and 28 day compressive and flexural strengths of blast furnace slag based geopolymer binders and mortars activated with sodium hydroxide and sodium silicate solutions (Puertas et al., 2003). It was concluded that the vinyl and polyacrylate copolymer superplasticizers did not improve the workability (Puertas et al., 2003). Furthermore, vinyl copolymer superplasticizer reduced the 2 and 28 day compressive and flexural strength compared to the specimens without superplasticizer due to the delay in activation of the slag, whereas polyacrylate copolymer superplasticizer had no significant on effect (Puertas et al., 2003).

Palacios and Puertas (2005) investigated the effect of five different superplasticizers (i.e., two polycarboxylate based, one melamine based, one naphthalene based, one vinyl copolymer based) and one shrinkage reducing admixture (i.e., polypropylene glycol derivative) on the workability, compressive strength, flexural strength, and setting time of blast furnace slag based geopolymer binders and mortars activated with sodium hydroxide and sodium silicate solutions (M. Palacios & Puertas, 2005). It was concluded that the alkaline environment altered the chemical structure of all the admixtures, excepting naphthalene based superplasticizer (M. Palacios & Puertas, 2005). As such, naphthalene based superplasticizer increased the workability, retarded the setting times, and increased both the compressive and flexural strengths compared to the specimens without superplasticizer (M. Palacios & Puertas, 2005).

Palacios et al. (2008) investigated the effect of four different superplasticizers (i.e., polycarboxylate-based, melamine formaldehyde derivative, naphthalene formaldehyde derivative, and vinyl copolymer) and one shrinkage- reducing admixture (i.e., polypropylene glycol derivative ) at dosages of 0, 0.3, 0.5, 1.0, 1.5, and 2.0 wt.% of the binder on the rheological parameters of blast furnace slag based geopolymer binders and mortars activated with sodium hydroxide and sodium silicate solutions (Marta Palacios et al., 2008). It was concluded that the superplasticizers did not have a significant effect on the rheological properties (Marta Palacios et al., 2008).

In 2009, Palacios investigated the adsorption effect of three different superplasticizers (i.e., melamine based, naphthalene based, and vinyl copolymer based) of blast furnace slag based geopolymer binders and mortars activated with sodium silicate solution and two sodium hydroxide solutions with concentrations of 0.005 M and 2.57 M (M. Palacios et al., 2009). It was concluded that the adsorption capacity of the superplasticizer is not dependent on the sodium hydroxide concentration (M. Palacios et al., 2009). Furthermore, naphthalene based superplasticizer and sodium hydroxide concentration of 2.57 M affected the rheological properties of the slag based binder (M. Palacios et al., 2009).

Based on the different tests and superplasticizers investigated for blast furnace slag based geopolymer binders, mortars, and concrete, it can be concluded that the naphthalene based superplasticizer is an alkali resistant superplasticizer which increases the workability, compressive strength, and rheological properties. As such, for slag based geopolymers, it is the go to superplasticizer.



### **2.8.2. Fly Ash**

Similar to slag based geopolymer materials, several studies have investigated the effect of type and dosage of superplasticizer on physical, mechanical, and rheological properties of fly ash based geopolymer materials.

Puertas et al. (2003) investigated the effect of two superplasticizers (i.e., vinyl and polyacrylate copolymers) on the workability and 2 and 28 day compressive strength of fly ash based geopolymer binders and mortars activated with an 8M sodium hydroxide solution (Puertas et al., 2003). It was concluded that both superplasticizers did not increase the workability of the binders or the compressive strength of the mortars (Puertas et al., 2003).

Hardjito et al. (2004) investigated the effect of naphthalene based superplasticizer (i.e., 0 to 3.5 wt.% of binder) on the workability and compressive strength of fly ash based concrete activated with sodium hydroxide solution and sodium silicate solutions (Hardjito et al., 2004). It was concluded that the addition of naphthalene based superplasticizer for all dosages enhanced the workability. However, the compressive strength reduced after exceeding a dosage of 2 wt.% (Hardjito et al., 2004).

Criado (2009) investigated the effect of three types of superplasticizers (i.e., lignosulfonate, melamine, and polycarboxylate based) on the rheology of fly ash based geopolymer binders activated with 12.5 M sodium hydroxide and sodium silicate solutions (Criado et al., 2009). Among the superplasticizers studied, it was concluded that polycarboxylate based superplasticizer at 0.8 wt.% of binder was the most effective superplasticizer (Criado et al., 2009).

Kong and Sanjayan (2010) investigated the effect of naphthalene and polycarboxylate based superplasticizer on the workability and compressive strength of fly ash based geopolymer

concrete activated with potassium hydroxide and sodium silicate solution (Kong & Sanjayan, 2010). It was concluded that the plasticizers did not improve the workability (Kong & Sanjayan, 2010). Furthermore, the compressive strength reduced upon the addition of superplasticizer by 54% and 22% for polycarboxylate and naphthalene based superplasticizer, respectively (Kong & Sanjayan, 2010).

Memon et al. (2012) investigated the effect of polycarboxylate based superplasticizer on the workability and compressive strength of fly ash based geopolymer concrete activated with sodium hydroxide and sodium silicate solutions (Memon et al., 2012). It was concluded that the addition of 3 to 7 wt.% (by mass of binder) polycarboxylate based superplasticizer increased the workability and compressive strength (Memon et al., 2012).

Jang et al. (2014) investigated the effect of polycarboxylate and naphthalene based superplasticizers on the workability, compressive strength, and setting time of a combination of fly ash and/or slag geopolymer binder activated with sodium hydroxide and sodium silicate solutions (Jang et al., 2014). It was concluded that the polycarboxylate based superplasticizer improved the workability and delayed the setting time compared to naphthalene based superplasticizer (Jang et al., 2014). However, exceeding 2 wt.% of the polycarboxylate based superplasticizer negatively affected the compressive strength (Jang et al., 2014).

Xie and Kayali (2016) investigated the effect of polycarboxylate and naphthalene based superplasticizer on the workability of class C and F fly ash based geopolymer binders activated with sodium hydroxide and sodium silicate solutions (Xie & Kayali, 2016). Based on the workability, it was concluded that polycarboxylate based superplasticizer was more effective for class C fly ash, but less effective for class F fly ash (Xie & Kayali, 2016). However, naphthalene

based superplasticizer performed similarly for both fly ash based geopolymer binders (Xie & Kayali, 2016).

Based on the different tests and superplasticizers investigated for fly ash based geopolymer binders, mortars, and concrete, it can be concluded that the addition of superplasticizer had a minimal effect on the workability, yet reduced the compressive strength in all cases. As such, there is a need to find an effective superplasticizer for fly ash based geopolymer materials.

### **2.8.3. *Metakaolin***

Pacheco-Torgal et al. (2011) investigated the effect of a superplasticizer (provided by MAISOL-FPR) on the workability, compressive strength, and flexural strength of metakaolin based geopolymer binder and mortar activated with sodium hydroxide and sodium silicate solutions (Pacheco-Torgal et al., 2011). It is important to know that the type of superplasticizer was not specified in this study. It was concluded that the superplasticizer dosage up to 3 wt.% of the binder did not have a significant effect on the workability or strengths (Pacheco-Torgal et al., 2011).

Al-Shathr et al. (2015) investigated the effect of sulphonated naphthalene polymer superplasticizer dosage (i.e., 6, 8, 10, 12, and 16 kg/m<sup>3</sup>) on the 7 day compressive strength of metakaolin based geopolymer concrete activated with sodium hydroxide and sodium silicate solutions (Al-Shathr et al., 2015). It was concluded that increasing superplasticizer dosage up to 12 kg/m<sup>3</sup> lead to an increase in compressive strength, yet exceeding 12 kg/m<sup>3</sup> will reduce the compressive strength (Al-Shathr et al., 2015).

Lee et al. (2020) investigated the effect of polycarboxylate superplasticizers and methyl isobutyl carbinol (MIBC) superplasticizer on the workability and 7 day compressive strength of metakaolin based geopolymer binder activated with a waterglass solution consisting of sodium

hydroxide or potassium hydroxide and fumed silica (Lee et al., 2020). It was concluded that MIBC improved the workability of sodium based metakaolin geopolymer binder (Lee et al., 2020). However, MIBC did not reduce the water demand (Lee et al., 2020). Furthermore, potassium based binder was much more workable compared to sodium based binder, yet sodium based binder presented a higher compressive strength (Lee et al., 2020).

Due to intercalation of polyethylene glycol (PEG) side chains into clay mineral interlayers, conventional superplasticizers based on polycarboxylate ether (PCE) are intolerant of clay minerals (Tutal et al., 2020). AAs such, PCE is not a suitable plasticizer for geopolymers. Tutal et al. (2020) investigated the effect of starch based superplasticizers modified with sodium sulfonate (Figure 2.10.a) and (3-chloro-2-hydroxypropyl) trimethylammonium chloride (Figure 2.10.b) on the workability, air content, shrinkage, compressive strength, flexural strength, and porosity of metakaolin based geopolymer binder and mortar activated with potassium silicate solution (Tutal et al., 2020). It was concluded that the starch based superplasticizers are stable in alkaline environment thus leading to the improvement of the workability by up to 40% at a dosage of 1 wt.% of the binder (Tutal et al., 2020). Furthermore, the superplasticizer did not impact the air content (Tutal et al., 2020). Moreover, the starch based superplasticizer increased the 7 and 28 day compressive and flexural strengths (Tutal et al., 2020).

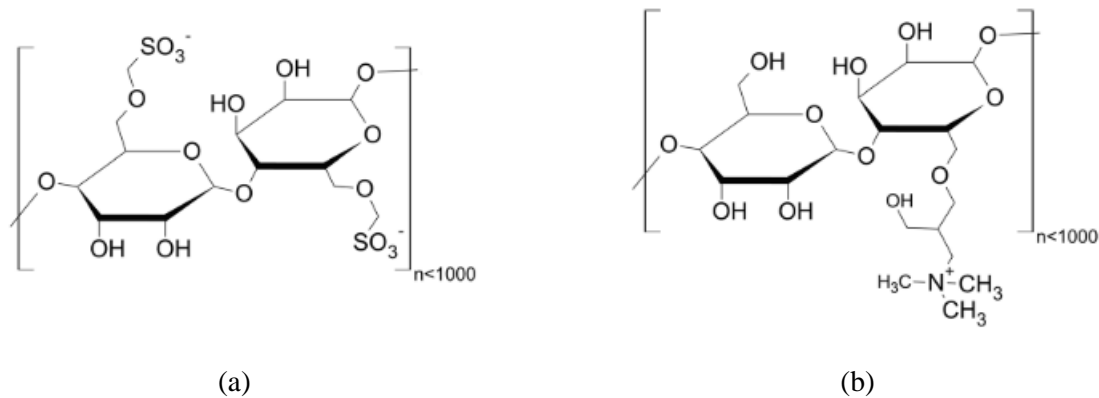


Figure 2.10. Starch Modified with (a) Sodium Sulfonate and (b) CHPTAC

## 2.9. Deterioration of Geopolymer Concrete

Conventional ordinary Portland cement concrete is the most utilized material in the world.

However, it is one of the main contributors to global warming as one ton of cement production produces an equivalent one ton of CO<sub>2</sub>. To reduce the CO<sub>2</sub> emissions, researchers began utilizing industrial by products (i.e., fly ash, slag, etc.) as supplementary cementitious materials (SCMs). However, to significantly reduce CO<sub>2</sub> emissions, the cementitious binder needed to be replaced with a less emission and energy intensive material. As a result, geopolymer concrete was developed. The following subsections will compare the durability of OPC and geopolymer based concrete.

### 2.9.1. Permeability

Permeability is defined as the property that governs the rate of flow of a fluid into a porous solid.

In OPC concrete, permeability is governed by the water to cement ratio (which determines the size, volume, and continuity of the pores in the cement binder) and maximum aggregate size (which influences the microcracks in the interfacial transition zone between the cement binder and aggregate) (Edvardsen, 1999). Similarly, in geopolymer concrete, permeability is governed by the water content and aggregate size (Abdulsalam Arafa et al., 2017). Furthermore, the

permeability of geopolymer concrete also depends on the alkaline activator solution (Abdulsalam Arafa et al., 2017). Abdulsalam et al. (2017) investigated the effect of fly ash to aggregate ratio, aggregate size (i.e., 5-10, 10-14, and 14-20 mm), fly ash to alkaline liquid ratio, and sodium hydroxide concentration (i.e., 8, 10, and 12 M) on the permeability and compressive strength of fly ash based pervious geopolymer concrete activated with sodium hydroxide and sodium silicate solutions (Abdulsalam Arafa et al., 2017). It was concluded that increasing aggregate content and aggregate size increased the permeability and significantly decreased the compressive strength (Abdulsalam Arafa et al., 2017). Furthermore, increasing the alkaline liquid content reduces the permeability and therefore increased the compressive strength (Abdulsalam Arafa et al., 2017). Moreover, increasing the concentration of the sodium hydroxide increases the permeability, yet the compressive strength increased with an increase in sodium hydroxide concentration up to 10 M (Abdulsalam Arafa et al., 2017). It is important to mention that the permeability and compressive strength of the concrete are inversely related.

### ***2.9.2. Freezing and Thawing***

In countries subjected to cold temperatures, the performance of concrete when subjected to freezing and thawing cycles is important. In general, concrete tends to deteriorate in cold weather as the water in cracks/capillary pores expand and convert into ice. This expansion causes internal stresses which in turn cause microcracks. It is important to mention that only a few studies were conducted to evaluate the effect of freezing and thawing cycles on geopolymer concrete. Based on the freeze-thaw studies conducted on geopolymer concrete, it can be concluded that geopolymer concrete is more durable to freeze-thaw resistance than regular concrete.

Fu et al. (2011) investigated the freeze-thaw resistance of slag based geopolymer concrete activated with sodium hydroxide and sodium silicate solutions (Fu et al., 2011). It was concluded

that the mass and relative dynamic modulus of elasticity (RDME) decreased after 25 freeze-thaw cycles (Fu et al., 2011).

Zhao et al. (2019) investigated the freeze-thaw resistance of class F fly-ash and slag based geopolymer concrete activated with sodium hydroxide and sodium silicate (Zhao et al., 2019). It was concluded that the freeze -thaw resistance of fly ash based geopolymer concrete with 50% slag replacement is slightly weaker than that of regular ordinary Portland cement concrete (Zhao et al., 2019).

Nazarpour and Jamali (2019) investigated the freeze-thaw resistance of ground granulated blast furnace slag based geopolymer concrete with 20, 30, and 40 wt.% recycled aggregate from concrete blocks as coarse aggregate replacement and activated with sodium hydroxide and sodium silicate (Nazarpour & Jamali, 2020). It was concluded that the compressive strength of the geopolymer concrete did not decrease significantly even after 300 freeze-thaw cycles (Nazarpour & Jamali, 2020).

Azarsa and Gupta (2020) investigated the freeze-thaw resistance of fly-ash and bottom-ash based geopolymer concrete activated with potassium hydroxide and potassium silicate. It was concluded that bottom ash based geopolymer concrete presented a better freeze-thaw resistance compared to fly ash based geopolymer concrete (Azarsa & Gupta, 2020). However, for both geopolymer concretes studied, the mass and relative dynamic modulus of elasticity decreased after 300 freeze-thaw cycles (Azarsa & Gupta, 2020).

Rashad and Sadek (2020) investigated the freeze-thaw resistance of fly-ash and slag based geopolymer binder activated with sodium silicate with and without waste rubber powder (Rashad & Sadek, 2020). The specimens were subjected to 5, 10, 15, and 20 accelerated freeze-thaw cycles where they were placed at -19 °C for 12 hours then in water for 12 hours (Rashad &

Sadek, 2020). It was concluded that the incorporation of rubber increased the freeze-thaw resistance due to the increased porosity of the matrix (Rashad & Sadek, 2020).

### ***2.9.3. Creep and Shrinkage***

Creep is a type of deformation which occurs when a material is subjected to an external sustained load. Unlike creep, drying shrinkage is independent of external sustained load. Drying shrinkage occurs as water is lost during the drying process and accounts for the large proportion of total long-term shrinkage. Factors affecting creep and shrinkage include the type and content of the binder, water content, and type and size of aggregate.

Hardjito et al. (2004) investigated the drying shrinkage, creep, and sulfate resistance of the best performing fly ash based geopolymer concrete activated with 8 M sodium hydroxide solution and sodium silicate solutions where the sodium silicate to sodium hydroxide ratio is 2.5 (Hardjito et al., 2004). For creep, the test specimens were loaded on the 7<sup>th</sup> day with a sustained stress of 22 MPa (i.e., approximately 40% of its compressive strength) (Hardjito et al., 2004). Based on Figure 2.11.

, the drying shrinkage and creep strains are extremely small where the creep factor (i.e., creep strain-to-elastic strain) is approximately 0.30 after 6 weeks (Hardjito et al., 2004). (Hardjito et al., 2004).



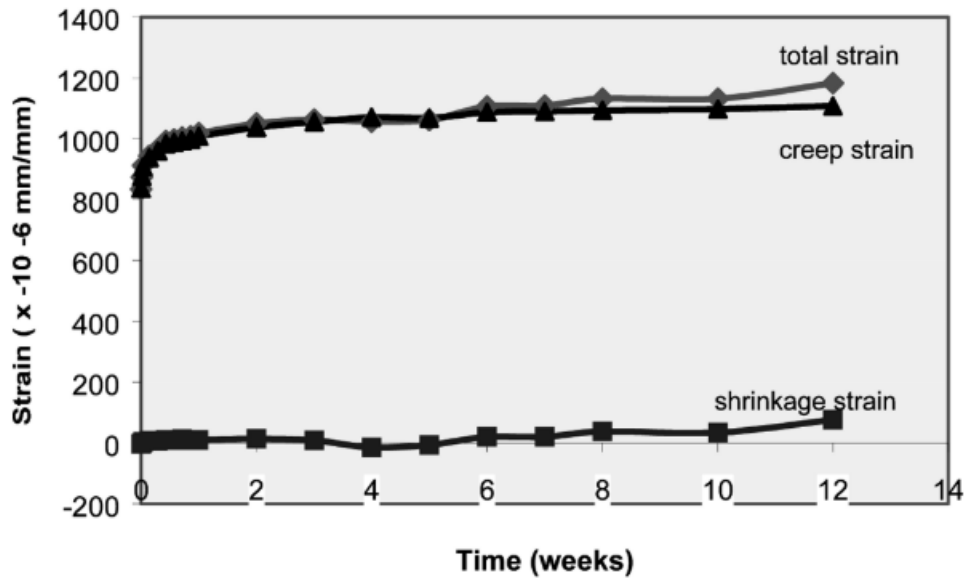


Figure 2.11. Drying Shrinkage and Creep Strains (Hardjito et al., 2004)

Wallah and Rangan (2006) investigated the drying shrinkage of heat cured fly ash based geopolymer concrete activated with 8 M sodium hydroxide solution and sodium silicate solutions (S E Wallah & Rangan, 2006). It was concluded that heat cured fly ash based geopolymer concrete exhibited very low drying shrinkage (S E Wallah & Rangan, 2006).

Deb et al. (2015) investigated the drying shrinkage of fly ash and slag based geopolymer concrete activated with 14 M sodium hydroxide solution and sodium silicate solutions where the sodium silicate to sodium hydroxide ratios are 1.5 and 2.5 (Deb et al., 2015). It was concluded that shrinkage reduced upon decreasing sodium silicate to sodium hydroxide ratios and increasing the slag content from 10 to 20 wt.% of the total precursor (Deb et al., 2015). It is important to mention that the drying shrinkage for all materials studied remained under 1000 microstrain, which is the criteria for normal concrete (Deb et al., 2015).

Castel et al. (2016) investigated the creep with sustained loads of 10 and 20 MPa and drying shrinkage of fly ash and slag based geopolymer concrete activated with sodium hydroxide solution and sodium silicate solutions (Castel et al., 2016). It was concluded that the creep and

shrinkage strains were very low, especially for the specimens cured for more time under elevated temperatures (Castel et al., 2016).

Singh et al. (2016) investigated the drying shrinkage of fly ash and slag based geopolymer concrete activated with sodium hydroxide and sodium silicate solutions (B. Singh et al., 2016). It was concluded that the drying shrinkage is very small after 6 months and falls significantly below the reported value of ordinary Portland cement concrete (B. Singh et al., 2016).

Yang et al. (2017) investigated the drying shrinkage of metakaolin based geopolymer binders and mortars containing 0-30 wt.% fly ash and activated with sodium hydroxide and sodium silicate solutions (T. Yang et al., 2017). It was concluded that the replacement of metakaolin with fly ash reduced the drying shrinkage strain (T. Yang et al., 2017).

Khan et al. (2019) investigated the tensile creep and shrinkage on early age cracking of fly ash and slag based geopolymer concrete using three different fly ash sources with two slag contents (i.e., 10 and 25 wt.%) and activated with sodium hydroxide and sodium silicate solutions (Khan et al., 2019). The specimens were subjected to two curing methods (i.e., ambient and heat cured) and two shrinkage tests (i.e., restrained and unrestrained) (Khan et al., 2019). It was concluded that the heat cured specimens presented viscoelastic characteristics where they had lower early age shrinkage and a higher tensile creep (Khan et al., 2019). Furthermore, compared to heat cured geopolymer concrete specimens, the ambient cured geopolymer concrete specimens developed high tensile stresses under restrained shrinkage causing early age cracking (Khan et al., 2019). As such, elevated curing is required for fly ash based geopolymer concrete to reduce early age cracking (Khan et al., 2019).

Ma et al. (2020) investigated the drying shrinkage of fly ash and slag based geopolymer binder activated with anhydrous sodium silicate and sodium sulfate (C. Ma et al., 2020). It was

concluded that the incorporation of anhydrous sodium sulfonate increased the volume of the specimen after 1 day of curing due to delay in crystallization (C. Ma et al., 2020). As such, the drying shrinkage after 120 days is significantly lower than the use of only sodium silicate (C. Ma et al., 2020).

#### ***2.9.4. Sulfate Attack***

Sulfate attack is a complex process in which the salt from groundwater, seawater, industrial waters, or rain from air pollution attacks the concrete leading to the degradation of concrete through expansion, cracking, progressive decrease in strength, and disintegration of the binder.

In general, geopolymer materials tend to resist sulfate attack better than ordinary Portland cement materials. This is attributed to the different materials chemistry. In cement based concrete, the deterioration due to sulfate attack is attributed to the formation of gypsum and ettringite which cause expansion, cracking, and spalling of concrete (B. V. Rangan, 2018).

However, in geopolymer concrete, the main component (i.e., binder) is not susceptible to sulfate attack without the presence of high calcium contents (B. V. Rangan, 2018). The following research has been conducted to evaluate the sulfate resistance of different geopolymer materials. Hardjito et al. (2004) investigated the resistance to sulfate attack of fly ash based geopolymer concrete activated with sodium hydroxide and sodium silicate solutions by placing the specimens in a 5% sodium sulfate solution for periods of time (Hardjito et al., 2004). After 12 weeks of exposure, the specimens showed no significant change in mass, dimensions, and compressive strength (Hardjito et al., 2004).

Wallah et al. (2005) investigated the resistance of sulfate attack of fly ash based geopolymer concrete activated with sodium hydroxide and sodium silicate solutions by placing the specimens in a 5% sodium sulfate solution for 12 weeks (Steenie E. Wallah et al., 2005). It was concluded

that sulfate attack did not have a significant effect on the compressive strength, mass, and dimensions of the specimens (Steenie E. Wallah et al., 2005).

Komljenović et al. (2013) investigated the resistance to sulfate attack of slag based geopolymer binders and mortars activated with sodium hydroxide and sodium silicate solutions (Komljenović et al., 2013). The specimens were cured for 28 days then placed in a 5% sodium sulfate solution for an additional 30, 60, and 90 days (Komljenović et al., 2013). It was concluded that sulfate attack did not decrease the strength (Komljenović et al., 2013). Furthermore, the geopolymer gel did not show significant structural change (Komljenović et al., 2013).

Duan et al. (2016) investigated the resistance to sulfate attack of fly ash based geopolymer binder where 0, 10, 15, 20, 25, and 30 wt.% of fly ash was replaced with metakaolin and activated with sodium hydroxide and sodium silicate solutions (Duan et al., 2016). The specimens were cured for 28 days then placed in a 5% sodium sulfate solution (which was renewed every 2 weeks) for an additional 28, 90, and 180 days (Duan et al., 2016). It was concluded that increasing the metakaolin content increases the compressive strength due to the denser geopolymer gel and becomes more resistant to sulfate attack (Duan et al., 2016). In fact, the specimens without metakaolin presented larger pore sizes and more microcracks after 28 days of curing, which made them more susceptible to sulfate attack (Duan et al., 2016).

Džunuzović et al. (2017) investigated the effect of external sulfate attack on fly ash and slag based geopolymer binder and mortar activated with sodium hydroxide and sodium silicate solutions (Džunuzović et al., 2017). After 28 days of curing, the specimens were placed in a 5% sodium sulfate solution for an additional 30, 90, and 180 days (Džunuzović et al., 2017). It was concluded that the exposure to sulfate did not cause any deterioration to the strength even after 180 days (Džunuzović et al., 2017).

Rashad and Sadek (2020) investigated the resistance to sulfate attack of fly-ash and slag based geopolymer binder activated with sodium silicate with and without waste rubber powder (Rashad & Sadek, 2020). The specimens were subjected to 5, 10, 15, and 20 cycles where they were placed in a 5% sodium sulfate solution for 15 hours followed by drying for 6 hours at 80 °C (Rashad & Sadek, 2020). It was concluded that the incorporation of rubber increased the resistance of sulfate attack (Rashad & Sadek, 2020).

### ***2.9.5. Alkali Silica Reaction***

Alkali silica reaction (ASR) occurs when the aggregates containing siliceous minerals react with alkali-metal ions ( $\text{Na}^+$  and  $\text{K}^+$ ) and hydroxyl ions ( $\text{OH}^-$ ) from the cementitious paste or geopolymeric gel to form expansive alkali silica gel. Geopolymer materials have shown to be substantially less vulnerable to alkali silica reaction than ordinary Portland cement materials.

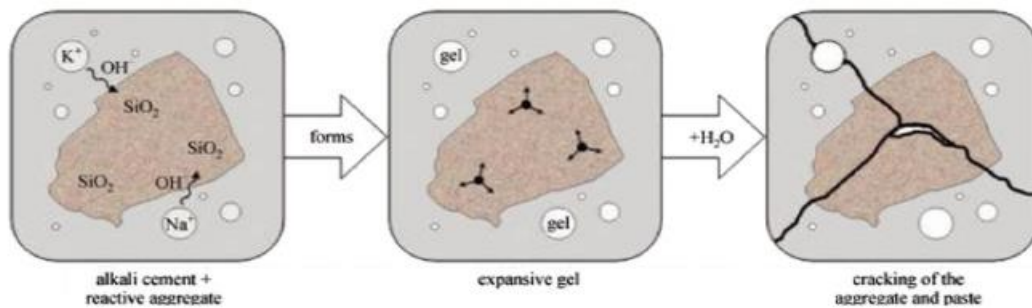


Figure 2.12. Mechanism of Alkali Silica Reaction (Annapurna et al., 2020)

Kupwade-Patil et al. (2013) investigates the alkali silica reaction resistance of fly ash based geopolymer concrete activated with sodium silica and 14 M sodium hydroxide solutions (Kupwade-Patil & Allouche, 2013). The alkali silica reactive aggregates used are limestone, sand- stone, and quartz (Kupwade-Patil & Allouche, 2013). It was concluded that fly ash based geopolymer concrete is significantly less vulnerable to alkali silica reaction than ordinary Portland cement concrete (Kupwade-Patil & Allouche, 2013).

Annapurna et al. (2019) investigated the alkali silica reaction resistance of fly ash and slag based geopolymer mortar activated with sodium hydroxide and sodium silicate solutions (Annapurna et al., 2020). The alkali silica reactive aggregates used are granite, quartz and black trap (Annapurna et al., 2020). It was concluded that geopolymer concrete is more resistant to alkali silica reaction compared to ordinary Portland cement concrete (Annapurna et al., 2020).

Lei et al. (2020) investigated the alkali silica reaction resistance of fly ash based geopolymer concrete activated with 10 M sodium hydroxide (Lei et al., 2020). The alkali silica reactive aggregates used contain quartz and albeit. It was concluded that the fly ash based geopolymer concrete exhibited significantly better alkali silica reaction resistance compared to ordinary Portland cement (Lei et al., 2020). In fact, the presence of aluminum in the pore solution enhanced the alkali silica reaction resistance of the geopolymer concrete (Lei et al., 2020).

## **2.10. Comparison between Geopolymer Concrete and Ordinary Portland Cement Concrete**

A comprehensive study was conducted Berndt et. al. (2013) to determine the difference between the physical and mechanical properties of geopolymer concrete and conventional concrete. According to Table 2.6., there is no clear difference between geopolymer concrete and conventional concrete. In fact, the results of the studies varied between different researchers. Nevertheless, it can be concluded that geopolymer concrete has higher early strength gain with higher compressive, flexural, and tensile strength. Furthermore, they have similar to higher bond strength to reinforcement. However, they typically have lower modulus of elasticity, density, poison's ratio, creep, shrinkage, chloride diffusion coefficient, and rapid chloride permeability. Based on the durability properties shown in Table 2.6., geopolymer concrete appeared to be more durable than conventional concrete.

Table 2.6. Comparison between Geopolymer and Conventional Concrete (Berndt et al., 2013)

Property	Geopolymer versus conventional concrete
Compressive Strength	Similar, higher rate of early strength gain
Tensile Strength	Indirect tensile strength typically higher for similar compressive strength
Flexural Strength	Similar to higher depending on alkali activator higher rate of early strength gain
Modulus of Elasticity	Typically lower
Density	Similar to lower
Poisson's Ratio	Typically lower or similar
Shrinkage	Lower to similar
Creep Coefficient	Lower
Bond Strength to Reinforcement	Similar for similar compressive strengths higher for higher compressive strengths
Carbonation Coefficient	Higher
Chloride Diffusion Coefficient	Lower (migration test); lower (core test)
Rapid Chloride Permeability	Lower to similar depending on mix proportions
Corrosion Rate of Embedded Steel	Limited research, particularly field exposure, prevents conclusive comparison.
Sulphate Resistance	Somewhat higher, depends on cation
Acid Resistance	More resistant to organic and inorganic acid attack
Alkali-Silica Reaction Susceptibility	Variable based on limited research
Fire Resistance	More resistant
Freeze-Thaw Durability	More durable
Permeability	Varies depending on mix proportions; higher
Water Absorption	Similar

## 2.11. Engineered Geopolymer Composites

The recent development of geopolymer (GP) binders offers a sustainable alternative to cement-based binders in production of ECCs (Nematollahi et al., 2016; Nematollahi, Sanjayan, & Ahmed Shaikh, 2015; Ohno & Li, 2014). In the literature, these composites are referred to as strain-hardening geopolymer composites (SHGC) or Engineered Geopolymer Composites (EGCs). According to previous studies discussed in section 2-10, GP matrices are comparable in compressive strength to cementitious matrices while exhibiting lower fracture toughness (C. Ma et al., 2018; Nematollahi et al., 2016; Nematollahi, Sanjayan, & Ahmed Shaikh, 2015; Ohno & Li, 2014). Compared to ECCs, EGCs are a relatively new material which follow the same

fracture mechanics and fiber/matrix micromechanics discussed in section 2.2.2 to achieve pseudo strain hardening behavior at relatively low fiber contents (i.e., less than 2%) (Nematollahi et al., 2014, 2016; Nematollahi, Sanjayan, & Shaikh, 2015; Ohno & Li, 2014, 2018). Ohno and Li (2014) were the first to develop EGCs. Since then, many researchers began studying the processing, curing, physical and mechanical properties, microstructure, etc. of these novel composites. Similar to geopolymer concrete, the most important factors affecting EGCs are the aluminosilicate source,  $\text{SiO}_2/\text{Al}_2\text{O}_3$  ratio of the binder, water to solids ratio, type and amount of alkali activator, mixing and curing conditions, etc. (Abdullah et al., 2012; Kan et al., 2019, 2020; Zahid & Shafiq, 2020).

#### ***2.11.1. Materials of Engineered Geopolymer Composites***

The geopolymer precursors studied to date include fly ash (Alrefaei & Dai, 2018; Kan et al., 2019, 2020; Nematollahi, Sanjayan, & Shaikh, 2015; Ohno & Li, 2018; Zahid & Shafiq, 2020), a combination of fly ash and ground granulated blast-furnace slag (GGBS) (Alrefaei & Dai, 2018; Ling et al., 2019), a combination of fly ash and metakaolin (Kan et al., 2019, 2020), and recently metakaolin (Constâncio Trindade et al., 2020; Trindade et al., 2020).

The activator solutions studied to date include commercially-available aqueous sodium silicate ( $\text{Na}_2\text{SiO}_3$ ) solution and sodium hydroxide (NaOH) pellets (Kan et al., 2019, 2020; Ohno & Li, 2018), aqueous 8 M NaOH and  $\text{Na}_2\text{SiO}_3$  (Nematollahi, Sanjayan, & Shaikh, 2015; Salami et al., 2016; Zahid & Shafiq, 2020), aqueous 8 M KOH and potassium silicate ( $\text{K}_2\text{SiO}_3$ ) (Nematollahi, Sanjayan, & Shaikh, 2015), anhydrous sodium metasilicate powder (Alrefaei & Dai, 2018), and laboratory manufactured waterglass solutions of potassium or sodium hydroxide pellets and silica fume dissolved in DI water (Constâncio Trindade et al., 2020; Trindade et al., 2020).



The type fine aggregate and content studied is microsilica sand at 0, 14.5, 20, 30, 40, 50, and 80 wt% (Alrefaei & Dai, 2018; Constâncio Trindade et al., 2020; Kan et al., 2019, 2020; Ohno & Li, 2018; Trindade et al., 2020; Zahid & Shafiq, 2020).

The fibers studied to produce EGCs with ductile PSH capabilities include 1.2 wt% oil coated and uncoated PVA (Constâncio Trindade et al., 2020; Kan et al., 2019, 2020; Nematollahi, Sanjayan, & Ahmed Shaikh, 2015; Ohno & Li, 2018; Salami et al., 2016; Trindade et al., 2020; Zahid & Shafiq, 2020), UHMWPE (Alrefaei & Dai, 2018; Trindade et al., 2020), and copper coated steel fibers (Alrefaei & Dai, 2018).

### ***2.11.2. Effect of Curing Regime on Engineered Geopolymer Composites***

Similar to geopolymer concrete, two types of curing methods were observed: ambient temperature curing (Alrefaei & Dai, 2018; Constâncio Trindade et al., 2020; Trindade et al., 2020) and heat curing (Alrefaei & Dai, 2018; Kan et al., 2019, 2020; Nematollahi, Sanjayan, & Ahmed Shaikh, 2015; Ohno & Li, 2018; Salami et al., 2016; Zahid & Shafiq, 2020). It is important to note that, among the same curing type, the researchers performed the curing differently. Alrefaei & Dai (2018) performed ambient curing by placing a wet burlap and plastic sheets on top of the EGC specimens for 24 hours then submerging the specimens in a water tank until testing day (Alrefaei & Dai, 2018), whereas Trindade et al. (2019, 2020) exposed the EGC specimens to the air for 48 hours then placed them in plastic bags until testing day (Constâncio Trindade et al., 2020; Trindade et al., 2020). In terms of heat curing, the researchers typically kept the EGC specimens in the mold for 24 hours, the demolded specimens were placed in an oven at a designated temperature ranging from 60 °C, and then placed then exposed them to the atmosphere until testing day (Alrefaei & Dai, 2018; Nematollahi, Sanjayan, & Ahmed Shaikh, 2015; Ohno & Li, 2018; Salami et al., 2016; Zahid & Shafiq, 2020). On the other hand, Kan et

al. (2019, 2020) placed the EGC specimens in an oven for 2h at 60, 70, and 80°C before exposing the specimens to the air (Kan et al., 2019, 2020). Kan et al. (2020) concluded that the most ductile composite was achieved by heat curing the EGC specimens at 80°C where the tensile strength and tensile strain capacities achieved are 3.8 MPa and 5.2%, respectively (Kan et al., 2020).

### ***2.11.3. Effect of Fiber Type and Content on Engineered Geopolymer Composites***

To increase the compressive, tensile, and flexural strengths of the geopolymer materials, PVA fiber contents ranging from 1 to 2 vol.% (Alrefaei & Dai, 2018; Constâncio Trindade et al., 2020; Kan et al., 2019, 2020; Nematollahi, Sanjayan, & Ahmed Shaikh, 2015; Ohno & Li, 2018; Salami et al., 2016; Trindade et al., 2020; Zahid & Shafiq, 2020). Ohno and Li (2018) conducted compression and uniaxial tensile tests on fly ash based PVA reinforced EGC specimens and concluded that 1.5 vol.% PVA was the optimum fiber content where the compressive strength, tensile strength, and tensile strain capacity are 43 MPa, 5.3 MPa, and 4.7%, respectively (Ohno & Li, 2018). Furthermore, Kan et al.(2020) studied fly ash based EGCs reinforced with 1.50, 1.65, and 1.8 vol.%. PVA fibers where 0, 0.8, 1.6 wt.% metakaolin was used as partial fly ash replacement (Kan et al., 2020). It was concluded that the optimum composite consisted of 1.6 wt.% metakaolin and 1.5 vol.% PVA cured at 80°C with a compressive strength, tensile strength, and tensile strain capacity of 17 MPa, 3.8 MPa, and 5.2%, respectively (Kan et al., 2020).

Trindade et al. (2020) studied the effect of 2 vol.% PVA and UHMWPE fibers on the quasi-static and dynamic loading of metakaolin based EGCs (Trindade et al., 2020). It was concluded that PVA fibers have a better bond strength under quasi-static loading whereas UHMWPE fibers perform better under dynamic loading (Trindade et al., 2020).

### **3. EFFECT OF FINE AGGREGATE AND PVA FIBER CONTENT ON THE PROPERTIES OF METAKAOLIN BASED ENGINEERED GEOPOLYMER COMPOSITES**

#### **3.1. Introduction**

Due to its high mechanical strength, durability, low cost, and wide availability, concrete is a widespread material in the build environment. However, concrete exhibits low tensile strength and ductility, which results in brittle failure and cracking. This in turn negatively affects the durability of concrete structures as cracks grant easy access of detrimental agents into the structure allowing for enhanced deterioration. As a response to this pervasive problem, over the past three decades, a new class of fiber-reinforced cementitious composites known as Engineered Cementitious Composites (ECCs) has been developed to mitigate the brittle nature of concrete. The uniqueness of ECCs arises from its high tensile strain capacity ranging between 1 to 8% (i.e., 100 to 800 times that of regular concrete), which is achieved at relatively low fiber contents (i.e., typically 1.5 to 2% volume fraction) (Alrefaei & Dai, 2018; Li, 2008; Li et al., 2004; Nematollahi, Sanjayan, & Ahmed Shaikh, 2015; Ohno & Li, 2018). To attain this, ECCs are distinctively designed based on micromechanics and fracture mechanics concepts to transform the Griffith crack propagation mode of regular concrete and fiber-reinforced concrete (FRC) to a steady-state flat crack propagation mode. Consequently, this enables a tensile pseudo strain-hardening (PSH) behaviour in ECCs through the formation of multiple steady-state microcracks, which gives rise to the extraordinary tensile ductility of these composites (Li, 2003).

ECCs are typically composed of cement, supplementary cementitious materials (SCMs), fine aggregate, water, admixtures, and polymer microfibers (Arce et al., 2019; Li, 2003, 2019b; Li et al., 2002; Reda Taha et al., 2002). Polyvinyl alcohol (PVA) fibers have been principally utilized to manufacture ECCs (Kan et al., 2019, 2020; Li et al., 2002, 2004; Ling et al., 2019; H.

Ma et al., 2015; Nematollahi, Sanjayan, & Ahmed Shaikh, 2015; Nematollahi, Sanjayan, & Shaikh, 2015; Pakravan et al., 2018; Redon et al., 2001a). However, ultra-high-molecular weight polyethylene (UHMWPE) fibers have also been utilized; yet, these have been mainly limited to the development of high performance ECCs due to its high cost (Alrefaei & Dai, 2018; Choi et al., 2016; Ding et al., 2018; Li et al., 2002; Osman et al., 2019; Yu et al., 2018). Since ECCs do not use coarse aggregate, the amount of cement required to manufacture these composites increases relative to conventional concrete. In turn, this increments ECCs environmental impact, as the cement industry consumes vast amounts of energy and produces immense amounts of carbon dioxide (CO<sub>2</sub>) emissions, which accounts for nearly 8% of CO<sub>2</sub> global anthropogenic emissions (N. B. Singh, 2018). As such, there is a significant motivation to find less emission-intensive binders that can replace cement in the manufacture of ECC materials without negatively affecting the mechanical properties of these novel composites. A promising alternative is the use of geopolymer binders, which can reduce CO<sub>2</sub> emissions by 44-64% compared to ordinary Portland cement (OPC) (Komnitsas, 2011; McLellan et al., 2011; Turner & Collins, 2013). Geopolymers (GPs) are inorganic aluminosilicate polymers, which can be processed at room temperature from natural materials (e.g., calcined clays, volcanic rocks, mine tailings, etc.) or industrial byproducts (e.g., fly ash, slag, rice husk ash, etc.) that provide for a rich source of soluble silicon (Si) and aluminum (Al) species (Davidovits et al., 2015; Provis & Deventer, 2009; Ryu et al., 2013). The formation of GP rigid gels emerges from the geopolymerization of Al and Si species, which occurs through the activation of the GP precursor with an alkaline solution. The geopolymerization process starts with the dissociation of the Al and Si species of the GP precursor in the alkaline solution. The hydrolyzed [AlO<sub>4</sub>]<sup>5-</sup> (aluminate) and [SiO<sub>4</sub>]<sup>4-</sup> (silicate) species react forming hardened polymer chains through the

polycondensation process releasing water as it cures (Davidovits et al., 2015; Provis & Deventer, 2009; Ryu et al., 2013). Three types of 3-dimensional amorphous polymer structures consisting of Si, O, and Al form during a geopolymerization chemical reaction: poly-sialate (Si-O-Al-O-), poly-sialate-siloxo (Si-O-Al-O-Si-O), and poly-sialate-disiloxo (Si-O-Al-O-Si-O-Si-O) (Davidovits et al., 2015; Provis & Deventer, 2009; Ryu et al., 2013). Sialate refers to the Si-O-Al link, while siloxo refers to the Si-O-Si link. The resulting chemical formula of a GP composition is  $M_n[-(SiO_2)_z - AlO_2]_n \cdot wH_2O$  where M is the alkali metal cation (usually  $Na^+$  or  $K^+$ ), n is the degree of polymerization, z is the Si/Al ratio, and w is the molar water quantity. Geopolymers are usually prepared with a Si/Al ratio of 1.8-2.2, a  $H_2O/(Al_2O_3+SiO_2)$  ratio of 2.0-5.0, and a M/Al ratio of 0.9-1.2 (Davidovits et al., 2015; Provis & Deventer, 2009; Ryu et al., 2013).

Recently, the first efforts to develop ECCs utilizing geopolymer (GP) binders have been reported in 2014 by Ohno and Li (Ohno & Li, 2014). These new GP-based ECCs are referred in the literature as Engineered Geopolymer Composites (EGCs). Since then, scientists around the world have begun studying these emerging composites including their processing, curing, mechanical properties, microstructure, etc. To date, EGCs utilizing mainly fly ash as precursor for GP binders have been studied (Alrefaei & Dai, 2018; Kan et al., 2019, 2020; Ohno & Li, 2018; Zahid & Shafiq, 2020). However, recent studies have also evaluated the use of combinations of fly ash and ground granulated blast-furnace slag (GGBS) (Alrefaei & Dai, 2018; Ling et al., 2019), and fly ash and metakaolin (Kan et al., 2019, 2020) as GP precursors. Most recently, the use of pure metakaolin-based GP binders have also been evaluated for the development of EGCs (Constância Trindade et al., 2020; Trindade et al., 2020). To date, the alkaline activators studied by researchers include commercially-available sodium silicate ( $Na_2SiO_3$ ) solution and sodium hydroxide (NaOH) flakes, potassium silicate solution ( $K_2O_3Si$ ),

calcium hydroxide, and laboratory made Na- or K-based waterglass solutions (Al-Qutaifi et al., 2018; Constâncio Trindade et al., 2020; Kong & Sanjayan, 2010; Nematollahi, Sanjayan, & Ahmed Shaikh, 2015; Trindade et al., 2020). Out of the previously stated activator solutions, commercially available sodium silicate solution was studied extensively. Researchers used either commercially-available sodium silicate solution or a combination of commercially available sodium silicate solution and NaOH solution (with varying molarity) (Al-Qutaifi et al., 2018; Kong & Sanjayan, 2010). Studies show that important factors affecting the strength of the EGCs include aluminosilicate source, Si/Al ratio in precursor materials, water to solids ratio used during synthesis, type and amount of alkali activator, and curing conditions. (Abdullah et al., 2012; Kan et al., 2019, 2020; Zahid & Shafiq, 2020).

Fibers studied to endow EGCs with ductile PSH capabilities include PVA (Kan et al., 2019, 2020; Nematollahi et al., 2016; Nematollahi, Sanjayan, & Ahmed Shaikh, 2015; Nematollahi, Sanjayan, & Shaikh, 2015; Ohno & Li, 2018; Zahid & Shafiq, 2020), UHMWPE (Alrefaei & Dai, 2018; Trindade et al., 2020), and copper coated steel (Alrefaei & Dai, 2018) fibers. PVA fibers at 1, 1.5, and 2 vol.% were utilized to increase the compressive, tensile, and flexural strengths (Constâncio Trindade et al., 2020; Kan et al., 2019, 2020; Nematollahi et al., 2016; Nematollahi, Sanjayan, & Ahmed Shaikh, 2015; Nematollahi, Sanjayan, & Shaikh, 2015; Ohno & Li, 2018; Zahid & Shafiq, 2020). After conducting compression and uniaxial tensile tests, Ohno and Li concluded that 1.5 vol.% was the optimum PVA fiber content balancing material sustainability indices (MSI) and compressive and tensile properties (Ohno & Li, 2018). Kan et al. further studied fly ash based PVA-EGCs utilizing metakaolin as partial fly ash replacement (at 0, 0.8, 1.6 wt.%) and PVA fiber at 1.50, 1.65, and 1.8 vol.%. It was concluded

that 1.5 vol.% PVA with 1.6 wt.% metakaolin cured at 80°C was the optimum composition due to its high compressive and tensile properties (Kan et al., 2019, 2020).

Recently, Trindade et al. investigated metakaolin-based EGCs by using K-based and Na-based waterglass activator solutions, 50 wt.% fine grained quartz sand (i.e., 0.2 mm maximum particle size), two types of fibers (i.e., oil-coated PVA and UHMWPE) at 2% volume fraction, and room temperature curing (Constâncio Trindade et al., 2020; Trindade et al., 2020). Trindade et al. concluded that under quasistatic tensile loading conditions and tensile impact loading conditions UHMWPE fibers produce composites with greater mechanical performance compared to PVA reinforced composites (Trindade et al., 2020). Furthermore, Na-based EGCs exhibited lower flowability and workability, however these composites resulted in a higher density, tensile, flexural, and compressive strengths as well as higher modulus of elasticity in comparison to the K-based EGCs (Constâncio Trindade et al., 2020). The use of metakaolin based GP binders for the development of EGCs are promising as the use of metakaolin as an aluminosilicate source can allow for better material formulation control and consistency in contrast to fly ash based EGCs. Furthermore, metakaolin based GP binders can produce EGC materials with high mechanical strength and ductility, which could be useful for transportation infrastructure applications where ECCs have already been implemented such as bridge deck link-slabs, shear keys, and patch repairs (Kim et al., 2004; Lepech & Li, 2009; Li, 2019b; Ozyildirim & Moruza, 2016). Nevertheless, metakaolin based EGCs remain at early stages of development and the compositional space of these composites must be further investigated to fully understand the effect of materials selection and proportions on the mechanical and physical properties of the composites.

### 3.2. Objective and Scope

The objective of this study was to develop and evaluate novel metakaolin (MK) based polyvinyl alcohol (PVA) fiber reinforced EGCs as a sustainable construction material alternative with superior mechanical performance. To this end, the present study focused on exploring several aspects of the compositional space of MK-PVA-EGCs beyond existing literature including binder composition, aggregate type, and fiber content, on the mechanical and physical properties of the proposed composites. For precise control of the GP binder chemistry, activator solutions utilized in this study were manufactured in the laboratory. Furthermore, a detailed microstructure characterization of the developed materials was conducted via SEM-EDS analysis.

### 3.1. Background

Like ECCs, the design of EGCs is guided by the same fiber/matrix micromechanics and fracture mechanics concepts, which allow for these composites to exhibit pseudo strain-hardening (PSH) behavior. In order for the PSH phenomenon to occur, two conditions must be met: the strength criterion and the energy criterion, which are presented in Equation 3.1. and Equation 3.2., respectively (Li, 2019b; Ohno & Li, 2018; E. Yang, 2008). The strength criterion assures that the composite will not fail (by fiber rupture or pullout) upon crack initiation from any defect site in the matrix (H. Ma et al., 2015; Ohno & Li, 2018; Redon et al., 2001a; E. H. Yang et al., 2008). Furthermore, the energy criterion guarantees steady-state flat crack propagation that occurs when the crack-tip matrix toughness ( $J_{tip}$ ) is lower than the complementary energy of the fiber bridging relation ( $J'_b$ ) as first demonstrated by Marshall and Cox using J-integral analysis (Marshall & Cox, 1988). When both criteria are satisfied, then PSH behavior of the composite is possible. Otherwise, the post-cracking strain-softening behavior commonly observed in regular fiber-reinforced concrete will prevail as illustrated in Figure 3.1.a.



Equation 3.1.

$$\sigma_{fc} \leq \sigma_0$$

where,

$\sigma_0$  = Fiber-bridging capacity; and

$\sigma_{fc}$  = First-cracking strength.

From Equation 3.1.,  $\sigma_{fc}$  is defined by the matrix fracture toughness ( $K_m$ ) and the initial flaw size and is determined by conducting a uniaxial tensile test , while  $\sigma_0$  depends on the fiber and fiber/matrix interface properties and is determined by conducting a single crack tensile (SCTT) test where a notch is created in middle section around the entire dogbone specimen to allow for the formation of a single crack. (Nematollahi et al., 2016; Ohno & Li, 2018).

Equation 3.2.

$$J'_b = \sigma_0 \delta_0 - \int_0^{\delta_0} \sigma(\delta) d\delta \geq J_{tip} \approx \frac{K_m^2}{E_m}$$

where

$J'_b$  = Complementary energy of the fiber-bridging relation;

$J_{tip}$  = Crack-tip matrix toughness;

$\delta_0$  = Crack opening corresponding to  $\sigma_0$ ;

$\sigma(\delta)$  = Fiber-bridging relationship;

$K_m$  = Fracture toughness of matrix; and

$E_m$  = Modulus of elasticity of matrix.

From Equation 3.2.,  $J_{tip}$  is governed by  $K_m$  and  $E_m$ , which depends on the matrix composition and is determined by conducting a fracture toughness test where a notch is cut into the middle of a mortar beam. On the other hand,  $J'_b$  is defined by the fiber-bridging relation, which depends on the properties of the fiber and fiber/matrix interface and is determined upon conducting the SCTT test. Figure 3.1.b illustrates  $J'_b$  and  $J_{tip}$  on a fiber-bridging curve, where  $\sigma_{ss}$  represents the steady-state cracking stress (i.e., when energy balance is achieved, and steady-state flat crack propagation occurs) and  $\delta_{ss}$  is the crack opening corresponding to  $\sigma_{ss}$ .

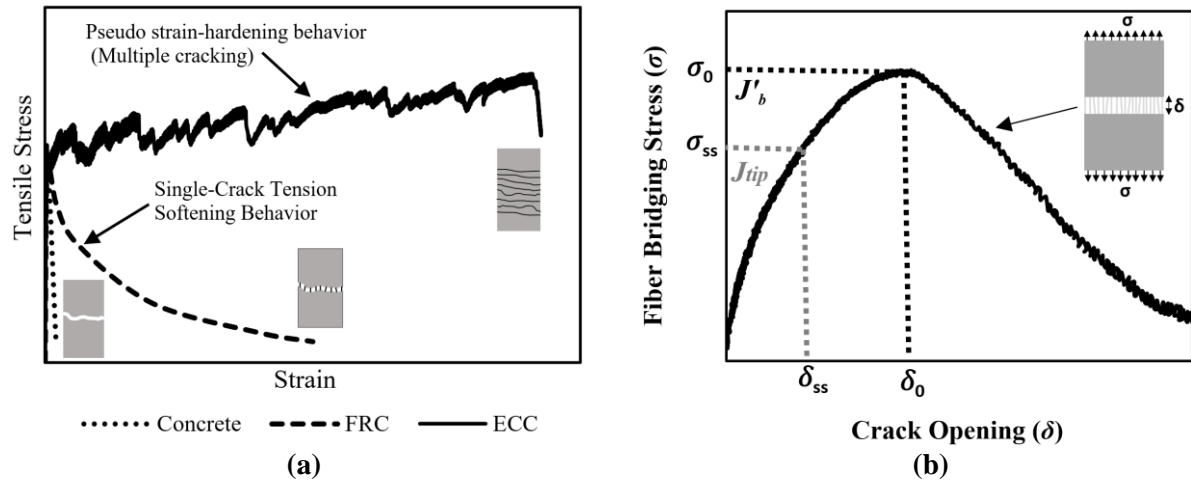


Figure 3.1. (a) Fiber Bridging Relation ( $\sigma$ - $\delta$  Curve) (b) Stress vs. Strain Behavior of Cementitious Materials in Tension (Adapted from (Noorvand et al., 2019))

Equation 3.1. and Equation 3.2. are typically expressed in the form of  $\sigma_0/\sigma_{fc} \geq 1$  and  $J'_b/J_{tip} \geq 1$  where the  $\sigma_0/\sigma_{fc}$  and  $J'_b/J_{tip}$  ratios are referred to as the PSH strength and the PSH energy performance indexes, respectively. As such, succesful design of ECCs or EGCs is achieved when both the PSH strength and PSH energy indexes are greater than one. However, it is important to note that Equation 3.1. and Equation 3.2. assume a perfectly homogeneous material; and therefore, for robust PSH behaviour of the composites, PSH perfomance indexes greater than one are necessary. Based on experimental evidence, it has been determined that PSH

strength and PSH energy indexes greater than 1.3 and 2.7, respectively, correlate well with robust PSH performance (Kanda & Li, 2006). Figure 3.1.a illustrates an ECC with robust PSH behavior.

## **3.2. Experimental Program**

### **3.2.1. Materials**

#### **3.2.1.1. *Activator Solution***

The geopolymer activator solutions utilized in this study consisted of a mixture of potassium hydroxide flakes (99.9% purity, Noah Technologies, TX), amorphous fumed silicon (IV) oxide (Alfa Aesar, MA), and deionized water.

#### **3.2.1.2. *Geopolymer Precursor***

The geopolymer precursor used in this study was metakaolin (MetaMax, BASF), which is an anhydrous calcined form of the clay mineral kaolinite. Per X-ray Fluorescence Spectroscopy (XRF), the metakaolin utilized in this study was mainly composed of  $\text{SiO}_2$  and  $\text{Al}_2\text{O}_3$ , with contents of 51.04 and 46.70% (atomic %), respectively. Furthermore, the loss on ignition (LOI) of the metakaolin material was 0.64%. The morphological details of the metakaolin particles are presented in the SEM micrograph in Figure 3.2. From this image, the irregular and porous microstructure of the metakaolin particles can be clearly observed.

#### **3.2.1.3. *Fine Aggregates***

In this study, two types of sand were evaluated: locally available river sand (RS) and microsilica sand (MS) (U.S. Silica Company, Ottawa, IL). Both sands are composed of crystalline silica. Furthermore, the specific gravity of the RS and MS were 2.62 and 2.65, respectively. To gain insight on the particle size distribution of the sands, a Beckman LS200 Laser Diffraction Particle Size Analyzer was utilized to determine the particle size distribution. The analysis was

performed in a micro-volume module where the sample was suspended in water and agitated for 60 seconds. The particle size distribution of both sands is presented in Figure 3.3. Furthermore, the mean particle size and maximum nominal particle size of both sands are also shown in Figure 3.3. As shown, RS consists of coarser particles than MS. Moreover, SEM images presenting the morphological details of MS and RS are shown in Figure 3.2.b and Figure 3.2.c, respectively, showing that MS have a highly angular particle shape in contrast to the more rounded shape of the RS particles.

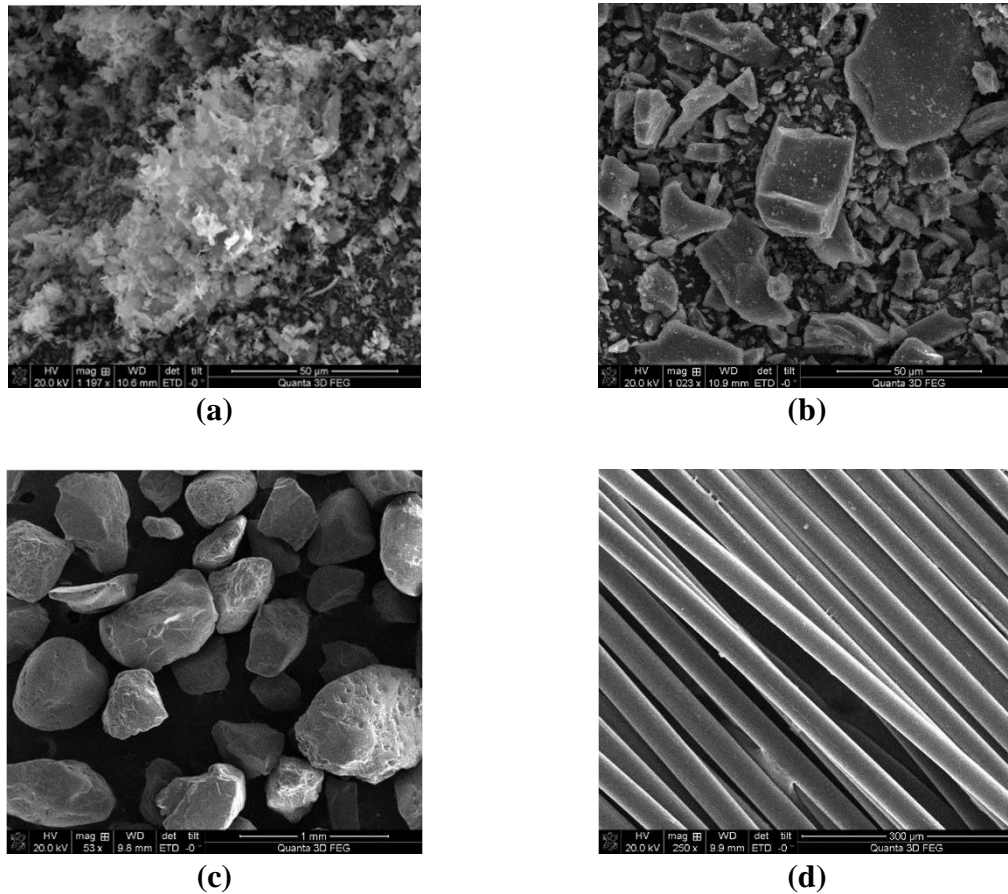


Figure 3.2. Secondary Electron SEM Images of (a) Metakaolin, (b) Microsilica Sand, (c) Silica Sand, and (d) PVA Fiber

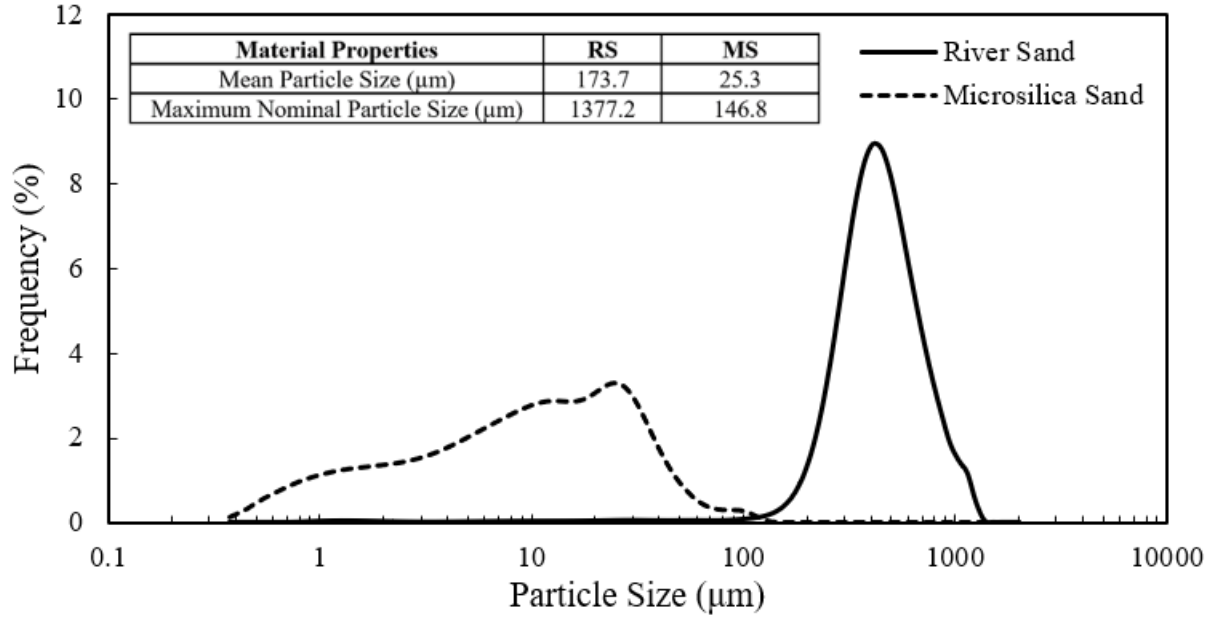


Figure 3.3. Particle Size Distribution of River Sand, and Microsilica Sand

#### 3.2.1.4. *Fibers*

The fibers used in this study were non-oil-coated RECS15 Polyvinyl Alcohol (PVA) fibers (Nycon, PA) in contrast to oil-coated PVA fibers used in previous studies (Constâncio Trindade et al., 2020; Trindade et al., 2020). Non-oil coated PVA fibers were used in the present study as these fibers are readily available in the US market. The fibers had a diameter of 38 μm, length of 8 mm, tensile strength of 1600 MPa, modulus of elasticity of 41 GPa, and specific gravity of 1.3. An SEM image presenting the morphology of the PVA fibers is shown in Figure 3.2.d.

#### 3.2.2. *Mixing Proportions and Mixing*

In this study, the GP binder compositions are labeled as KXYZ, where the first letter denotes the alkali metal cation, i.e., potassium (K), while X, Y, and Z are numbers, which denote the molar ratios of SiO<sub>2</sub>/Al<sub>2</sub>O<sub>3</sub>, water to solids (W/S), and K<sub>2</sub>O/Al<sub>2</sub>O<sub>3</sub> (K/Al), respectively (Lizcano, Gonzalez, et al., 2012). Two GP binder types (i.e., K321 and K331), two sand types (i.e., RS and

MS), and three different levels of PVA fiber content were evaluated (i.e., 0.8%, 1.2%, and 1.6% volume fraction). It is important to mention that the two GP binders utilized were selected based on preliminary experimentation, where these compositions exhibited satisfactory strength, and setting characteristics. In total, 12 different GP materials were manufactured in this study including pure GP binders, GP mortars, and fiber-reinforced GP mortars (i.e., EGCs). Table 3.1. presents the mixture proportions in  $\text{kg/m}^3$  for all the GP materials produced in this study. As shown, the binder consisted of a mixture of the GP precursor (i.e., metakaolin) and the activator solution (i.e., a combination of  $\text{SiO}_2$ ,  $\text{KOH}$ , and  $\text{H}_2\text{O}$ ). For all GP mortar and fiber-reinforced GP mortar mixtures, the sand to GP solids ratio was maintained constant at 0.36.

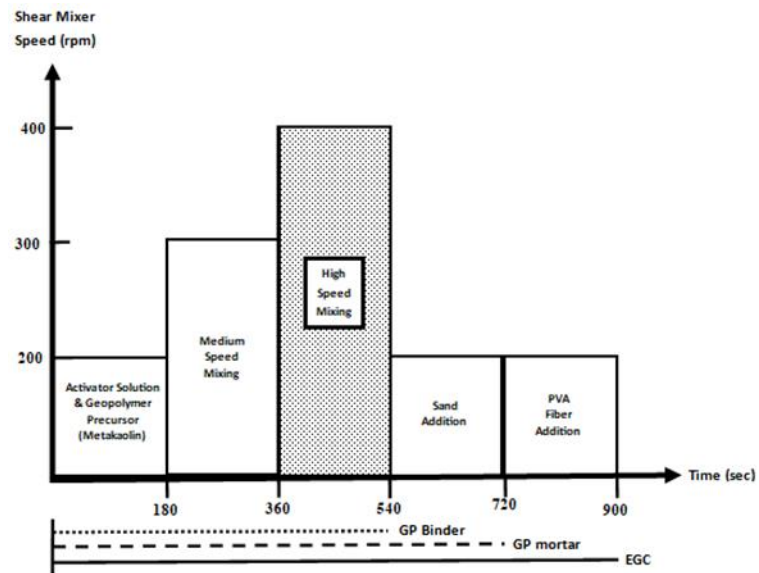
To produce GP materials, a VPM2 Vacuum Shear Mixer (Whip Mix, KY), shown in Figure 3.4.a, was used for mixing. The manufacturing procedure started by mixing metakaolin with the activator solution for 180 seconds at 200 rpm to produce GP binder. After the initial mixing, the GP binder was further mixed at speeds of 300 and 400 rpm for 180 seconds each (for a total of 360 seconds) (Lizcano, Kim, et al., 2012). In the case of GP mortar manufacturing, after the completion of the GP binder mixing process, sand was added and mixed at 200 rpm for 180 seconds. For GP mortars containing fibers (i.e., EGCs), fibers were added to the material upon completion of the mortar mixing procedure and preliminary dispersed using a steel spatula. Subsequently, the fibers and the GP mortars were mixed for an additional 180 seconds at 200 rpm. The mixing procedure is illustrated in Figure 3.4.b.

In an attempt to further enhance fiber dispersion and explore the potential of MK-based GP matrices for EGC application, a modified mixing procedure using a tabletop planetary mixer was also evaluated. The mixing procedure was similar to that presented in Figure 3.4.b, however, in the modified mixing procedure more time was allowed for fiber mixing. In the modified

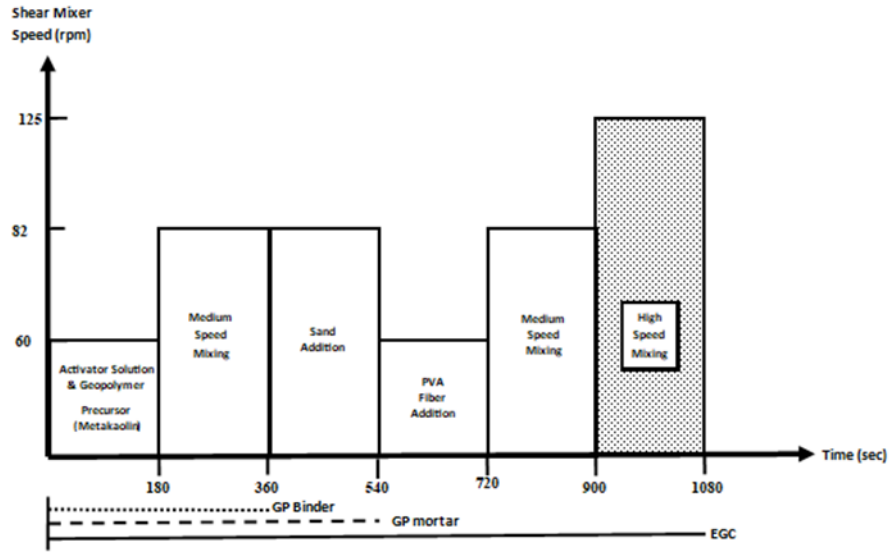
mixing procedure, the GP binder was manufactured by slowly mixing metakaolin with activator solution at stir (i.e., 60 rpm) for 180 seconds and then at level 2 (i.e., 82 rpm) for 180 seconds. Subsequently, to make GP mortar, the sand was added for a period of 60 seconds and mixed for an additional 120 seconds at level 2. Finally, the fibers were mixed until homogeneity was achieved (i.e., when meaningful fiber agglomeration was no longer detected by visual inspection and touch). This occurred approximately after 6 minutes of additional mixing (compared to the original mixing procedure). The modified mixing procedure sequence is summarized in Figure 3.4.c.



(a)



(b)



(c)

Figure 3.4. Geopolymer Manufacturing (a) Vacuum Shear Mixer (b) Mixing Procedure (c) Modified Mixing Procedure

Table 3.1. Mixture Proportions (units in kg/m<sup>3</sup>)

Mix Type	Binder Type	Mix ID	Binder				Fine Aggregate		Fiber
			GP Precursor	Activator Solution			RS	MS	
				Metakaolin	SiO <sub>2</sub>	KOH			
Pure Binder	K321	GP	685.0	218.9	353.5	453.6	-	-	-
	K331	GP	558.3	178.4	288.1	554.6	-	-	-
Mortar	K321	GP-RS	584.1	186.6	301.4	386.8	386.0	-	-
		GP-MS	585.0	186.9	301.9	387.4	-	386.6	-
	K331	GP-RS	489.4	156.4	252.6	486.1	323.4	-	-
		GP-MS	490.1	156.6	252.9	486.8	-	323.9	-
Composite	K321	GP-RS-0.8%PVA	579.3	185.1	298.9	383.6	382.8	-	10.7
		GP-RS-1.2%PVA	576.9	184.3	297.7	382.0	381.2	-	16.0
		GP-RS-1.6%PVA	574.5	183.6	296.5	380.4	379.7	-	21.3
		GP-MS-0.8%PVA	580.2	185.4	299.4	384.2	-	383.5	10.7
		GP-MS-1.2%PVA	577.9	184.6	298.2	382.6	-	381.9	16.0
		GP-MS-1.6%PVA	575.4	183.9	297.0	381.1	-	380.3	21.3



Upon completion of the preparation of the different GP materials, the mixtures were casted into cube and dog-bone shaped molds to prepare specimens for uniaxial compressive and tensile tests, respectively. Immediately after casting, the specimens were placed inside sealed plastic bags to prevent moisture loss as shown in Figure 3.5.a. Cube specimens were demolded within 24 hours; yet dogbone specimens were demolded after 48 hours. This was the case since dogbone specimens are thin and prone to cracking at early stages of curing; therefore, additional time was given to these specimens to allow for strength gain prior to demolding. Right after demolding, specimens were placed back in sealed plastic bags and allowed to cure until their respective testing date (as shown in Figure 3.5.b). Specimens were always maintained under ambient laboratory conditions (i.e.,  $22\pm1^{\circ}\text{C}$ ).



Figure 3.5. Casting and Curing of GP Materials (a) Dogbone Specimens after Casting (b) Cube Specimens during Curing

### 3.2.3. EGC Experimental Testing

#### 3.2.3.1. Compressive Strength Test

The compressive strength of the different GP materials were evaluated according to ASTM C109 on 2-inch cube specimens after 28 days of curing (ASTM C109, 2009). Three specimens were prepared and tested for each material listed in Table 3.1. The experimental tests were performed

by applying pressure with a constant loading rate of 1800 N/sec. The experimental setup is shown in Figure 3.6. during the evaluation of an EGC cube specimen.



Figure 3.6. Experimental Setup for Compressive Strength Test

#### 3.2.3.2. *Uniaxial Tensile Test*

To evaluate the tensile performance of the developed composites, uniaxial tensile tests were conducted in accordance to recommendations of the Japan Society of Civil Engineers (Zhang et al., 2015). Three dog-bone shaped specimens (Figure 3.7.a) were tested at  $28 \pm 1$  days of curing for each selected material. The uniaxial tensile test was conducted using a deformation-controlled loading rate of 0.5 mm/min. The deformation of the specimens in the testing area was recorded by using two linear displacement sensors, one attached to each side of the specimen as shown in Figure 3.7.b.

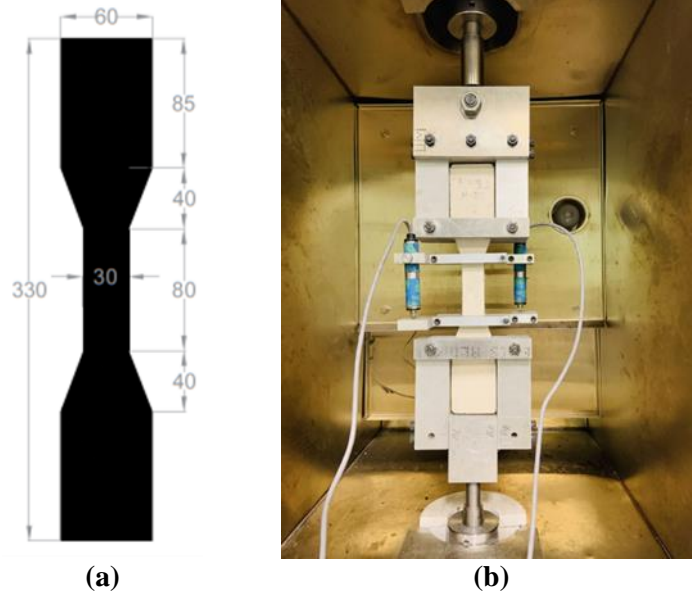


Figure 3.7. (a) Dog-bone Specimen Dimensions (in mm) and (b) Uniaxial Tensile Test Setup

#### 3.2.3.3. *Setting Time*

The initial and final setting time for K321 and K331 GP binders were evaluated per ASTM C191 (ASTM C191, 1987). The Vicat initial setting time was calculated based on the initial contact of metakaolin and activator solution and the time when the penetration is measured or calculated to be 25 mm (ASTM C191, 1987). The Vicat final setting time is the time between the initial contact of metakaolin and the activator solution and the time where the needle does not leave a complete circular impression on the GP surface (ASTM C191, 1987).

#### 3.2.3.4. *Microstructure Characterization*

The microstructure of the different GPs produced in this study was investigated through SEM-EDS. A Quanta™ 3D Dual Beam™ FEG FIB-SEM with EDAX Pegasus EDS/EBSD detectors was utilized. Six GP specimens were prepared for the analysis by vacuum epoxy impregnation and polishing (Figure 3.8.). EpoThin 2 epoxy resin and hardener were utilized for epoxy impregnation. For polishing, the following grit silicon carbide papers were utilized: 120,

240, 400, 600, 800, and 1200 grades. After polishing, the specimens were sputter coated with platinum. The accelerating voltage and current used in the analysis were 20kV and 4nA, respectively.

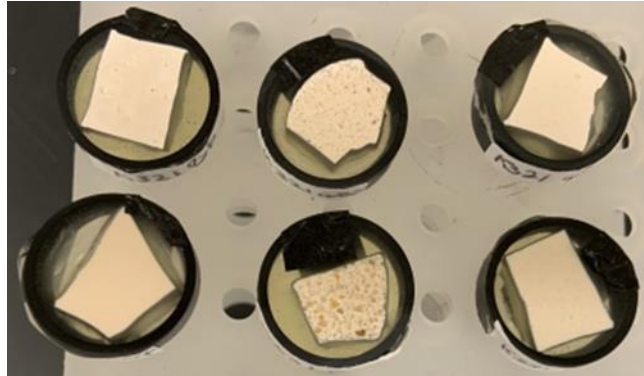


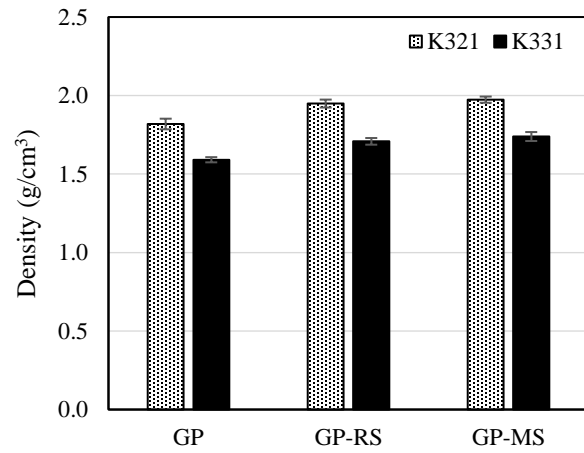
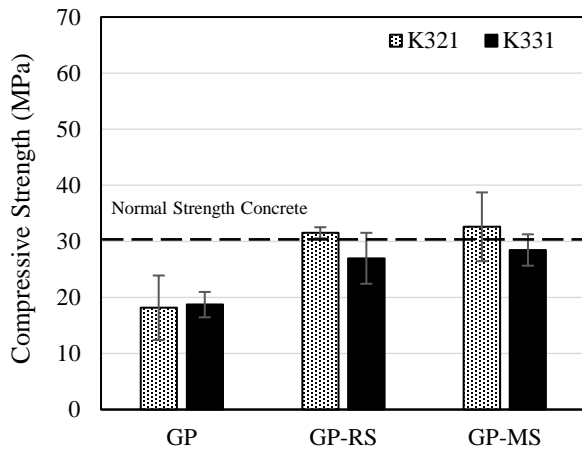
Figure 3.8. Epoxy Impregnated and Polished GP Materials for SEM Analysis

### 3.3. RESULTS AND ANALYSIS

#### 3.3.1. *Compressive Strength Test*

The 28-day compressive strength and density of all the pure GP binders and GP mortars evaluated in this study are presented in Figure 3.9. As shown, pure GP binders exhibited the lowest compressive strength, where the K331 GP binder marginally outperformed the K321 GP binder (i.e., by 3.1%), yet differences were not statistically significant (i.e.,  $p$ -value = 0.90). Interestingly, the incorporation of RS and MS produced dramatic increases in the compressive strength of both K321 and K331 GP binders (of up to 79.6% and 52.1% for K321 and K331, respectively). In cement-based concrete materials, it is established that during a compressive strength test, failure occurs by the propagation and growth of microcracks existing at the generally weak binder/aggregate interfacial transition zone (ITZ) and cracks forming at defect sites (i.e., voids) within the cementitious matrix, which interconnect to form a failure plane

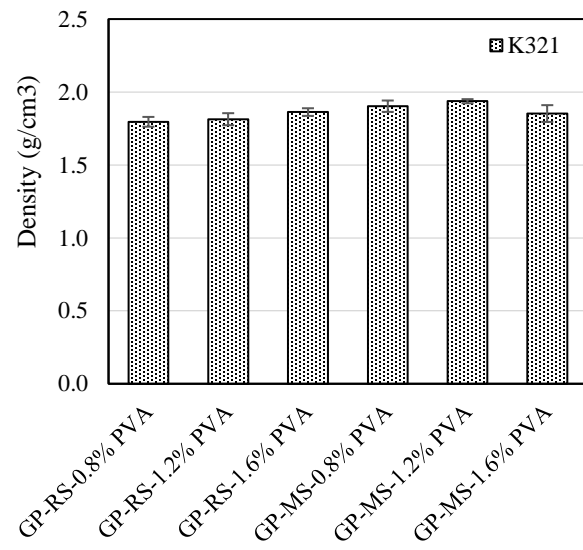
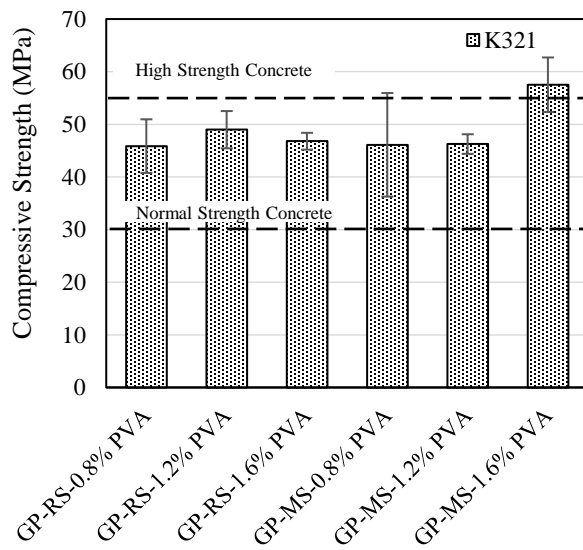
(Paulo & Monteiro, 2006). It is well known, however, that GPs tend to form strong and small ITZs with aggregate in contrast to cement-based binders (Ren & Zhang, 2018; B. Singh et al., 2016). The effect of aggregate in substantially enhancing the compressive strength of GP binders is attributed to the increased tortuosity in the propagation path of microcracks during compressive loading. As cracks propagate within the binder, they intersect aggregate particles and are deflected or continue propagating around the ITZ. This in turn, requires additional energy, especially when strong ITZs exist. Consequently, this is reflected in the increase in the observed compressive strength. Another distinctive trend observed was that the compressive strength of K321 GP mortars exceeded that of K331 GPs. This was expected since K331 binders are processed with a higher amount of water, which has been demonstrated to be detrimental for strength development of GPs (Lizcano, Gonzalez, et al., 2012); however, workability of the binder is improved. It is important to mention that in the case of K331 GP-RS mortar, aggregate segregation was observed, which was attributed to the high workability of the K331 binder (in contrast to that of K321) and the relatively large particle size of RS in contrast to the GP precursor. As a result, only K321 GP mortars were considered as GP matrices for the evaluation of fiber-reinforced composites in the present study (as shown in Table 3.1.).



(a)

(b)

Figure 3.9. GP Binders and Mortars (a) Average 28-Day Compressive Strength (b) Density



(a)

(b)

Figure 3.10. GP Composites (a) Average 28-Day Compressive Strength (b) Density

Figure 3.11. presents the 28-day compressive strength and density of the fiber-reinforced GP composites produced with K321 GP matrices. Comparing the results in Figure 3.11. with those presented in Figure 3.9., it can be observed that the inclusion of PVA fibers produced an important additional increase in the compressive strength of all K321 GP mortars (up to 55.4% and 76.5% for K321 mortars using RS and MS, respectively). In the case of GP mortars

incorporating MS, the highest compressive strength was achieved at the highest fiber content of 1.6%. On the other hand, for GP mortars incorporating RS, 1.2 vol.% of PVA fibers presented the highest compressive strength. It is important to mention that besides increasing the compressive strength, fibers changed the brittle failure mode of the GP mortars to a more ductile-like failure mode. Figure 3.11. shows K321 fiber-reinforced GP mortar specimens after completion of the compressive strength test presenting large deformation and splitting columnar vertical cracks similar to a Type 3 fracture pattern as per ASTM C39. It is noted that pure GP specimens crumbled into pieces upon failure in compression while GP mortars developed a conical failure similar to a Type 1 fracture pattern per ASTM C39; yet, upon removal of the specimens from the testing machine, specimens crumbled. Therefore, pictures of pure GP binder and plain GP mortar specimens are not included in Figure 3.11. The effect of PVA fibers in enhancing the compressive strength and ductility of GP mortars is attributed to the crack-bridging mechanism of fibers. When fibers are added to the system, they can initially act as defect sites for crack initiation when their stiffness is lower than that of the matrix or when fiber/matrix interfacial defects exist. However, upon the initiation of micro-cracks, fibers help to mitigate crack propagation and growth; thus, leading to a delayed failure, which increases the ductility of the composite and can also increase its load carrying capacity depending on the fiber properties and fiber/matrix interfacial characteristics (Naaman, 2018).

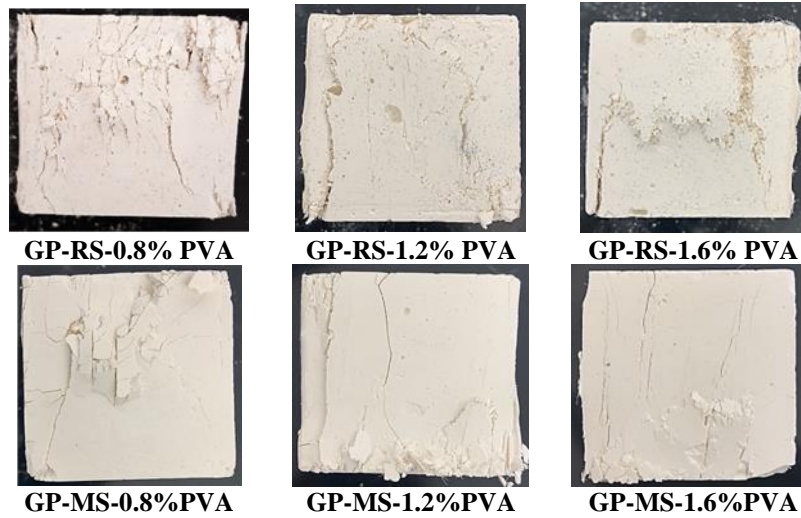


Figure 3.11. Compressive Strength Failure Mode of K321 EGCs

As shown in Figure 3.9. and Figure 3.10., except for GP-RS-1.2%PVA (in contrast to GP-MS-1.2%PVA), plain and fiber-reinforced GP mortars incorporating MS presented a higher compressive strength in contrast to those using RS. Nevertheless, differences in strength between materials incorporating MS and RS were generally marginal, excepting the K321 fiber-reinforced GP mortars with 1.6 vol.% PVA, where the strength increment for the material incorporating MS in contrast to the material using RS was noticeable (i.e., 22.9%). The enhancements in strength generally observed for specimens using MS in contrast to those implementing RS, were attributed mainly to the effect of aggregate size on fiber dispersion and matrix microstructure. When aggregate particle size decreases, the potential for fiber agglomeration is reduced (Sahmaran et al., 2009). Given that MS particles are substantially smaller than those of RS (as presented in Figure 3.3.), materials incorporating MS presented a lower probability of presenting significant fiber agglomeration, which generate weak areas within the composite. Consequently, this is likely the main cause for the enhancements in strength observed for fiber-reinforced materials incorporating MS relative to those using RS. Furthermore, due to its small particles size, MS can act as a filler material, thus enhancing



particle packing and the microstructure of the matrix. In turn, this can allow for improvements in compressive strength of both plain and fiber-reinforced GP mortars.

Figure 3.9.b and Figure 3.10.b present the density of all the produced GP materials, which was assessed by dividing the mass of the cube specimens (measured prior to the compressive strength test) by their volume. The densities of the GP materials developed ranged between 1.59 and 1.97 g/cm<sup>3</sup>, which is significantly lower than the density of regular concrete (i.e., 2.40 g/cm<sup>3</sup>). Despite the relatively low density, all fiber-reinforced GP materials exhibited a compressive strength beyond that of regular concrete (i.e., 30 MPa). Furthermore, the GP material having the highest compressive strength (i.e., K321 GP-MS-1.6%PVA) exceeded the compressive strength of high-strength concrete (i.e., 55 MPa) as defined by the ACI Committee 363 while having a density 22.9% lower than that of regular concrete. As such, this highlights the excellent mechanical properties of the novel MK based composites developed in the present study.

### ***3.3.2. Uniaxial Tensile Test***

In this study, the uniaxial tensile test was conducted on fiber-reinforced GP composites to evaluate whether EGC-like tensile performance was achieved. Furthermore, tests were conducted solely on mixtures containing the highest fiber content (i.e., 1.6% volume fraction) in order to evaluate the maximum tensile performance potential of the developed composites. As such, mixtures K321-GP-RS-1.6%PVA and K321-GP-MS-1.6%PVA were evaluated at 28±1 days of curing.

The uniaxial tensile test stress vs. strain curves are presented in Figure 3.12. It can be observed that for K321-GP-RS-1.6%PVA, specimens exhibited a tensile behavior closer to that

of conventional FRC than that of EGC. In fact, only one specimen presented multiple cracks (i.e., 3 cracks) before failure. On the other hand, for K321-GP-MS-1.6%PVA, two specimens exhibited a multiple cracking pseudo strain-hardening behavior similar to that of EGC materials; yet the PSH performance was not robust. As reported in Figure 3.13.a, the average tensile strain capacity (i.e., the strain corresponding to the tensile strength) of K321-GP-RS-1.6%PVA and K321-GP-MS-1.6%PVA was 0.22 and 0.46%, respectively, which is relatively low for EGC or ECC materials (which typically exhibit tensile strain capacities ranging from 1 to 8%). While the tensile ductility of the developed K321-GP-RS-1.6%PVA and K321-GP-MS-1.6%PVA composites was relatively low for EGC materials, it is important to note that these outperformed the tensile strain capacity of regular concrete or FRC (which is approximately 0.01%) by ~22 and 46 times, respectively; thus, highlighting the distinct tensile characteristics of these materials. Regarding the material composition, it was clearly noticeable that MS was more effective in promoting the PSH behavior of the composites as K321-GP-MS-1.6%PVA exceeded the tensile strain capacity of K321-GP-RS-1.6%PVA by more than 2.1 times. This was attributed to the small particles size of MS in contrast to RS, which can enhance fiber distribution that is paramount for tensile performance of the composite (as this allows for theoretical  $\sigma_0$  and  $J'_b$  values to be neared at any plausible crack plane in the material) (Sahmaran et al., 2009). Furthermore, the reduction in aggregate size can decrease the tortuosity of the propagation path of cracks in the matrix leading to a reduction in  $J_{tip}$  (Li, 2019b; Sahmaran et al., 2009). In turn, this can increase the PSH energy index ( $J'_b/J_{tip}$ ), thus promoting a more ductile response of the composite. This highlights the importance of using aggregate with small particle size in the processing EGC materials.

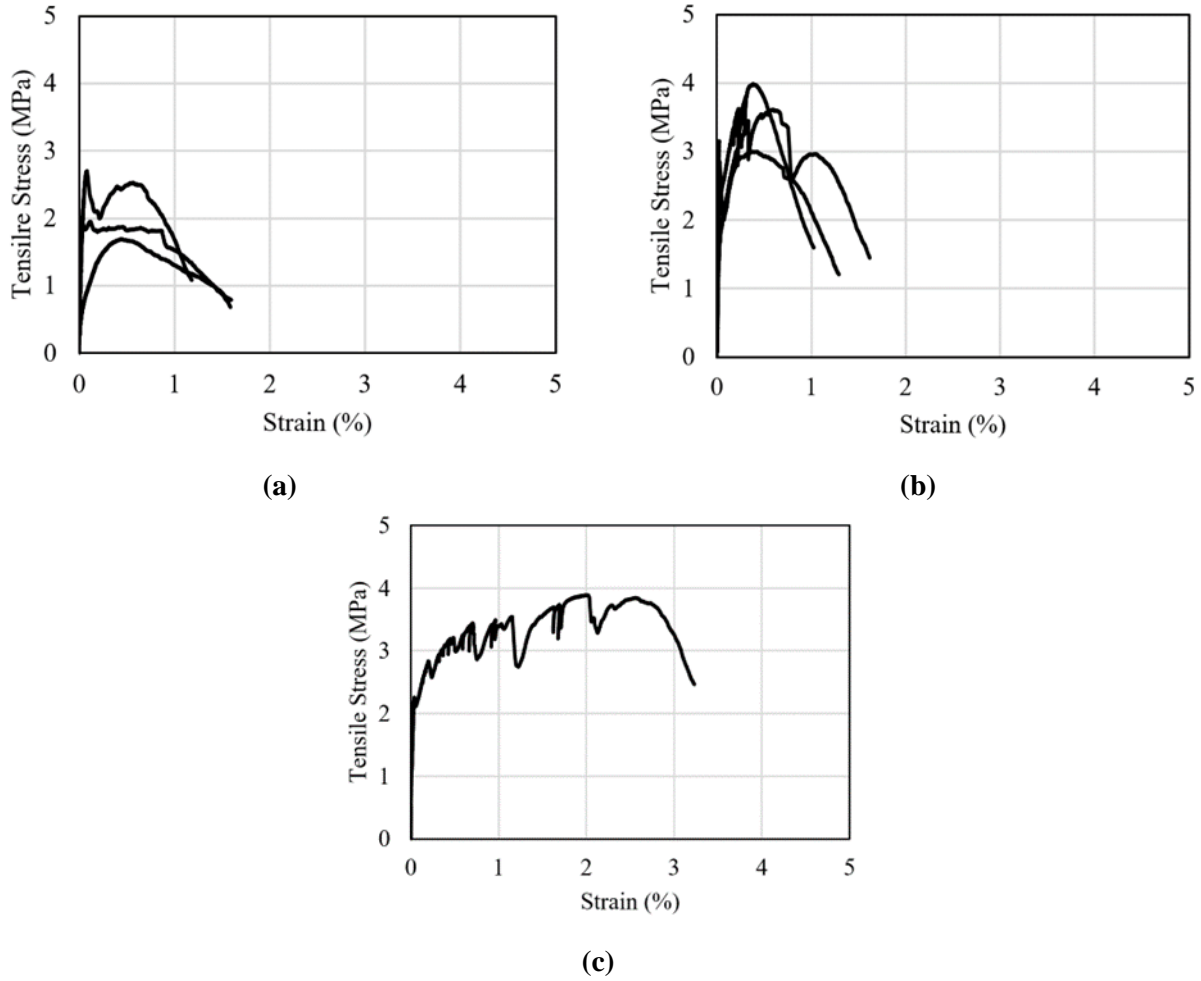


Figure 3.12. Tensile Stress vs. Strain Curves of (a) K321 GP-RS-1.6%PVA (b) K321 GP-MS-1.6%PVA (c) K321 GP-MS-1.6% Using Modified Mixing Procedure

As shown in Figure 3.13.b, the first-cracking strength and ultimate tensile strength of K321-GP-RS-1.6%PVA were 2.10 and 2.12 MPa, respectively. These values reflect a low matrix cracking strength and a low fiber-bridging capacity, as the tensile strength of K321-GP-RS-1.6%PVA significantly underperformed that of normal ECC (which ranges from 4 to 8 MPa) (Li, 2019b). Furthermore, the difference between the first-cracking strength and the tensile strength of the composite was negligible; thus, highlighting the lack of appropriate fiber-bridging capacity to carry the tensile load beyond the cracking strength of the matrix. It is relevant to mention that a low fiber-bridging capacity ( $\sigma_0$ ) can produce a low PSH strength index ( $\sigma_0/\sigma_{fc}$ )

and low complementary energy ( $J'_b$ ), which can prevent the PSH behavior of the composites from occurring. It is hypothesized that the lack in fiber-bridging capacity observed is mainly related to issues in fiber distribution. While mixing the K321-GP-RS-1.6%PVA, fiber clumping was observed due to the highly viscous nature of the K321 GP binder and the relatively large particle size of the RS aggregate. As such, future research should be aimed in ways to enhance fiber distribution by means of rheological control of the mixture to exploit the full potential of these composites.

In the case of K321-GP-MS-1.6%PVA, the first-cracking strength and tensile strength were 3.15 MPa and 3.53 MPa, respectively. This translates into an increase of 12.1% from the first-cracking strength to the tensile strength of the composite, which was superior to that observed for K321-GP-RS-1.6%PVA. Furthermore, the tensile strength of K321-GP-MS-1.6%PVA vastly exceeded that of K321-GP-RS-1.6%PVA (i.e., by 66.5%); thus, demonstrating a substantial improvement in the fiber-bridging capacity of the composite using MS in contrast to that incorporating RS. This behavior is mainly attributed to the enhanced fiber distribution achieved when implementing MS in contrast to RS. Another mechanism, which likely contributed to an enhancement in the fiber-bridging capacity of the K321-GP-MS-1.6%PVA composite was the improved particle packing due to the fine particle size of the MS in contrast to RS, which can improve the fiber/matrix frictional bond. It is important to mention that while K321-GP-MS-1.6%PVA exhibited the best performance, fiber distribution was not optimum as some fiber agglomeration could be identified when checking for homogeneity of the mixture (by visual inspection and touch). In an attempt to further enhance fiber dispersion and explore the potential of MK-based GP matrices for EGC application, three K321-GP-MS-1.6%PVA tensile specimens were manufactured using the modified mixing procedure presented in Figure 3.4.c

using a tabletop planetary mixer. Figure 3.12.c, shows the tensile stress vs. strain curve of a K321-GP-MS-1.6%PVA specimen manufactured using the modified mixing procedure. It is important to mention that only one specimen is shown since two specimen exhibited failure outside of the testing zone (i.e., neck failure). As it can be observed, in Figure 3.12.c, the K321-GP-MS-1.6%PVA specimen showed a clear PSH behavior with a tensile strain capacity of 2.02%, which is ~202 times higher than that of conventional concrete or FRC. Furthermore, in contrast to specimens prepared using the original mixing procedure, the K321-GP-MS-1.6%PVA specimen prepared with the modified procedure exhibited an enhancement in tensile strain capacity of 339% (from 0.46 to 2.02%). This exceptional improvement in tensile ductility observed highlights the importance of fiber distribution in the performance of the composites. Moreover, this shows the potential of MK GP matrices for the development of EGCs. To fully exploit the potential of MK GPs in the manufacture of EGCs, future research should be directed towards optimizing the rheological characteristics of MK GPs as well as mixing procedures to assure proper fiber dispersion. This will not only improve the mechanical properties of the composites, but also reduce variability in their mechanical properties, which is key for implementation in civil infrastructure. In the present study, high variability observed in the mechanical properties of some of the materials prepared, was mainly attributed to the issue of fiber dispersion. Nevertheless, the limited number of specimens (i.e., 3 specimens) evaluated did also exacerbate variability. It is relevant to mention that given that the PVA fibers used in the present study were not oil-coated, and therefore a strong fiber/matrix chemical bond ( $G_d$ ) may have developed, thus negatively affecting the tensile ductility of the composites. In cement-based composites, oil-coating of PVA fibers has been shown to be effective to reduce the fiber/matrix chemical bond, thus reducing the slope of the rising part of the fiber-bridging relation curve and

therefore increasing  $J'_b$ , which promotes the PSH behavior of the composites (Redon et al., 2001b). Consequently, future research should also focus on assessing the fiber/matrix interfacial characteristics of oil-coated PVA fibers in contrast to those of pristine PVA fibers in MK-based GP matrices.

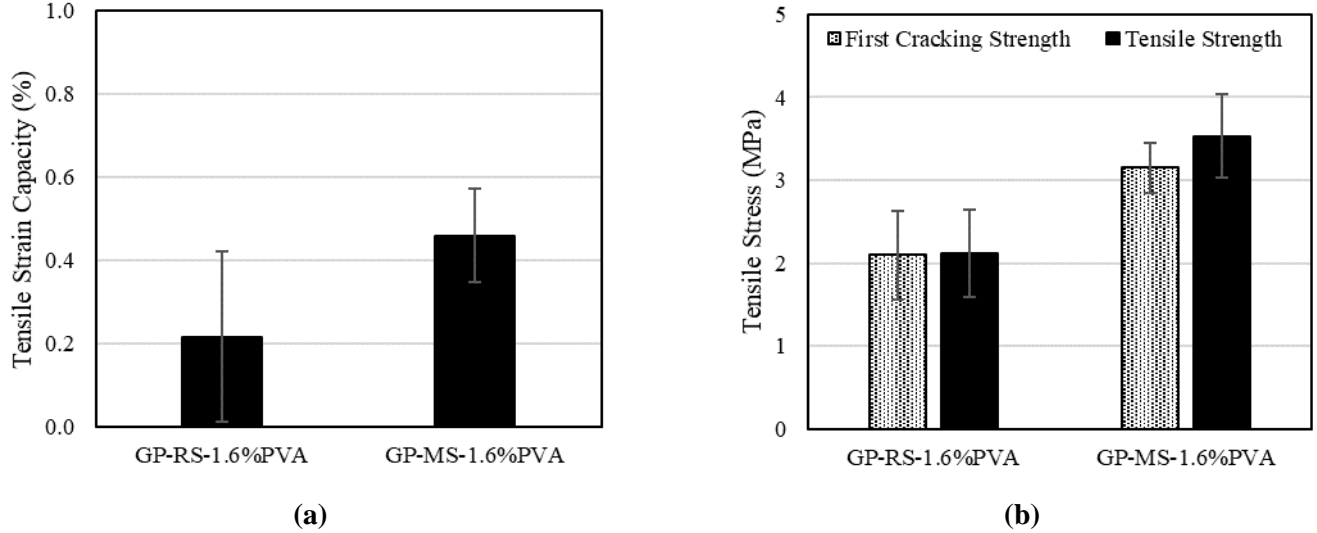


Figure 3.13. Average Tensile Test Results (a) Tensile Strain Capacity (b) First-Cracking Strength and Tensile Strength

### 3.3.3. Microstructure Characterization

The SEM-BSE images of different GP binders evaluated in this study after 14 weeks of curing, are presented in Figure 3.14. As shown in Figure 3.14.a and b, most likely due to presence of some unreacted metakaolin particles (i.e., white particles) were encountered within the geopolymer gel in both binders; thus, signaling an incomplete polymerization reaction in some areas of the binder. To gain insight on the chemical composition of the different GPs prepared in this study, EDS spectra were collected under spot mode for all the GP binders and mortars evaluated in this study. The EDS spectra collected were obtained from the binder portion of the different GP materials. A total of 184 EDS spectra were collected for the analysis.

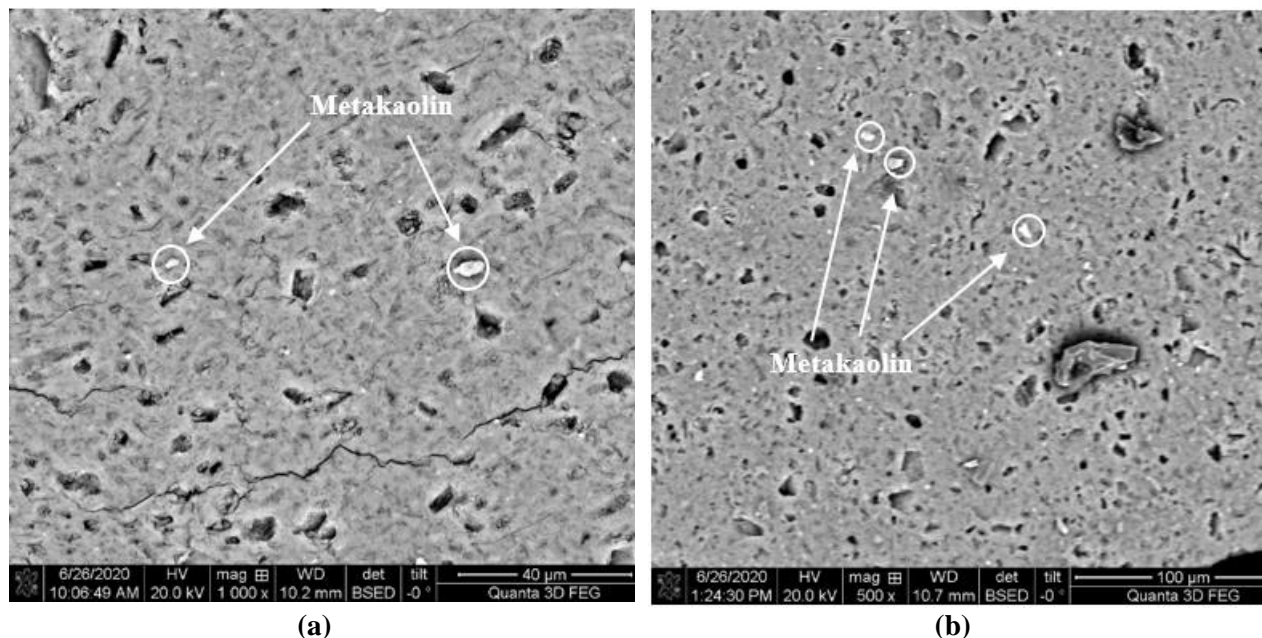


Figure 3.14. BSE Images of (a) K321 GP Binder (b) K331 GP Binder

Based on the EDS data,  $\text{SiO}_2/\text{Al}_2\text{O}_3$  vs.  $\text{K}/\text{Al}$  atomic ratio plots were generated as shown in Figure 3.15. for K321 and K331 GP materials, respectively. Furthermore, the average  $\text{SiO}_2/\text{Al}_2\text{O}_3$  and  $\text{K}/\text{Al}$  ratios were calculated for all GP materials and are also presented in Figure 3.15. It can be observed in this figure that the average  $\text{SiO}_2/\text{Al}_2\text{O}_3$  and  $\text{K}/\text{Al}$  ratios for K321 pure GP binder were 3.04 and 1.13, respectively. As such, in contrast to the K321 target binder composition, differences of 1.48 and 12.92% were encountered for  $\text{SiO}_2/\text{Al}_2\text{O}_3$  and  $\text{K}/\text{Al}$  atomic ratios, respectively. In the case of the K331 pure GP binder, the average  $\text{SiO}_2/\text{Al}_2\text{O}_3$  and  $\text{K}/\text{Al}$  ratios obtained were 3.02 and 1.08, respectively; thus, exhibiting differences of 0.78 and 7.69% for  $\text{SiO}_2/\text{Al}_2\text{O}_3$  and  $\text{K}/\text{Al}$  targeted atomic ratios, accordingly. Consequently, for both K321 and K331 GP binders, a close agreement was encountered between the design composition and the actual chemical composition of the geopolymer gel encountered through EDS analysis; thus, validating the composition of the GP materials produced.

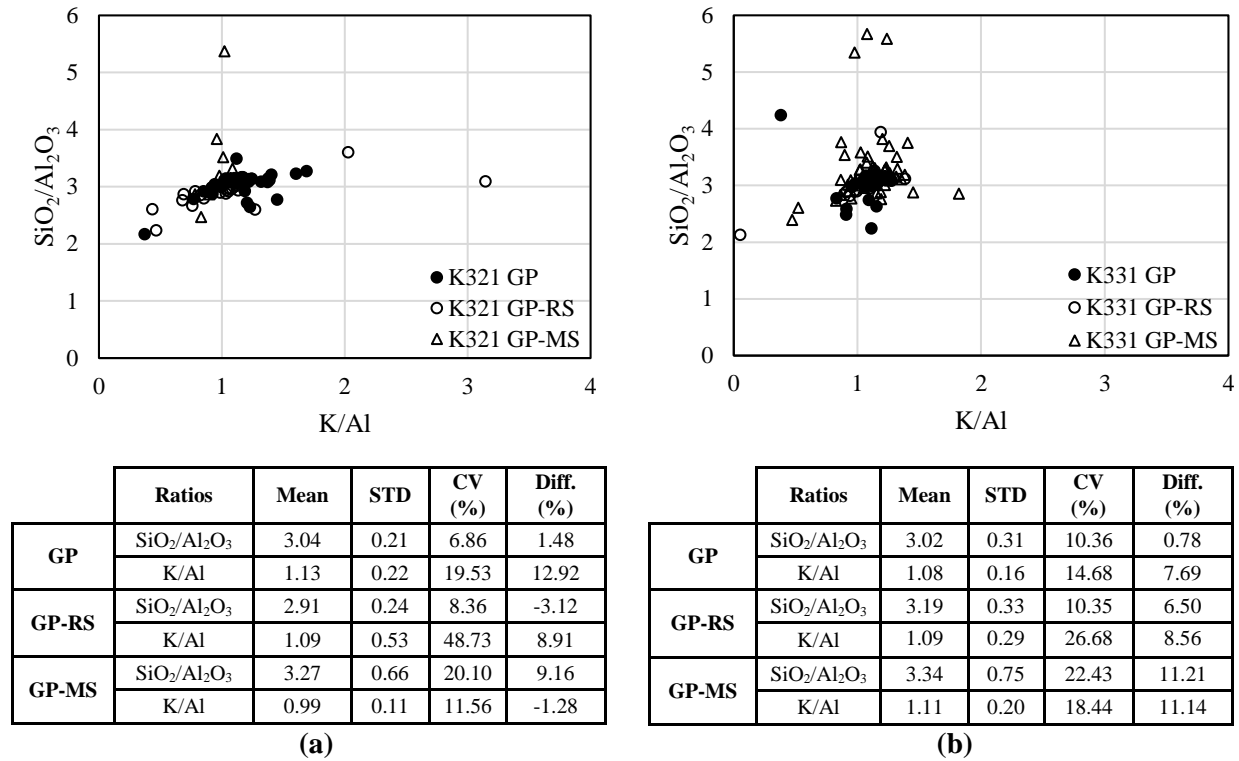


Figure 3.15. Atomic Ratio Plot for (a) K321 and (b) K331 GPs

In the case of GP mortars, a similar situation to that of pure GP binders was observed, where the SiO<sub>2</sub>/Al<sub>2</sub>O<sub>3</sub> and K/Al ratios were in close agreement to those of the target GP composition. Furthermore, based on an analysis of variance (ANOVA) conducted at a significance level of 0.05, no statistically significant differences were encountered in the SiO<sub>2</sub>/Al<sub>2</sub>O<sub>3</sub> and K/Al ratios of the different GP materials (i.e., GP, GP-RS, and GP-MS) for each binder type (i.e., K321 and K331). For materials using K321-based GP materials SiO<sub>2</sub>/Al<sub>2</sub>O<sub>3</sub> and K/Al p-values were 0.60 and 0.88, respectively. On the other hand, p-values for K331-based GP materials were 0.75 and 0.99 for the SiO<sub>2</sub>/Al<sub>2</sub>O<sub>3</sub> and K/Al ratios, respectively. This in turn, indicated that the addition of sand did not have a significant effect on the GP binder composition. It is worth noting that the differences in chemical composition and variability observed in Figure 3.15. arise mainly from the contribution of X-rays from phases other than the GP binder. While the EDS spectra were targeted to the binder phase of the material, due to the interaction volume



generated by the electron beam, the resolution of the analysis is usually larger than that of an individual phase. As such, X-ray contributions from other phases within the material such as silica sand particles and unreacted metakaolin or KOH particles may occur, thus adding error. This phenomenon is evident in Figure 3.15., where materials containing sand exhibited several EDS spectra with high Si/Al ratios.

#### ***3.3.4. Setting Time***

The setting time of the different GP binders produced in this study was investigated per ASTM C191. Figure 3.16. present the Vicat needle penetration vs. time curves for both GP binders as well as the initial and final setting times. As seen in Figure 3.16., the K331 GP binder exhibited higher initial and final setting time compared to K321 GP binder. The increase in initial and final setting time for K331 in contrast to K321 was of 96.9% (i.e., from 127 to 250 minutes) and 90.9% (i.e., from 165 to 315), respectively. This was attributed to the increased amount of water used to process the K331 GP binder in contrast to K321. It is relevant to mention that the relatively rapid setting characteristics of the K321 GP binder, which was used for the development of fiber-reinforced GP composites, may be useful for transportation infrastructure applications such as patch repairs.

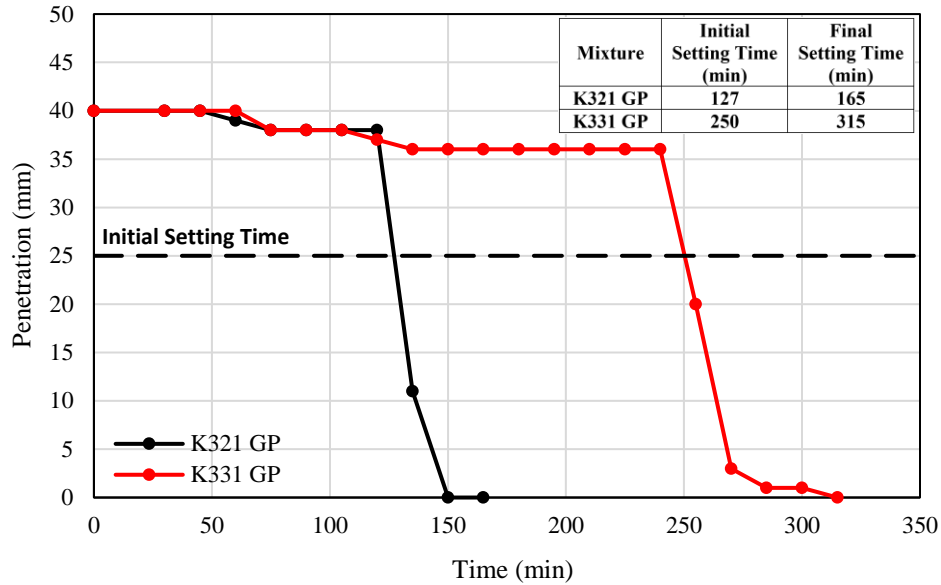


Figure 3.16. Setting Time Experimental Results

### 3.4. RESULTS AND CONCLUSION

This study investigated the effect of binder type, aggregate type, and PVA fiber content on the properties of metakaolin-based GP mortars and fiber-reinforced GP composites, i.e., EGCs.

Based on the experimental results, the following conclusions can be drawn:

- The compressive strength of GP mortars was substantially greater to that of pure GP binders. This was attributed to the likely formation of a strong aggregate/binder ITZ and the increased tortuosity of the propagation path of microcracks. Furthermore, GP mortars implementing the K321 GP binder exhibited a greater compressive strength in contrast to those using the K331 GP binder. This was explained by the higher amount of water used to process K331 GP binders in contrast to K321. K331 GP mortars implementing RS exhibited noticeable aggregate segregation attributed mainly to the high workability of the K331 GP binder. Consequently, only K321 GP mortars were considered as GP matrices for the evaluation of fiber-reinforced composites.

- The incorporation of fibers in GP mortars produced important enhancements in compressive strength, where the greatest compressive strength occurred for the GP composite implementing K321 GP binder, microsilica sand, and the highest fiber content evaluated of 1.6% volume fraction. In the case of aggregate type, generally, the use of MS (in contrast to RS) tended to produce higher compressive strengths in both fiber-reinforced GP composites and plain GP mortars. Higher compressive strengths reported for materials implementing MS were attributed to the ability of MS to improve the particle packing and microstructure of the GP matrix as well as enhance fiber dispersion (due to the small particle size of MS in contrast to RS). All fiber-reinforced GP composites evaluated in this study exceeded the compressive strength of regular concrete (i.e., 30 MPa). Furthermore, these materials exhibited low densities (i.e., from 1.80 to 1.94 g/cm<sup>3</sup>) relative to conventional concrete; as such, the strength to weight ratio exhibited by fiber-reinforced GP composites is notable.
- Tensile PSH behavior of novel MK based PVA-EGCs was confirmed by uniaxial tensile test of composites implementing MS and PVA fiber at 1.6% volume fraction. However, the PSH behavior was not robust due to the lack of proper fiber dispersion. It was observed that the utilization of MS produces a superior tensile performance in contrast to RS. This was attributed to an enhanced fiber dispersion and improved particle packing and microstructure, which can improve the fiber/matrix frictional bond.
- SEM BSE images revealed unreacted metakaolin particles in some areas within the geopolymer gel of both GP binders evaluated in this study; therefore, suggesting incomplete geopolymerization. Furthermore, SEM-EDS microchemical analysis of geopolymer gel

encountered close agreement between the target composition of the binders and the actual chemical composition encountered in the specimens evaluated, which validated the composition of the GP materials produced.

- Incrementing the processing water used for GP binder synthesis increased the initial and final setting time of the materials. Furthermore, the GP binder containing the least amount of water (i.e., K321), which was used for the development of fiber-reinforced GP composites, exhibited a relatively rapid initial and final setting time, which may be useful for applications such as patch repairs.

Overall, the best performing composite developed, K321-GP-MS-1.6%PVA, exhibited a compressive strength of 57.5 MPa, a tensile strength of 3.53 MPa, and a tensile strain capacity up to 2.02%. As such, this material can be classified as a high-strength concrete while simultaneously exhibiting a tensile ductility two orders of magnitude greater to that of conventional concrete or FRC. While excellent mechanical properties were achieved, to fully exploit the potential of these novel composites, future research is encouraged to solve poor fiber dispersion through rheology modification of the fresh GP matrix. Furthermore, evaluating alternative fine aggregate exhibiting similar characteristics to that of microsilica sand is encouraged for future research as microsilica sand is expensive and the use of coarser sands can limit the PSH behavior of the composites. EGCs may be an excellent material alternative for use in the repair of transportation infrastructure due to its high strength and ductility. To this end, evaluating the dimensional stability of EGCs and bond characteristics with PCC is of great interest for future research.

### **3.5. ACKNOWLEDGEMENTS**

The authors of the paper greatly appreciate the financial support of Tran-SET through the 19CLSU04 grant as well as the support from the Louisiana Transportation Research Center (LTRC). The authors would also like to acknowledge BASF and US Silica for providing the metakaolin and microsilica sand utilized in this study. Finally, the authors would like to acknowledge the contribution of Zhen Sang.

### **3.6. AUTHOR CONTRIBUTIONS**

The authors confirm contribution to the paper as follows: study conception and design: Gabriel Arce, Marwa Hassan, Miladin Radovic, Svetlana Sukhishvili, Ruwa AbuFarsakh; data collection: Ruwa AbuFarsakh; analysis and interpretation of results: Gabriel Arce, Ruwa AbuFarsakh, Marwa Hassan, Miladin Radovic, Svetlana Sukhishvili, Oscar Huang; draft manuscript preparation: Ruwa AbuFarsakh, Gabriel Arce, Marwa Hassan, Oscar Huang, Miladin Radovic, Svetlana Sukhishvili. All authors reviewed the results and approved the final version of the manuscript.

#### 4. SUMMARY AND CONCLUSIONS

The deterioration of the civil infrastructure shed a spotlight on the environmental impacts, such as increased global anthropogenic emission, associated with rehabilitation and rebuilding which require vast amounts of Portland cement concrete (PCC). However, to reduce the environmental impacts, there is a need to develop a less emission intensive and more energy efficient, durable, and resilient material as a sustainable alternative to PCC. Furthermore, there is a need to develop a material with a longer lifespan. To this end, geopolymer based binders were developed as an alternative to the cementitious binder in engineered cementitious composite. Also known as engineered geopolymer composites, this new sustainable material is designed to increase durability to achieve infrastructure with a longer lifespan.

The goal of this study was to develop metakaolin based engineered geopolymer composites as a sustainable alternative to engineered cementitious composites. To achieve this goal, 1 inch cylinder potassium activated metakaolin geopolymer binders and mortars were manufactured with a VPM2 vacuum shear mixer at Texas A&M with  $\text{SiO}_2/\text{Al}_2\text{O}_3$  and water/GP solids ratios ranging from 2 to 4 and sand to binder (mass ratio) of 2.75. Furthermore, they were tested in compression and the best performing material/s were chosen based on workability and compressive strength. Pure binder, mortars, and fiber reinforced mortars of the two best performing binder compositions (i.e., K321 and K331) were then scaled up at LSU to make 2-inch cubes for compressive strength test. Furthermore, uniaxial tensile test dogbone specimens were manufactured for the fiber reinforced mortar with the highest fiber content (i.e., 1.6%PVA) to produce engineered geopolymer composites. Moreover, a modified mixing procedure (using a planetary tabletop mixer instead of a VPM2 vacuum shear mixer) was used to enhance the fiber dispersion for the best performing engineered geopolymer composite. The microstructure of the

binders and mortars were analyzed via SEM-EDS to validate the binder composition produced. Lastly, the setting time of the binders were determined.

The compressive strength results revealed that GP mortars were significantly greater than pure GP binders as the geopolymers tend to develop strong aggregate/binder ITZ resulting in an increased tortuosity of the microcracks. Furthermore, due to the use of more water in the processing of K331 GP materials, K321 GP materials have greater compressive strength. Nevertheless, the increased workability of K331 GPs implementing RS resulted in the segregation of the RS particles. As such, only K321 GP mortars were considered as GP matrices for the evaluation of fiber-reinforced composites. As a matter of fact, the addition of PVA fibers in the K321 GP mortars produced a significant improvement in compressive strength where the fiber reinforced composite with the greatest compressive strength (i.e., 57.52 MPa) is K321 MS-1.6%PVA classifying it as high strength concrete per ACI Committee 363. In the case of aggregate type, microsilica sand tended to produce higher compressive strength than river sand for both GP mortars and fiber reinforced composites as a result of the improved particle packing and fiber dispersion associated with the smaller particle size of microsilica sand in contrast to river sand. In conclusion, all fiber reinforced composites evaluated exhibited low densities (i.e., from 1.80 to 1.94 g/cm<sup>3</sup>) relative to conventional concrete (i.e., 2.3 g/cm<sup>3</sup>) while exceeding the compressive strength of regular concrete (i.e., 30 MPa).

Upon conducting uniaxial tensile test for the fiber reinforced composites consisting of the highest fiber content (1.6%PVA), tensile pseudo strain hardening behavior was confirmed for the K321 MS-1.6%PVA composite with a tensile strength and strain capacity of 3.5 MPa and 0.46%. However, the PSH behavior was not robust due to the lack of fiber dispersion. For this reason,

only K321 MS-1.6%PVA composite was manufactured using a modified mixing procedure. As expected, the tensile strength and strain capacity increased by 11% (from 3.53 to 3.89 MPa) and 339% (from 0.46 to 2.02%) indicating better fiber dispersion. To be classified as an engineered geopolymer composite, the tensile strength and strain capacity must be greater than 2 MPa and 1%. As such, K321 MS-1.6%PVA qualifies as an engineered geopolymer composite.

Scanning electron microscopy results indicated incomplete polymerization reaction in some areas of both GP binders. Additionally, scanning electron microscopy accompanied with electron dispersive spectroscopy results revealed that the pure geopolymer compositions manufactured were in close agreement with the design composition. However, for both K321 and K331 mortars, the addition of sand did not have a significant effect on the GP binder composition. The setting time of binders indicated that incrementing the water increases the initial and final setting times of the GP binder from 127 to 250 minutes and 165 to 315 minutes.

In conclusion, K321 MS-1.6%PVA composite can be deemed as the best performing material with a compressive strength of 57.5 MPa, a tensile strength up to 3.89 MPa, and a tensile strain capacity up to 2.02%. As such, this material can be classified as a high strength concrete and engineered geopolymer composites. Furthermore, its rapid setting time can be useful for repair applications.



## 5. FUTURE WORK

Based on the results of this study, geopolymers based binders can be used to manufacture Engineered Geopolymer Composites (EGCs). Therefore, the results of this study leads to future research opportunities, including:

- Future research studies should be conducted to evaluate different types of fibers (i.e., ultrahigh molecular weight polyethylene, polypropylene, etc.) as an alternative to PVA.
- Future studies should also aim to evaluate the effect of sand type and content to find the optimum sand content rather than assuming a sand to binder ratio similar to that of cement-based composites of 0.36 wt.%. Future studies should also aim at evaluating the effect of cation type and content (e.g., 75 mol% potassium and 25 mol% sodium) along with different cation to aluminum ratios (e.g., 0.8). as an alternative cation to potassium and cation to aluminum ratio of 1.

## APPENDIX. COPYRIGHT PERMISSION

Dear Ruwa Abufarsakh,

Per the SAGE Author Archiving and Re-Use Guidelines (found in full at <https://us.sagepub.com/en-us/nam/journal-author-archiving-policies-and-re-use>):

**You may use the Final Published PDF** (or **Original Submission** or **Accepted Manuscript**, if preferred) in your dissertation or thesis, including where the dissertation or thesis will be posted in any electronic Institutional Repository or database.

***Provided that:***

- Access to the Original Submission and Accepted Manuscript is provided at no charge.
- Any re-use terms for users of websites and repositories (where your **Original Submission** or **Accepted Manuscript** are posted) are restricted to non-commercial and no derivative uses.
- You may not post the **Final Published PDF** on any unrestricted website or repository without permission from SAGE.
- You may not republish or translate any version of your Contribution in another journal without prior permission from SAGE.
- The journal as the original publication of your Contribution is appropriately credited by including the full citation information each time your Contribution, or excerpts, are further distributed or re-used:
  - After your Contribution has been accepted for publication and until it is assigned a DOI, please include a statement that your Contribution has been accepted for publication in the journal.
  - Once full citation information for your Contribution is available, please include this with your posted Contribution, in a format similar to the following:  
**Author(s), Contribution Title, Journal Title (Journal Volume Number and Issue Number) pp. xx-xx. Copyright © [year] (Copyright Holder). DOI: [DOI number].**

Best,  
Kisna

Transportation Research Record Editorial Office  
Transportation Research Board  
The National Academies of Sciences, Engineering, and Medicine  
[trr@nas.edu](mailto:trr@nas.edu) | [www.TRB.org](http://www.TRB.org)  
Transportation Research Record - [trr.editorialmanager.com](http://trr.editorialmanager.com)  
TRB Annual Meeting Paper Submission - [trbam.editorialmanager.com](http://trbam.editorialmanager.com)

*The National Academies of*  
SCIENCES • ENGINEERING • MEDICINE



## REFERENCES

- A. M. Aguirre-Guerrero, R. A. Robayo-Salazar, and R. M. de G. (2017). A novel geopolymer application: Coatings to protect reinforced concrete against corrosion. *Application Clay Scientific*, 135, 437–446.
- Abdullah, M. M. A. B., Razak, R. A., & Yahya, Z. (2012). *Geopolymer Composite for High Temperature Exposure*.
- Abdulsalam Arafa, S., Mohd Ali, A. Z., Rahmat, S. N., & Lee, Y. L. (2017). Optimum Mix for Pervious Geopolymer Concrete (GEOCRETE) Based on Water Permeability and Compressive Strength. *MATEC Web of Conferences*, 103, 1–9. <https://doi.org/10.1051/mateconf/201710301024>
- Advanced Steel Fibers for Ultra High Performance Concrete*. (2020). HiPer Fiber.LLC.
- Al-Qutaifi, S., Nazari, A., & Bagheri, A. (2018). Mechanical properties of layered geopolymer structures applicable in concrete 3D-printing. *Construction and Building Materials*, 176, 690–699. <https://doi.org/10.1016/j.conbuildmat.2018.04.195>
- Al-Shathr, B. S., Al-Attar, T. S., & Hasan, Z. A. (2015). Optimization of Geopolymer Concrete Based on Local Iraqi Metakaolin. *The 2nd International Conference of Buildings, Construction and Environmental Engineering*, 45, 97–100. [https://www.uotechnology.edu.iq/dep-building/IMACT\\_FACTOR/dr-basil-2016-2.pdf](https://www.uotechnology.edu.iq/dep-building/IMACT_FACTOR/dr-basil-2016-2.pdf)
- Al-Shether, B., Al-Attar, T., & A. Hassan, Z. (2016). Effect of Curing System on Metakaolin Based Geopolymer Concrete. *Journal of University of Babylon - Engineering Sciences*, 24(3), 569–576.
- Alrefaei, Y., & Dai, J. G. (2018). Tensile behavior and microstructure of hybrid fiber ambient cured one-part engineered geopolymer composites. *Construction and Building Materials*, 184, 419–431. <https://doi.org/10.1016/j.conbuildmat.2018.07.012>
- American Sugarcane League. (2022). *Louisiana Sugarcane Statistics*.
- Annapurna, D., Kishore, R., & Anil, K. (2020). *Effect of Different Aggregates on Alkali Silica Reaction of Geopolymer Concrete*. <http://www.springer.com/series/16172>
- Arce, G., Hassan, M., Radovic, M., Sukhishvili, S., AbuFarsakh, R., Huang, O., Zhen, S., Cornejo, M., & Baykara, H. (2020). Engineered Geopolymer Composites (EGCs) for Sustainable Transportation Infrastructure. In *Publications* (Issue 19). [https://digitalcommons.lsu.edu/transet\\_pubs/89](https://digitalcommons.lsu.edu/transet_pubs/89)
- Arce, G., Noorvand, H., Hassan, M., Rupnow, T., & Hungria, R. (2019). Cost-Effective ECC with Low Fiber Content for Pavement Application. *MATEC Web of Conferences*, 271, 07001. <https://doi.org/10.1051/mateconf/201927107001>
- ASTM C109. (2009). Standard Test Method for Compressive Strength of Hydraulic Cement

- Mortars (Using 2-in. or [50-mm] Cube Specimens). *Engineered Concrete*, 29–31. <https://doi.org/10.1201/9781420091175-c5>
- ASTM C191. (1987). *Standard Test Methods for Time of Setting of Hydraulic Cement by Vicat Needle*. 1–8. <https://doi.org/10.1520/C0191-19.2>
- ASTM C618. (2019). *Standard Specification for Coal Fly Ash and Raw or Calcined Natural Pozzolan for Use*. 1–5. <https://doi.org/10.1520/C0618-19.2>
- ASTM C989. (2019). *Standard Specification for Slag Cement for Use in Concrete and Mortars. ASTM*, 1–7. <https://doi.org/10.1520/C0989>
- Azarsa, P., & Gupta, R. (2020). Freeze-thaw performance characterization and leachability of potassium-based geopolymer concrete. *Journal of Composites Science*, 4(2). <https://doi.org/10.3390/jcs4020045>
- Bakharev, T. (2005). Resistance of geopolymer materials to acid attack. *Cement and Concrete Research*, 35(4), 658–670. <https://doi.org/10.1016/j.cemconres.2004.06.005>
- Bakharev, T., Sanjayan, J. G., & Cheng, Y. B. (2000). Effect of admixtures on properties of alkali-activated slag concrete. In *Cement and Concrete Research* (Vol. 30, Issue 9, pp. 1367–1374). [https://doi.org/10.1016/S0008-8846\(00\)00349-5](https://doi.org/10.1016/S0008-8846(00)00349-5)
- BASF. (2007). *MetaMax* ®. 2007.
- Berndt, M. L., Sanjayan, J. G., Sagoe-Crentsil, K., & Heidrich, C. (2013). Overcoming barriers to implementation of geopolymer concrete. *Concrete* 2013, 1.
- C. Tennakoon, A. Shayan, J. G. Sanjayan, and A. X. (2017). Chloride ingress and steel corrosion in geopolymer concrete based on long term tests. *Material Design*, 116, 287–299.
- Castel, A., Foster, S. J., Ng, T., Sanjayan, J. G., & Gilbert, R. I. (2016). Creep and drying shrinkage of a blended slag and low calcium fly ash geopolymer Concrete. *Materials and Structures/Materiaux et Constructions*, 49(5), 1619–1628. <https://doi.org/10.1617/s11527-015-0599-1>
- Chem Europe. (n.d.). *Ultra-high-molecular-weight polyethylene*. Chem Europe. [https://www.chemurope.com/en/encyclopedia/Ultra-high-molecular-weight\\_polyethylene.html](https://www.chemurope.com/en/encyclopedia/Ultra-high-molecular-weight_polyethylene.html)
- Choi, J. Il, Lee, B. Y., Ranade, R., Li, V. C., & Lee, Y. (2016). Ultra-high-ductile behavior of a polyethylene fiber-reinforced alkali-activated slag-based composite. *Cement and Concrete Composites*, 70, 153–158. <https://doi.org/10.1016/j.cemconcomp.2016.04.002>
- Constância Trindade, A. C., Curosu, I., Liebscher, M., Mechtcherine, V., & de Andrade Silva, F. (2020). On the mechanical performance of K- and Na-based strain-hardening geopolymer composites (SHGC) reinforced with PVA fibers. *Construction and Building Materials*, 248(118558). <https://doi.org/10.1016/j.conbuildmat.2020.118558>

- Criado, M., Palomo, A., Fernández-Jiménez, A., & Banfill, P. F. G. (2009). Alkali activated fly ash: Effect of admixtures on paste rheology. *Rheologica Acta*, 48(4), 447–455. <https://doi.org/10.1007/s00397-008-0345-5>
- Davidovits, J., Davidovitis, J., & Davidovits, J. (2015). *Geopolymer Chemistry & Applications* (4th ed.). Institut Geopolymer.
- Deb, P. S., Nath, P., & Sarker, P. K. (2015). Drying shrinkage of slag blended fly ash geopolymer concrete cured at room temperature. In *Procedia Engineering* (Vol. 125, pp. 594–600). <https://doi.org/10.1016/j.proeng.2015.11.066>
- Ding, Y., Yu, K. Q., Yu, J. tao, & Xu, S. lang. (2018). Structural behaviors of ultra-high performance engineered cementitious composites (UHP-ECC) beams subjected to bending-experimental study. *Construction and Building Materials*, 177, 102–115. <https://doi.org/10.1016/j.conbuildmat.2018.05.122>
- Douglas, E., & Brandstetr, J. (1990). A PRELIMINARY STUDY ON THE ALKALI ACTIVATION OF GROUND GRANULATED BLAST-FURNACE SLAG. *CEMENT and CONCRETE RESEARCH*, 20, 746–756.
- Duan, P., Yan, C., & Zhou, W. (2016). Influence of partial replacement of fly ash by metakaolin on mechanical properties and microstructure of fly ash geopolymer paste exposed to sulfate attack. In *Ceramics International* (Vol. 42, Issue 2, pp. 3504–3517). <https://doi.org/10.1016/j.ceramint.2015.10.154>
- Duxson, P., Fernández-Jiménez, A., Provis, J. L., Lukey, G. C., Palomo, A., & Deventer, J. S. J. Van. (2007). *Geopolymer technology: The current state of the art* (vol. 42, n). J. Mater. Sci.
- Džunuzović, N., Komljenović, M., Nikolić, V., & Ivanović, T. (2017). External sulfate attack on alkali-activated fly ash-blast furnace slag composite. In *Construction and Building Materials* (Vol. 157, pp. 737–747). <https://doi.org/10.1016/j.conbuildmat.2017.09.159>
- Edvardsen, C. (1999). Water permeability and autogenous healing of cracks in concrete. *ACI Materials Journal*, 96(4). <https://doi.org/10.14359/645>
- Ekaputri, J. J., Junaedi, S., & Wijaya. (2017). Effect of Curing Temperature and Fiber on Metakaolin-based Geopolymer. In *Procedia Engineering* (Vol. 171, pp. 572–583). <https://doi.org/10.1016/j.proeng.2017.01.376>
- Fu, Y., Cai, L., & Yonggen, W. (2011). Freeze-thaw cycle test and damage mechanics models of alkali-activated slag concrete. In *Construction and Building Materials* (Vol. 25, Issue 7, pp. 3144–3148). <https://doi.org/10.1016/j.conbuildmat.2010.12.006>
- Hake, S. L., Damgir, R. M., & Patankar, S. V. (2015). State of Art-Investigation of method of curing on geopolymer concrete. *IOSR Journal of Mechanical and Civil Engineering Ver. II*, 12(3), 2278–1684. <https://doi.org/10.9790/1684-12324044>
- Hardjito, D., Wallah, S. E., Sumajouw, D. M. J., & Rangan, B. V. (2004). On the development of

- fly ash-based geopolymer concrete. *ACI Materials Journal*, 101(6), 467–472.  
<https://doi.org/10.14359/13485>
- He, J. (2012). Synthesis and characterization of geopolymers for infrastructural applications. *LSU Digital Commons*.
- He, P., Wang, M., Fu, S., Jia, D., Yan, S., Yuan, J., Xu, J., Wang, P., & Zhou, Y. (2016). Effects of Si/Al ratio on the structure and properties of metakaolin based geopolymer. *Ceramics International*, 42(13), 14416–14422. <https://doi.org/10.1016/j.ceramint.2016.06.033>
- Heah, C. Y., Kamarudin, H., Mustafa Al Bakri, A. M., Binhussain, M., Luqman, M., Khairul Nizar, I., Ruzaidi, C. M., & Liew, Y. M. (2011). Effect of curing profile on kaolin-based geopolymers. In *Physics Procedia* (Vol. 22, pp. 305–311).  
<https://doi.org/10.1016/j.phpro.2011.11.048>
- Huang, O. D., Kim, C., Lies, N. J., Castaneda, H., & Radovic, M. (2021). Parametric Study of Reinforced Metakaolin-Based Geopolymer Concrete against Chloride-Induced Corrosion. *American Society of Civil Engineers*, 373–385.
- Ilić, B. R., Mitrović, A. A., & Miličić, L. R. (2010). Thermal treatment of kaolin clay to obtain metakaolin. *Hemijska Industrija*, 64(4), 351–356.  
<https://doi.org/10.2298/HEMIND100322014I>
- Inada, S., Kobayashi, S., Taniguchi, J., Mizuki, S., Kamada, H., & Nishiyama, M. (2004). *High-absorbent polyvinyl alcohol fibers and nonwoven fabric comprising them* (Patent No. US 6783852 B2).
- Jang, J. G., Lee, N. K., & Lee, H. K. (2014). Fresh and hardened properties of alkali-activated fly ash\_slag pastes with superplasticizers. *Construction and Building Materials*, 50, 169–176.
- Japan Society of Civil Engineers. (2008). Recommendations for Design and Construction of High Performance Fiber Reinforced Cement Composites with Multiple Fine Cracks ( HPFRCC ). *Concrete Engineering*, 82.
- Kan, L. li, Lv, J. wei, Duan, B. bei, & Wu, M. (2019). Self-healing of Engineered Geopolymer Composites prepared by fly ash and metakaolin. *Cement and Concrete Research*, 125(105895). <https://doi.org/10.1016/j.cemconres.2019.105895>
- Kan, L. li, Wang, W. song, Liu, W. dong, & Wu, M. (2020). Development and Characterization of Fly ash based PVA Fiber Reinforced Engineered Geopolymer Composites Incorporating metakaolin. *Cement and Concrete Composites*, 108(103521).  
<https://doi.org/10.1016/j.cemconcomp.2020.103521>
- Kanda, T., & Li, V. C. (2006). Practical Design Criteria for Saturated Pseudo Strain Hardening Behavior in ECC. *Journal of Advanced Concrete Technology*, 4(1), 59–72.
- Khan, I., Xu, T., Castel, A., Gilbert, R. I., & Babaei, M. (2019). Risk of early age cracking in geopolymer concrete due to restrained shrinkage. *Construction and Building Materials*,

229. <https://doi.org/10.1016/j.conbuildmat.2019.116840>
- Kim, Y. Y., Fischer, G., & Li, V. C. (2004). Performance of bridge deck link slabs designed with ductile engineered cementitious composite. *ACI Structural Journal*, 101(6), 792–801. <https://doi.org/10.14359/13454>
- Kiron, M. I. (2013). *Polypropylene Fiber: Properties, Manufacturing Process and Applications*. Textile Learner. <https://textilelearner.net/polypropylene-fiber-properties-applications/>
- Komljenović, M., Bašćarević, Z., Marjanović, N., & Nikolić, V. (2013). External sulfate attack on alkali-activated slag. In *Construction and Building Materials* (Vol. 49, pp. 31–39). <https://doi.org/10.1016/j.conbuildmat.2013.08.013>
- Komnitsas, K. A. (2011). Potential of geopolymer technology towards green buildings and sustainable cities. *Procedia Engineering*, 21, 1023–1032. <https://doi.org/10.1016/j.proeng.2011.11.2108>
- Kong, D. L. Y., & Sanjayan, J. G. (2010). Effect of elevated temperatures on geopolymer paste, mortar and concrete. *Cement and Concrete Research*, 40(2), 334–339. <https://doi.org/10.1016/j.cemconres.2009.10.017>
- Kumaravel, S. (2014). Development of various curing effect of nominal strength Geopolymer concrete. *Journal of Engineering Science and Technology Review*, 7(1), 116–119.
- Kupwade-Patil, K., & Allouche, E. N. (2013). Impact of Alkali Silica Reaction on Fly Ash-Based Geopolymer Concrete. *Journal of Materials in Civil Engineering*, 25(1), 131–139. [https://doi.org/10.1061/\(asce\)mt.1943-5533.0000579](https://doi.org/10.1061/(asce)mt.1943-5533.0000579)
- Lee, S., Kim, B., Seo, J., & Cho, S. (2020). Beneficial use of MIBC in metakaolin-based geopolymers to improve flowability and compressive strength. *Materials*, 13(17). <https://doi.org/10.3390/MA13173663>
- Lei, J., Fu, J., & Yang, E. H. (2020). Alkali-silica reaction resistance and pore solution composition of low-calcium fly ash-based geopolymer concrete. *Infrastructures*, 5(11), 1–15. <https://doi.org/10.3390/infrastructures5110096>
- Lepech, M. D., & Li, V. C. (2009). Application of ECC for bridge deck link slabs. *Materials and Structures/Materiaux et Constructions*, 42(9), 1185–1195. <https://doi.org/10.1617/s11527-009-9544-5>
- Li, V. C. (1993). From Micromechanics Engineering Design for Compo- of Cementitious Engineering. *JSCE Journal of Structural Mechanics Earthquake Eng.*, 471(I–24), 37s–48s.
- Li, V. C. (2003). On Engineered Cementitious Composites (ECC) A Review of the Material and Its Applications. In *Journal of Advanced Concrete Technology* (Vol. 1, Issue 3).
- Li, V. C. (2008). Engineered cementitious composite (ecc): Material, structural, and durability performance. *Concrete Construction Engineering Handbook, Second Edition*, 1001–1048.

- Li, V. C. (2019a). Engineered Cementitious Composites (ECC). In *Engineered Cementitious Composites (ECC)*. <https://doi.org/10.1007/978-3-662-58438-5>
- Li, V. C. (2019b). Engineered Cementitious Composites (ECC) Bendable Concrete for Sustainable and Resilient Infrastructure. In *Engineered Cementitious Composites (ECC)*. <https://doi.org/10.1007/978-3-662-58438-5>
- Li, V. C., Horikoshi, T., Ogawa, A., Torigoe, S., & Saito, T. (2004). Micromechanics-based durability study of polyvinyl alcohol-engineered cementitious composite. *ACI Materials Journal*, 101(3), 242–248. <https://doi.org/10.14359/13120>
- Li, V. C., Wu, C., Wang, S., Ogawa, A., & Saito, T. (2002). Interface tailoring for strain-hardening polyvinyl alcohol-engineered cementitious composite (PVA-ECC). *ACI Materials Journal*, 99(5), 463–472. <https://doi.org/10.14359/12325>
- Ling, Y., Wang, K., Li, W., Shi, G., & Lu, P. (2019). Effect of slag on the mechanical properties and bond strength of fly ash-based engineered geopolymer composites. *Composites Part B: Engineering*, 164(February), 747–757. <https://doi.org/10.1016/j.compositesb.2019.01.092>
- Lizcano, M., Gonzalez, A., Basu, S., Lozano, K., & Radovic, M. (2012). Effects of water content and chemical composition on structural properties of alkaline activated metakaolin-based geopolymers. *Journal of the American Ceramic Society*, 95(7), 2169–2177. <https://doi.org/10.1111/j.1551-2916.2012.05184.x>
- Lizcano, M., Kim, H. S., Basu, S., & Radovic, M. (2012). Mechanical properties of sodium and potassium activated metakaolin-based geopolymers. *Journal of Materials Science*, 47(6), 2607–2616. <https://doi.org/10.1007/s10853-011-6085-4>
- M. Sufian Badar, K. Kupwade-Patil, S. A. Bernal, J. L. Provis, and E. N. A. (2014). Corrosion of steel bars induced by accelerated carbonation in low and high calcium fly ash geopolymer concretes. *Construction and Building Materials*, 61, 79–89.
- Ma, C., Long, G., Shi, Y., & Xie, Y. (2018). Preparation of cleaner one-part geopolymer by investigating different types of commercial sodium metasilicate in China. *Journal of Cleaner Production*, 201, 636–647. <https://doi.org/10.1016/j.jclepro.2018.08.060>
- Ma, C., Zhao, B., Wang, L., Long, G., & Xie, Y. (2020). Clean and low-alkalinity one-part geopolymeric cement: Effects of sodium sulfate on microstructure and properties. *Journal of Cleaner Production*, 252, 119279. <https://doi.org/10.1016/j.jclepro.2019.119279>
- Ma, H., Qian, S., Zhang, Z., Lin, Z., & Li, V. C. (2015). Tailoring Engineered Cementitious Composites with local ingredients. *Construction and Building Materials*, 101(Part 1), 584–595. <https://doi.org/10.1016/j.conbuildmat.2015.10.146>
- Marshall, D. B. ., & Cox, B. N. N. (1988). A J-Integral Method for Calculating Steady-State Matrix Cracking Stresses in Composites. *Mechanics of Materials*, 7(2), 127–133.
- McCormac, J. C., & Brown, R. H. (2016). *Design of Reinforced Concrete* (Tenth). Wiley.



- McLellan, B. C., Williams, R. P., Lay, J., Van Riessen, A., & Corder, G. D. (2011). Costs and carbon emissions for geopolymer pastes in comparison to ordinary portland cement. *Journal of Cleaner Production*, 19(9–10), 1080–1090. <https://doi.org/10.1016/j.jclepro.2011.02.010>
- Memon, F. A., Nuruddin, M. F., Demie, S., & Shafiq, N. (2012). Effect of superplasticizer and extra water on workability and compressive strength of self-compacting geopolymer concrete. *Research Journal of Applied Sciences, Engineering and Technology*, 4(5).
- Michalske, T. A., & Freiman, S. W. (1982). *A molecular Interpretation of Stress Corrosion in Silica*. 295(February), 511–512.
- Mighty Mono*. (2020). FORTA.
- Mindess, S., Young, F. J., & Darwin, D. (2003). *Concrete* (2nd ed.). Prentice Hall.
- Morsy FA, El-Sherbiny S, Hassan MS, M. H. (2014). *Modification and evaluation of Egyptian kaolinite as pigment for paper coating*. 264,430-438. <https://doi.org/10.1016>
- Naaman, A. E. (2008). High performance fiber reinforced cement composites. In *High-performance construction materials: science and applications*. (pp. 91–153). Singapore: World Scientific Publishing.
- Naaman, A. E. (2018). *Fiber Reinforced Cement and Concrete Composites*. 765.
- Nazarpour, H., & Jamali, M. (2020). Mechanical and freezing cycles properties of geopolymer concrete with recycled aggregate. *Structural Concrete*, 21(3), 1004–1012. <https://doi.org/10.1002/suco.201900317>
- Nematollahi, B., Sanjayan, J., & Ahmed Shaikh, F. U. (2015). Tensile strain hardening behavior of PVA fiber-reinforced engineered geopolymer composite. *Journal of Materials in Civil Engineering*, 27(10), 1–12. [https://doi.org/10.1061/\(ASCE\)MT.1943-5533.0001242](https://doi.org/10.1061/(ASCE)MT.1943-5533.0001242)
- Nematollahi, B., Sanjayan, J., & Shaikh, F. U. A. (2014). Comparative deflection hardening behavior of short fiber reinforced geopolymer composites. *Construction and Building Materials*, 70, 54–64. <https://doi.org/10.1016/j.conbuildmat.2014.07.085>
- Nematollahi, B., Sanjayan, J., & Shaikh, F. U. A. (2015). Strain hardening behavior of engineered geopolymer composites: Effects of the activator combination. *Journal of the Australian Ceramic Society*, 51(1), 54–60.
- Nematollahi, B., Sanjayan, J., & Shaikh, F. U. A. (2016). Matrix design of strain hardening fiber reinforced engineered geopolymer composite. *Composites Part B: Engineering*, 89, 253–265. <https://doi.org/10.1016/j.compositesb.2015.11.039>
- Nematollahi, B., Vijay, P., Sanjayan, J., Nazari, A., Xia, M., Nerella, V. N., & Mechtcherine, V. (2018). Effect of polypropylene fibre addition on properties of geopolymers made by 3D printing for digital construction. *Materials*, 11(12). <https://doi.org/10.3390/ma11122352>

- Noël, J., Djobo, Y., Elimbi, A., & Tchakouté, H. K. (2017). *Volcanic ash-based geopolymer cements / concretes : the current state of the art and perspectives*. 4433–4446. <https://doi.org/10.1007/s11356-016-8230-8>
- Noorvand, H., Arce, G., Hassan, M., Rupnow, T., & Mohammad, L. N. (2019). Investigation of the Mechanical Properties of Engineered Cementitious Composites with Low Fiber Content and with Crumb Rubber and High Fly Ash Content. *Transportation Research Record*, 2673(5), 418–428. <https://doi.org/10.1177/0361198119837510>
- Nurruddin, M. F., Haruna, S., Mohammed, B. S., & Galal, I. (2018). *International Journal of Advanced and Applied Sciences Methods of curing geopolymer concrete : A review*. 5(1), 31–36.
- Nuruddin, M. F. N., Kusbiantoro, A. K., Qazi, S. Q., Darmawan, M. S. D., & Husin, N. A. H. (2011). Development of Geopolymer Concrete with Different Curing Conditions. *IPTEK The Journal for Technology and Science*, 22(1), 24–28. <https://doi.org/10.12962/j20882033.v22i1.54>
- NYCON. (2022). *NYCON-PVA RECS15*. Nycon. [www.nycon.com](http://www.nycon.com)
- Ohno, M., & Li, V. C. (2014). A feasibility study of strain hardening fiber reinforced fly ash-based geopolymer composites. *Construction and Building Materials*, 57, 163–168. <https://doi.org/10.1016/j.conbuildmat.2014.02.005>
- Ohno, M., & Li, V. C. (2018). An integrated design method of Engineered Geopolymer Composite. *Cement and Concrete Composites*, 88, 73–85. <https://doi.org/10.1016/j.cemconcomp.2018.02.001>
- Osman, B. H., Sun, X., Tian, Z., Lu, H., & Jiang, G. (2019). Dynamic Compressive and Tensile Characteristics of a New Type of Ultra-High-Molecular Weight Polyethylene (UHMWPE) and Polyvinyl Alcohol (PVA) Fibers Reinforced Concrete. *Shock and Vibration*, 2019. <https://doi.org/10.1155/2019/6382934>
- Ozyildirim, H. C., & Moruza, G. M. (2016). High-performance grouting materials in shear keys between box beams. *Transportation Research Record*, 2577(2577), 35–42. <https://doi.org/10.3141/2577-05>
- Pacheco-Torgal, F., Moura, D., Ding, Y., & Jalali, S. (2011). Composition, strength and workability of alkali-activated metakaolin based mortars. *Construction and Building Materials*, 25(9), 3732–3745. <https://doi.org/10.1016/j.conbuildmat.2011.04.017>
- Pakravan, H. R., Jamshidi, M., & Latifi, M. (2018). The effect of hydrophilic (polyvinyl alcohol) fiber content on the flexural behavior of engineered cementitious composites (ECC). *Journal of the Textile Institute*, 109(1), 79–84. <https://doi.org/10.1080/00405000.2017.1329132>
- Palacios, M., & Puertas, F. (2005). Effect of superplasticizer and shrinkage reducing admixtures on alkali activated slag pastes and mortars. *Cement and Concrete Research*, 35, 1358 –

- Palacios, M., Puertas, F., Bowen, P., & Houst, Y. F. (2009). Effect of PCs superplasticizers on the rheological properties and hydration process of slag-blended cement pastes. *Journal of Materials Science*, 44(10), 2714–2723. <https://doi.org/10.1007/s10853-009-3356-4>
- Palacios, Marta, Banfill, P. F. G., & Puertas, F. (2008). Rheology and setting of alkali-activated slag pastes and mortars: Effect if organic admixture. *ACI Materials Journal*, 105(2), 140–148. <https://doi.org/10.14359/19754>
- Panesar, D. K. (2019). *Developments in the Formulation and Reinforcement of Concrete* (2nd ed.).
- Patil, A. A., Chore, H. S., & Dode, P. A. (2014). Effect of Curing Condition on Strength of Geopolymer Concrete. *Advances in Concrete Construction*, 2(1), 29–37. <https://doi.org/10.1088/1755-1315/982/1/012031>
- Paulo, P. K. M., & Monteiro, P. (2006). *Concrete: microstructure, properties, and materials* (Issue 1). <https://doi.org/10.16309/j.cnki.issn.1007-1776.2003.03.004>
- Perera, D. S., Uchida, O., Vance, E. R., & Finnie, K. S. (2007). Influence of curing schedule on the integrity of geopolymers. *Journal of Materials Science*, 42(9), 3099–3106. <https://doi.org/10.1007/s10853-006-0533-6>
- Provis, J. L., & Deventer, J. S. J. Van. (2009). *Geopolymers Structure, processing, properties and industrial applications*.
- Puertas, F., Palomo, A., Fernández-Jiménez, A., Izquierdo, J. D., & Granizo, M. L. (2003). Effect of superplasticisers on the behaviour and properties of alkaline cements. *Advances in Cement Research*, 15(1). <https://doi.org/10.1680/adcr.2003.15.1.23>
- Rangan, B., & Hardjito, D. (2005). Studies on fly ash-based geopolymer concrete. *Proc. 4th World ...*, November.
- Rangan, B. V. (2018). *Chapter 11. Engineering Properties of geopolymer concrete*. 293–295. [https://doi.org/10.1007/978-3-319-73568-9\\_110](https://doi.org/10.1007/978-3-319-73568-9_110)
- Rashad, A. M., & Sadek, D. M. (2020). Behavior of alkali-activated slag pastes blended with waste rubber powder under the effect of freeze/thaw cycles and severe sulfate attack. In *Construction and Building Materials* (Vol. 265). <https://doi.org/10.1016/j.conbuildmat.2020.120716>
- Reda Taha, M. M., Xiao, X., Yi, J., & Shrive, N. G. (2002). Evaluation of flexural fracture toughness for quasi-brittle structural materials using a simple test method. *Canadian Journal of Civil Engineering*, 29(4), 567–575. <https://doi.org/10.1139/102-044>
- Redon, C., Li, V. C., Wu, C., Hoshiro, H., Saito, T., & Ogawa, A. (2001a). Measuring and Modifying Interface Properties od PVA fibers in ECC Matrix. *Manager*, 13(6), 399–406.

- Redon, C., Li, V. C., Wu, C., Hoshiro, H., Saito, T., & Ogawa, A. (2001b). Measuring and Modifying Interface Properties of PVA Fibers in ECC Matrix. *Journal of Materials in Civil Engineering*, 13(6), 399–406. [https://doi.org/10.1061/\(ASCE\)0899-1561\(2001\)13:6\(399\)](https://doi.org/10.1061/(ASCE)0899-1561(2001)13:6(399))
- Ren, X., & Zhang, L. (2018). Experimental study of interfacial transition zones between geopolymers binder and recycled aggregate. *Construction and Building Materials*, 167, 749–756. <https://doi.org/10.1016/j.conbuildmat.2018.02.111>
- Rovnaník, P. (2010). Effect of curing temperature on the development of hard structure of metakaolin-based geopolymer. In *Construction and Building Materials* (Vol. 24, Issue 7, pp. 1176–1183). <https://doi.org/10.1016/j.conbuildmat.2009.12.023>
- Rozek, P., Krol, M., & Mozgawa, W. (2019). Geopolymer-zeolite composites\_ A review \_ Elsevier Enhanced Reader.pdf. *Journal of Cleaner Production*, 230, 557–579.
- Ryu, G. S., Lee, Y. B., Koh, K. T., & Chung, Y. S. (2013). The mechanical properties of fly ash-based geopolymer concrete with alkaline activators. *Construction and Building Materials*, 47, 409–418. <https://doi.org/10.1016/j.conbuildmat.2013.05.069>
- Sahmaran, M., Lachemi, M., Hossain, K. M. A., Ranade, R., & Li, V. C. (2009). Influence of aggregate type and size on ductility and mechanical properties of engineered cementitious composites. *ACI Materials Journal*, 106(3), 308–316. <https://doi.org/10.14359/56556>
- Salami, B. A., Megat Johari, M. A., Ahmad, Z. A., & Maslehuddin, M. (2016). Impact of added water and superplasticizer on early compressive strength of selected mixtures of palm oil fuel ash-based engineered geopolymer composites. *Construction and Building Materials*, 109, 198–206. <https://doi.org/10.1016/j.conbuildmat.2016.01.033>
- Sata, V., Sathonsaowaphak, A., & Chindaprasirt, P. (2012). Resistance of lignite bottom ash geopolymer mortar to sulfate and sulfuric acid attack. *Cement and Concrete Composites*, 34(5), 700–708. <https://doi.org/10.1016/j.cemconcomp.2012.01.010>
- Singh, B., Rahman, M. R., Paswan, R., & Bhattacharyya, S. K. (2016). Effect of activator concentration on the strength, ITZ and drying shrinkage of fly ash/slag geopolymer concrete. *Construction and Building Materials*, 118, 171–179. <https://doi.org/10.1016/j.conbuildmat.2016.05.008>
- Singh, N. B. (2018). Fly ash-based geopolymer binder: A future construction material. *Minerals*, 8(299). <https://doi.org/10.3390/min8070299>
- Subedi, S., Arce, G., Hassan, M., Kumar, N., Barbato, M., & Gutierrez-Wing, M. T. (2019). Influence of Production Methodology on the Pozzolanic Activity of Sugarcane Bagasse Ash. *Tran-SET Conference*.
- Swapp, S. (2017). *Scanning Electron Microscopy ( SEM )*. Geochemical Instrumentation and Analysis.
- Tar buck, E. J., Lutgens, F. K., & Lutgens FK, T. E. (2017). *Earth; an Introduction to Physical*

*Geology* (12th ed.). Pearson.

- Trindade, A. C. C., Heravi, A. A., Curosu, I., Liebscher, M., de Andrade Silva, F., & Mechtcherine, V. (2020). Tensile behavior of strain-hardening geopolymer composites (SHGC) under impact loading. *Cement and Concrete Composites*, 113(103703). <https://doi.org/10.1016/j.cemconcomp.2020.103703>
- Turner, L. K., & Collins, F. G. (2013). Carbon dioxide equivalent (CO<sub>2</sub>-e) emissions: A comparison between geopolymer and OPC cement concrete. *Construction and Building Materials*, 43, 125–130. <https://doi.org/10.1016/j.conbuildmat.2013.01.023>
- Tutal, A., Partschefeld, S., Schneider, J., & Osburg, A. (2020). Effects of Bio-Based Plasticizers, Made From Starch, on the Properties of Fresh and Hardened Metakaolin-Geopolymer Mortar: Basic Investigations. *Clays and Clay Minerals*, 68(5), 413–427. <https://doi.org/10.1007/s42860-020-00084-8>
- Vickers, L., Riessen, A. van, & Rickard, W. (2015). Fire-resistant Geopolymers: Role of Fibres and Fillers to Enhance Thermal Properties. In *SpringerBriefs in Materials*.
- Vijai, K., Kumutha, R., & Vishnuram, B. G. (2010). Effect of types of curing on strength of geopolymer concrete. *International Journal of Physical Sciences*, 5(9), 1419–1423.
- W. JIANG, WU, X., & ROY, D. M. (1993). ALKALI-ACTIVATED FLY ASH-SLAG CEMENT BASED NUCLEAR WASTE FORMS. *Materials Research Society Symposium*, 294, 255–260.
- Wallah, S E, & Rangan, B. V. (2006). *Low-Calcium Fly Ash Based*. 1–107.
- Wallah, Steenie E., Sumajouw, D. M. J., Hardjito, D., & Rangan, B. V. (2005). Performance of geopolymer concrete under sulfate exposure. *American Concrete Institute, ACI Special Publication, SP-225*(April), 27–36. <https://doi.org/10.14359/14375>
- Weissberger, A. (2020). *Technique of Organic Chemistry* (3rd ed.).
- Xie, J., & Kayali, O. (2016). Effect of superplasticiser on workability enhancement of Class F and Class C fly ash-based geopolymers. In *Construction and Building Materials* (Vol. 122, pp. 36–42). <https://doi.org/10.1016/j.conbuildmat.2016.06.067>
- Yang, E. (2008). *Designing Added Functions in Engineered Cementitious Composites*. The University of Michigan.
- Yang, E. H., Wang, S., Yang, Y., & Li, V. C. (2008). Fiber-bridging constitutive law of engineered cementitious composites. *Journal of Advanced Concrete Technology*, 6(1), 181–193. <https://doi.org/10.3151/jact.6.181>
- Yang, T., Zhu, H., & Zhang, Z. (2017). Influence of fly ash on the pore structure and shrinkage characteristics of metakaolin-based geopolymer pastes and mortars. In *Construction and Building Materials* (Vol. 153, pp. 284–293).

<https://doi.org/10.1016/j.conbuildmat.2017.05.067>

- Yewale, V. V., Shirsath, M. N., & Hake, S. L. (2016). Evaluation of Efficient Type of Curing for Geopolymer Concrete. *International Journal of New Technologies in Science and Engineering*, 3(8), 10–14.
- Yu, K. Q., Yu, J. T., Dai, J. G., Lu, Z. D., & Shah, S. P. (2018). Development of ultra-high performance engineered cementitious composites using polyethylene (PE) fibers. *Construction and Building Materials*, 158, 217–227. <https://doi.org/10.1016/j.conbuildmat.2017.10.040>
- Zahid, M., & Shafiq, N. (2020). *Effects of Sand / Fly Ash and the Water / Solid Ratio on the Mechanical Properties of Engineered Geopolymer*.
- Zhang, Z., Zhang, Q., Qian, S., & Li, V. C. (2015). Low E modulus early strength engineered cementitious composites material development for ultrathin whitetopping overlay. *Transportation Research Record*, 2481, 41–47. <https://doi.org/10.3141/2481-06>
- Zhao, R., Yuan, Y., Cheng, Z., Wen, T., Li, J., Li, F., & Ma, Z. J. (2019). Freeze-thaw resistance of Class F fly ash-based geopolymer concrete. In *Construction and Building Materials* (Vol. 222, pp. 474–483). <https://doi.org/10.1016/j.conbuildmat.2019.06.166>

## **VITA**

Ruwa AbuFarsakh was born in 1996 in Baton Rouge, Louisiana. In 2019, she finished her Bachelor of Science in Civil Engineering from Louisiana State University, Baton Rouge, Louisiana. In 2019, she decided to pursue a Master of Science in Material Science and Engineering while doing her doctoral studies. She plans to receive her Master this December 2022. Her interests include sustainable construction materials, concrete materials, concrete materials, material characterization, and novel materials.